ORGANICALLY MODIFIED SILICA NANOPARTICLE BASED APPROACHES FOR IMPROVING EFFICACY OF DRUGS FOR CANCER THERAPY

By

SURYA PRAKASH SINGH

Enrolment No. – LIFE03200904001

Raja Ramanna Center for Advanced Technology, Indore, India

A thesis submitted to the
Board of Studies in Life Sciences
In partial fulfillment of requirements
For the Degree of

DOCTOR OF PHILOSOPHY
of
HOMI BHABHA NATIONAL INSTITUTE

June, 2015

Homi Bhabha National Institute

Recommendations of the Viva Voce Committee

As members of the Viva Voce Committee, we certify that we have read the dissertation prepared by **Surya Prakash Singh** entitled **"Organically modified Silica Nanoparticle based approaches for improving efficacy of drugs for cancer therapy"** and recommend that it may be accepted as fulfilling the thesis requirement for the award of Degree of Doctor of Philosophy.

Chairman – Dr. P.K. Gupta P. K. Gupta **Date:** 8/02/16

Guide / Convener – Dr. M. Sharma S. Mrinalini Sharma **Date:** 8/02/16

Co-guide – Dr. K. Das Kaustuv Das **Date:** 8/2/16

Member 1– Dr. Indira Priyadarsini K. Indira Priyadarsini **Date:** 8.2.2016

Member 2– Dr. A. Dube **Date:** 8/2/16

External Examiner Dr. R. Jayakumar **Date:**

Final approval and acceptance of this thesis is contingent upon the candidate's submission of the final copies of the thesis to HBNI.

We hereby certify that we have read this thesis prepared under our direction and recommend that it may be accepted as fulfilling the thesis requirement.

Date: 8/02/2016

Place: RRCAT, Indore

S. Mrinalini Sharma
Guide
(Dr. M. Sharma)

Kaustuv Das
Co-guide
(Dr. K. Das)

STATEMENT BY AUTHOR

This dissertation has been submitted in partial fulfillment of requirements for an advanced degree at Homi Bhabha National Institute (HBNI) and is deposited in the Library to be made available to borrowers under rules of the HBNI.

Brief quotations from this dissertation are allowable without special permission, provided that accurate acknowledgement of source is made. Requests for permission for extended quotation from or reproduction of this manuscript in whole or in part may be granted by the Competent Authority of HBNI when in his or her judgment the proposed use of the material is in the interests of scholarship. In all other instances, however, permission must be obtained from the author.

Surya Prakash Singh

(Surya Prakash Singh)

DECLARATION

I, hereby declare that the investigation presented in the thesis has been carried out by me. The work is original and has not been submitted earlier as a whole or in part for a degree / diploma at this or any other Institution / University.

Surya Prakash Singh

(Surya Prakash Singh)

List of Publications arising from the thesis

Journals:

a) Published

1. "Enhancement of phototoxicity of curcumin in human oral cancer cells using silica nanoparticles as delivery vehicle", **S. P. Singh**, M. Sharma, P. K. Gupta, *Lasers Med Sci.*, **2014**, 29: 645-52.

2. "Extra cellular pH influences uptake and photodynamic action of pyropheophorbide–a entrapped in folate receptor targeted organically modified silica nanoparticle", **S. P. Singh**, M. Sharma, H. Patel, P. K. Gupta, *Photodiagnosis Photodyn Ther.*, **2014**, 11: 156-64.

3. "Evaluation of phototoxic effects of curcumin loaded in organically modified silica nanoparticles in tumor spheroids of oral cancer cells", **S.P. Singh**, M. Sharma, P. K Gupta. *BioNanoScience*, **2015**, 5: 10-21.

4. "Cytotoxicity of curcumin silica nanoparticle complexes conjugated with hyaluronic acid on colon cancer cells", **S. P. Singh**, M. Sharma, P. K. Gupta, *Int J Biol Macromol.*, **2015** 74: 162-70.

b) To be communicated

1. "Biodistribution and clearance studies of pyropheophorbide–a entrapped in folate receptor targeted organically modified silica nanoparticle in tumor bearing mice", **S. P. Singh**, K. Sahu, M. Sharma, P.K. Gupta.

In conferences proceedings:

1. "Effect of complexing with silica nanoparticle on the photodynamic toxicity of curcumin", **S. P. Singh**, M. Sharma, P. K. Gupta, National Laser Symposium, Mumbai, February, 2013.

2. "Effect of pH on uptake and phototoxicity of folate receptor targeted organically modified silica nanoparticles entrapped with pyropheophorbide-a on breast and oral cancer cells", **S. P. Singh**, M. Sharma, B. Jain and P. K. Gupta, National Symposium on Radiation and Photochemistry, NEHU, Shillong, March, 2013.

3. "Effect of hyaluronic acid conjugated curcumin entrapped with organically modified silica nanoparticles on cancer cells", **S. P. Singh**, M. Sharma, P. K. Gupta, International conference on NanoSciTech 2014, Panjab University, Panjab, February, 2014.

Surya Prakash Singh

(Surya Prakash Singh)

Dedicated

To

My Beloved

Family

ACKNOWLEDGEMENTS

It gives me great pleasure to thank all those people who have contributed in their own ways for the successful completion of this work.

First and foremost, I would like to express my sincere gratitude to my guide Dr. Mrinalini Sharma, for her invaluable guidance, encouragement and continuous support throughout my research work.

I wish to express my sincere thanks to Professor P. K. Gupta, Head, Laser Bio-medical Application and Instrumentation Division (RRCAT, Indore). He has been very supportive since the days I began working. His advice, helpful suggestions and motivating words were the source of inspiration for carrying out my research work.

It is also a great pleasure to express my sincere thanks to my co-guide Dr. Kaustuv Das. His valuable guidance on nanoparticle preparation and the scientific discussions related to it helped me to complete this study successfully.

I am grateful to my doctoral committee members, Professor K. I. Priyadarsini, Head, Radiation Chemistry and Biology Section (BARC, Mumbai) and Dr. Alok Dube for their suggestions and discussions during the progress of my thesis work.

I express my sincere thanks to Mr. Khageswar Sahu for providing useful comments, help in animal studies and his constant support. I am also thankful to Mr. H.S. Patel for providing help for confocal imaging studies.

I would like to express special thanks Dr. Beena Jain and Dr. Rashmi Shrivastava for proof reading of this thesis.

I would also like to thank Dr. Biplab Bose, Dr. Abha Uppal, Dr. Mahesh Swami, Dr. Yogesh Verma and Dr Shovan Majumdar for useful discussion during my research work.

My heartfelt thanks to my seniors Dr. Arpana Parihar, Dr. R.K. Saini, Dr. B. Ramakrishna and friends G. K. Varshney, Paromita, Pooja, S. R. Kintali, Shyam Sunder, Sudhir and Pankaj for their support.

I would also like to thank Mrs. Harsha Bansal, Mr. Y. Deshpande, Mr. Anupam Chowdhary, Mr. Gyan Singh and all other members of Laser Biomedical Applications and Instrumentation Division for their kind co-operation. I would also like to acknowledge all my Ph.D. friends of HBNI for providing their moral support.

A special thanks to my family. My words cannot express how grateful I am for my parents. Your prayers and blessings are always with me. I am thankful to my brother Chandra Prakash Singh, my bhabhi Beena Singh for her selfless support and encouragement. I want to thank, my nephew Tanu, who is a constant source of joy. At the end I would like to express appreciation to my dearest wife Mamta Singh for her support and sacrifice.

(Surya Prakash Singh)

CONTENTS

Page No.

SYNOPSIS

Cancer remains one of the most lethal diseases and leading cause of death worldwide. Cancer-related morbidity and mortality is close to 8 million annually and incidence of cancer is increasing due to change in lifestyles and increase life expectancy [1]. Current modalities of cancer treatment such as radiation and chemotherapy lack selectivity induce serious side effects and also cancers develop resistance to these treatments. To overcome these limitations treatment modalities which are more selective, safer and effective than chemotherapy or radiation therapy are being investigated. Of late, there is a considerable interest in exploring the use of natural herbal compounds which have anticancer activities. One such natural product that has attracted attention is curcumin. This is a hydrophobic polyphenol derived from the herb *Curcuma longa* commonly called turmeric [2] and is well known for its antioxidant, anti-inflammatory, cancer preventive, chemotherapeutic and wound healing properties [3]. Curcumin also exhibits photosensitizing activity. This property has been explored for enhancing anticancer effects and antibacterial activity of curcumin [4, 5]. However, the use of this natural polyphenol for therapeutic applications is limited by its poor water solubility, rapid intestinal and hepatic metabolism. To enhance its biological effectiveness various polymer drug conjugates, liposomes, polymeric nanoparticles are being explored as drug carriers [6, 7]. Although curcumin loaded liposomes /polymeric nanoparticles, and curcumin polymer conjugates have shown improved water-solubility, stability and bioavailability, many of these systems have low drug loading efficiency and also have short storage life as these are prone to biofouling.

Among different inorganic nanomaterials, Organically modified silica nanoparticles (SiNp) have received a lot of attention as a delivery vehicle for photosensitizers and genetic materials. These are biocompatible, resistant to pH changes, optically transparent, have porous structure, allows easy encapsulation of hydrophobic drugs thus protect them from degradation. Also selectivity of drug delivery of these Nps can be enhanced by covalently conjugating ligands of interest with their surface functionalized of groups [8]. Therefore, SiNp is expected to be a good delivery agent for hydrophobic curcumin. One of the objectives of this study was to explore the use of SiNp for improving bioavailability and targeted delivery of curcumin.

Another attractive approach for cancer treatment is Photodynamic therapy (PDT). Compared to radiation and chemo therapy, PDT provides better tumor selectivity and fewer side effects [9]. It involves the administration of photosensitizer (PS) which preferentially gets accumulated in tumor. Photosensitizer localized in tumor when excited with light of appropriate wavelength leads to generation of reactive oxygen species (ROS) which is cytotoxic to cancer cells. The efficacy of PDT depends upon selective accumulation of PS in malignant cells and its photophysical and photochemical properties. The important parameters that an ideal PS should have for PDT include high quantum yield for ROS, amphiphilic nature to ensure higher accumulation in cancer cell and a strong absorbance in the red region (660-800 nm) for deeper penetration in tumor tissue [9]. In this respect, pyropheophorbide–a (PPa), a chlorophyll-a based second generation photosensitizer is attractive because it possess significantly high absorption in the longer wavelength region, is chemically well characterized and has good singlet oxygen yield [10]. However, this photodynamic agent in native form is poorly soluble in water and its photodynamic efficacy gets reduced due to aggregation. Entrapping this photosensitizer in hydrophobic core of SiNp is expected to improve its photodynamic efficiency. Evaluation of the

photodynamic efficacy of pyropheophorbide–a (PPa) entrapped in SiNp, was the second objective of this thesis work.

The thesis is organized as follows:

Chapter 1: In this chapter, we present an overview of the use of nanoparticles for delivery of drugs in cancer therapy. First, we discuss briefly cancer treatments and their limitations. Use of nanoparticle for drug delivery in cancer therapy, in particular mesoporous and organically modified silica nanoparticle (SiNp) is discussed next. Literature on *in vitro* and *in vivo* studies pertaining to use of SiNp for delivery of photodynamic drugs for therapeutic applications and gene delivery is described next. We also summarize the literature related to anticancer and photosensitizing property of curcumin, a natural herbal agent and use of different nanoformulations for improving its bioavailability. Basic principle of photodynamic therapy, characteristics of ideal photosensitizer, photophysical, and photobiological effects of PPa, conjugates of PPa based PS and nanoformulations prepared for improving their drug delivery is also briefly described.

Chapter 2: In this chapter, details of preparation and the methods used for characterization of SiNp and their complexes with curcumin and PPa are described. Next, we describe the experimental protocols used for cell culture, including spheroid cultures, methods for measuring drug uptake, cell viability, mode of cell death, protein expression, biochemical assays and photo irradiation of cells. Procedure used for tumor induction in mice, methods for measuring distribution of PS in different organs and histology has been described subsequently.

Chapter 3: In this chapter, we describe the results of our investigation on uptake and phototoxicity of curcumin loaded SiNp in human oral cancer cells grown in monolayer. Results

showed that the uptake of curcumin-SiNp complex (cur-SiNp) by these cells was ~5 times higher than that for free curcumin. This was attributed to the enhancement in stability of curcumin incorporated in SiNp which was ascertained by absorption spectroscopic measurements. Studies carried out on cytotoxicity (dark, as well as light induced), showed that as compared to free curcumin, cur-SiNp led to enhanced cell killing and inhibition in the activity of NF-κB and its regulated proteins involved in invasion (MMP-9), angiogenesis (VEGF), and inflammation (TNF-α).

Chapter 4: In view of the encouraging results obtained in monolayer culture, the efficacy of SiNp was investigated in tumor spheroids which are a better model system as these have three dimensional organization, extracellular matrix, complex biochemical and biomechanical environments as in tumors under in vivo conditions. In this chapter, we describe the results of our investigations on relative uptake efficacy and phototoxic potential of free curcumin and its cur-SiNp complex in multicellular spheroids of human oral cancer cells (Nt-8e) cells. Result showed that uptake of nanoformulated curcumin was ~1.7 times higher than free curcumin in spheroids of size ~195 μm. Increase in uptake of cur-SiNp resulted in enhancement of phototoxicity by ~2.7 times when spheroids were irradiated with blue light. However, phototoxic efficacy of nanoformulated curcumin decreased with increase in size of spheroids (>195 μm). Spheroids treated with nanoformulation and light led to larger inhibition in growth and migration of cells and enhanced reactive oxygen species (ROS) generation as compared to spheroids treated with free curcumin under similar conditions. To further confirm the involvement of ROS in cur-SiNp induced phototoxicity, experiments were carried out in presence of a ROS scavenger, glutathione (GSH). The results showed that irradiation in presence of GSH decreased the phototoxic effects induced by cur-SiNp. This was ascertained by

observation of reduced cell death, reduced inhibition of growth and migration of cells in spheroids and thus confirmed phototoxicity induced by nanoformulation involves ROS.

Chapter 5: In this chapter, results of our investigations on uptake and cytotoxic efficacy of Hyaluronic acid (HA) conjugated SiNp-cur (HA-SiNp-cur) on human colon carcinoma (colo-205) cells are presented. SiNp-cur complex was conjugated with HA as the later has strong affinity for CD44 receptor which is over expressed in cancer cells. Results showed that uptake of curcumin delivered through HA-SiNp-cur was significantly higher in monolayer and spheroid cultures as compared to free curcumin and HA free SiNp-cur. This resulted in higher cytotoxicity. The involvement of receptor in uptake of HA-SiNp-cur by cells was confirmed by observation of reduction in accumulation of curcumin in presence of free HA. Studies carried out on cytotoxicity, showed that cell death, inhibition in growth and migration of cells was higher in spheroids treated with HA-SiNp-cur complex as compared untargeted complex and free curcumin. Experiments done in cell free system showed, a time dependent increase in fluorescence of curcumin in release media when HA-SiNp-cur was incubated with hyaluronidase. This suggests involvement of enzyme in release of curcumin from nanoparticle under intracellular conditions.

Chapter 6: Use of SiNp for targeted delivery of PPa, a potential PS for photodynamic therapy of cancer has been described in this chapter. We investigated the effect of pH on the uptake and photodynamic action of plain SiNp entrapping PPa and its folic acid conjugate in two cell lines squamous cell carcinoma (Nt-8e, oral), and adenocarcinoma of breast (MCF-7) cells as pH of tumor strongly influence the outcome of anticancer drugs by affecting their uptake and as well as the expression of many receptors in cells. Confocal and fluorescence spectroscopic study showed

that while the uptake of untargeted (Np-PPa) was independent of pH of the incubation media for both the cell lines, for FR-Np-PPa, uptake of PPa increased with decrease in pH from 7.4 to 6.5. These studies also showed that in presence of free folic acid, the uptake of FR-Np-PPa was lower than the uptake of Np-PPa. These results suggest that acidic pH influences the level of folate receptor expression and binding of FR-Np-PPa to cells. Phototoxicity for untargeted Np-PPa was independent of pH of the incubation media for both the cell lines and was consistent with uptake studies. For FR targeted SiNp phototoxicity was more at pH 6.5. These results suggest that photodynamic efficacy of FR-targeted nanoformulated PPa is higher under acidic pH.

Chapter 7: To understand the *in vivo* effects of SiNp entrapped with PPa (Np-PPa) and its folic acid conjugate (FR-Np-PPa), biodistribution of Np-PPa and FR-Np-PPa and possible toxicity of these formulations was studied in mice bearing mammary tumors. The results of these studies are presented in this chapter. Biodistribution of different formulations of PPa injected in mice were studied by measuring the fluorescence of PPa extracted from tumor tissue and other organs. Results of this study showed that at 24h, PPa accumulation was ~ 2.2 times and ~1.4 times higher in FR-Np-PPa, Np-PPa than the animals injected with free PPa. Clearance study showed nanoformulated PPa was excreted mainly by hepatobiliary pathway. The possible oxidative stress induced by these particles in liver has also been evaluated by measuring lipid peroxidation and GSH content. The results showed that there was no significant change in oxidative stress markers. Histology of liver and kidney were normal even after 15 days of administrating nanoparticles. This indicated that SiNp did not cause any long term toxicity.

Finally in **Chapter 8** a brief summary of the results obtained are presented along with the possible future research work.

References

[1] Siegel R, Ward E, Brawley O, Jemal A. Cancer statistics, the impact of eliminating socioeconomic and racial disparities on premature cancer deaths. CA Cancer J Clin. 2011; 61: 212-36.

[2] Sharma RA, Gescher AJ, Steward WP. Curcumin: the story so far, Eur J Cancer. 2005; 41: 1955-68

[3] Gupta SC, Patchva S, Koh W, Aggarwal BB. Discovery of curcumin, a component of golden spice, and its miraculous biological activities. Clin Exp Pharmacol Physiol. 2012; 39: 283-99.

[4] Koon H, Leung AW, Yue KK, Mak NK. Photodynamic effect of curcumin on NPC/CNE2 cells. J Environ Pathol Toxicol Oncol. 2006; 125: 205–15.

[5] Ribeiro AP, Pavarina AC, Dovigo LN, Brunetti IL, Bagnato VS, Vergani CE, Costa CA. Phototoxic effect of curcumin on methicillin-resistant Staphylococcus aureus and L929 fibroblasts. Lasers Med Sci 2013; 28: 391–98.

[6] Li L, Ahmed B, Mehta K, Kurzrock R. Liposomal curcumin with and without oxaliplat, effects on cell growth, apoptosis, and angiogenesis in colorectal cancer. Mol Cancer Ther 2007; 6: 1276–82.

[7] Bisht S, Feldmann G, Soni S, Ravi R, Karikar C, Maitra A, Maitra A. Polymeric nanoparticle-encapsulated curcumin (“nanocurcumin”): a novel strategy for human cancer therapy J Nanobiotechnol, 2007; 5: 1–18.

[8] Ohulchanskyy TY, Roy I, Goswami LN, Chen Y, Bergey EJ, Pandey RK, Oseroff AR, Prasad PN. Organically modified silica nanoparticles with covalently incorporated photosensitizer for photodynamic therapy of cancer. Nano Lett. 2007; 7: 2835-42.

[9] Triesscheijn M, Baas P, Schellens JH, Stewart FA. Photodynamic therapy in oncology. Oncologist. 2006; 11: 1034-44.

[10] Stamati I, Kuimova MK, Lion M, Yahioglu G, Phillips D, Deonarain MP. Novel photosensitisers derived from pyropheophorbide-a: uptake by cells and photodynamic efficiency in vitro photochemistry. Photochem Photobiol Sci. 2010; 9: 1033-41.

LIST OF SCHEMES

Scheme No. **Page No.**

LIST OF TABLES

Table No. **Page No.**

LIST OF FIGURES

Figure No. **Page No.**

LIST OF ABBREVIATIONS

µl	Microliter
µM	Micromolar
APTES	3-aminopropyl-triethoxysilane
AFM	Atomic force microscopy
BSA	Bovine Serum Albumin
BCA	Bicinchoninic acid
BuOH	1-Butanol
Chl-a	Chlorophyll- a
CTAB	Cetyltrimethylammonium bromide
Cur	Curcumin
DTNB	(5,5'-dithiobis-(2-nitrobenzoic acid)
DMBA	7,12-Dimethyl- benz (a) anthracene
DMEM	Dulbecco's modified essential Media
DMF	Dimethyl formamide
DMSO	Dimethyl sulfoxide
DLS	Dynamic light scattering
EDTA	Ethylene diamine tetra acetate
EDC	Ethyl-3-(3-dimethylamino) propyl carbodiimide hydrochloride
ELISA	Enzyme-linked immunosorbent assay
ER	Endoplasmic reticulum
ECM	Extracellular matrix

FBS	Foetal bovine serum
FCS	Foetal calf serum
GSH	Reduced glutathione
GSSG	Glutathione disulfide
HA	Hyaluronic acid
H2DCFDA	2, 7'-dichlorodihydrofluorescein diacetate
HEPES	N-2-hydroxyethylpiperazine-N'-2- ethanesulphonic acid
HPPH	2-(1-hexyloxyethyl)-2-devinyl Pyropheophorbide-a
MTT	3(4,5-dimethylthiazol-2-yl)2,5 diphenyltetrazolium bromide
MSNs	Mesoporous silica nanoparticles
NaOH	Sodium Hydroxide
NHS	N-hydroxysuccinimide
NF-kB	Nuclear factor kappa-light-chain-enhancer of activated B cells
NP	Nanoparticle
OSCC	Oral squamous cell carcinoma
ORMOSIL	Organically modified silica nanoparticles
PAGE	Polyacrylamide gel
PBS	Phosphate buffer saline
PDT	Photodynamic therapy

PMT	Photomultiplier tube
PS	Photosensitizer
PI	Propidium Iodide
PPa	Pyropheophorbide-a
RPMI 1640	Roswell Park Memorial Institute media
ROS	Reactive oxygen species
SDS	Sodium dodecyl sulphate
SEM	Standered error of mean
SH	Sulfhydryls
SiNp	Silica nanoparticle
TBARS	Thiobarbituric acid reactive substance
TBS	Tris buffered saline
TCA	Trichloroacetic acid
TEM	Transmission Electron Microscopy
TNF-α	Tumor Necrosis Factor- α
VTMS	Vinyltrimethoxysilane
VTES	Vinyltriethoxysilane
VEGF	Vascular endothelial growth Factor

CHAPTER 1

INTRODUCTION AND REVIEW OF LITERATURE

Cancer remains one of the leading causes of death worldwide. According to data compiled by International Agency for Research on Cancer, a World Health Organization, it was reported that in 2012 there were about 8.2 million cancer deaths, about 14.1 million new cancer cases and 32.6 million people living with cancer worldwide. It was speculated that cancer incidences will rise from 14 million to as many as 22 million in ten years due to the change in life styles and the increase in life expectancy [1]. Cancer prevention and treatment therefore has become one of the most important priorities in public health.

Surgery, radiotherapy and chemotherapy are the standard approaches for cancer treatment. These strategies often fail to improve the survival rates and prevent recurrence of cancer due to several drawbacks. While early stages of cancer can be treated with surgery, for metastatic tumors and tumors located in sensitive regions surgery may not be effective, also surgery may lead to disfigurement especially for oral and mouth related cancers. Radiotherapy and chemotherapy are associated with many side effects as these treatment modalities are not selective. Also, there is always a possibility of recurrence of cancer. Further can cancers can develop resistance to these treatments due to inadequate drug dose or radiation exposure. Investigations have now focused on developing alternate treatment modalities that may be safer and more effective than chemotherapy and radiation therapy. During the last two decades, there has been increased interest in exploring the use of natural herbal compounds for anticancer activities. One such natural product that has attracted immense attention is curcumin which is a hydrophobic polyphenol derived from the herb Curcuma longa commonly called turmeric [2]. Unlike conventional cancer therapeutic drugs, curcumin is capable of targeting cancers via several pathways and also known to have better therapeutic effects alone or in combination with other therapies [3]. However, the usage of this natural polyphenols is limited by poor water solubility.

Another promising approach for cancer treatment is photodynamic therapy (PDT). This approach involves the use of photosensitizers (PS) which preferentially localizes in tumor. Excitation of PS with light (visible) of appropriate wavelength results in the generation of reactive oxygen species (ROS) which kills cancer cells. A major advantage of PDT over conventional chemotherapy is that the PS itself is not toxic in the absence of light and hence PS accumulation in non-specific tissues causes minimum or no systemic toxicity. Furthermore, unlike radiotherapy, the light used for activating the PS is non-ionizing and hence its effect on tissues without the PS is not harmful. Hence, PDT can be repeated with minimal damage to healthy tissue [4] and is a useful approach for treatment of recurrent tumors [5]. Several PSs which have good photosensitizing properties including absorption in the long wavelength region of visible light that penetrate deeper in tissue are hydrophobic in nature. These aggregate in water and therefore their *in vivo* application is limited [6]. Utilization of these requires a suitable delivery system.

1.1. Nanoparticles for cancer therapy

Nanotechnology has attracted lot of attention in cancer therapy. Materials developed at the nanoscale level have been used in drug delivery, diagnostic and medical imaging. Use of nanotechnology based drug delivery systems can overcome many of the limitations associated with chemotherapeutic drugs, PS and natural anticancer agents.

1.2. Advantages offered by nanocarriers

The most unique property of nanocarriers/nanoparticles (Nps) is their size in nanoscale and high surface to volume ratio due to which they have high drug carrying capacity. Use of nanocarriers

can overcome problems associated with solubility and stability of many good anti-cancer drugs and improve their bioavailability. For example, uptake and delivery of poorly soluble drugs may be increased by enveloping the compound in a hydrophilic nanocarrier [7]. Encapsulation of anti-cancer agents into nanocarriers or coupling to polymers may also protect the drugs from enzymatic degradation and rapid elimination of the drug and prolong the circulation time of drugs under *in vivo* conditions. This will facilitate Nps to accumulate preferably at the tumor site as they have leaky intra tumoral blood vessels with gaps between 100 nm and 800 nm of size [8] through phenomenon known as enhanced permeability and retention effect (EPR) [9] or passive targeting. Further, to improve selectivity of anti-tumor drugs, and to overcome the limitation that affect the efficacy of drugs delivered by passive targeting due to heterogeneity of the tumor such as a hypoxic gradient, increased interstitial fluid pressure [10] nanocarriers can also be developed to deliver drugs specifically to tumors which is known as active targeting [11]. Targeted delivery is ensured by attaching a ligand to nanocarrier which has a high affinity to the receptor present on the surface of tumor [12]. A wide range of ligands to receptors over expressed in cancer cells such as growth factors (folate, epidermal growth factor, transferrin), hormones (insulin, HER-2), CD44, low density lipoproteins have been used for such purposes. The ligands include small molecules, carbohydrates or macromolecules such as peptides, antibodies [13]. Nanocarriers can also be designed to release drugs loaded in them in response to stimuli for enhancing the therapeutic efficacy of drugs [14, 15]. For example, drugs whose delivery is not pH-dependent, such as doxorubicin, can be conjugated with a pH sensitive Np carrier to increase cellular drug uptake and intracellular delivery [16]. Another important feature is nanocarrier mediated drug uptake may decrease resistance of tumors against anti-cancer drugs as they are internalized by

cells through endocytotic pathway. This uptake pathway avoids nonspecific uptake by multidrug resistant / ATP pump driven drug elimination [17].

1.3. Nanoparticles used for drug delivery

Depending on composition, Nps can be divided into lipid-based vehicles (liposomes, solid lipid Nps and micelles), polymer carriers (hydrogel Nps, dendrimers), protein based, metallic Nps (gold, iron), and inorganic Nps (silica-based).

1.3.1. Lipid based carriers

Liposomes are lipid based Nps which have spherical structure and made up of one or several lipid bilayer, with hollow aqueous core. These are amphiphilic in nature have hydrophilic head and hydrophobic tail. They have attracted attention as drug delivery systems because they can encapsulate both hydrophilic and/or lipophilic drugs, also they are biodegradable and non immunogenic [18, 19]. They are internalized in cells either by adsorption or by endocytosis [20, 21]. Hydrophobic drugs can be incorporated into liposomes with 100% trapping efficiencies**.** Some of the lipid carriers approved by the US Food and Drug Administration (FDA) in 1995 for clinical use are liposomal doxorubicin (Doxil® or Caelyx®), non-pegylated liposomal doxorubicin (Myocet®), non-pegylated liposomal daunorubicin (DaunoXome®), non-pegylated liposomal cytarabine (DepoCyt®), vincristine sulfate liposomes (Marqibo®), and liposomal mifamurtide (Mepact®) [22]. The problems encountered with liposomes are, they are poorly soluble in water, stability is low, they are prone to oxidative degradation and also they are rapidly cleared from the body due to capture by reticuloendothelial system (RES) [23, 24].

Functionalization with biopolymer such as polyethylene glycol (PEG) can delay hydrolysis and improve their stability and circulation time. However, use of PEG can hinder the binding of the liposome to the target site [25].

Solid Lipid Nanoparticles (SLN) are alternative to liposomes. They are made up of lipids which are solid at both room and body temperatures [26]. Drugs in SLN are stable and their release occurs in controlled manner, both lipophilic and hydrophilic drugs can be incorporated in them, and the toxicity of SLN is minimal. The disadvantage of SLN is that the drugs are expulsed from the carrier during storage owing to transformations.

Micelles are another lipid based drug delivery systems which have attracted significant interest. These are formed by self-assembly of amphiphilic copolymer. Use of micelles improves solubility of hydrophobic drugs, circulation time via evading recognition by RES and passive targeting ability of tumor tissues by the EPR effect [27, 28]. One of the significant disadvantages of normal self-assembled polymeric micelles is that micelles are not stable and they may dissociate upon dilution [29].

1.3.2. Polymeric nanoparticles

Polymeric Nps are submicron sized (< 1µm) colloidal systems, made up of biodegradable or non-biodegradable polymers. The most common biodegradable polymers used include Poly(Lactide-co-Glycolide) (PLGA), chitosan, poly-alkyl-cyanoacrylates (PACA), polylactic acid (PLA) and polycaprolactone.

Chitosan is a modified natural carbohydrate made up of biopolymer chitin after partial N-deacetylation. Several drug molecules incorporated in these have been tested under *in vivo*

condition. Their clinical application is limited because of poor reproducibility and stability. These are also prone to contamination by microbes [30].

PLGA based Nps are more biocompatible and biodegradable, easily undergoes hydrolysis in the body than other polymers. PLGA nanoparticles protect poorly soluble and unstable drugs. Surface of the PLGA Np can be modified for specifically to target the cancer cells [31]. Many of the chemotherapeutic drugs (cisplatin, dexamethasone, 9-nitrocamptothecin, DOX (Doxorubicin), 5-FU (5-fluorouracil), PTX (paclitaxel), triptorelin and curcumin have been successfully encapsulated in PLGA [30]. Their degradation products such as glycolic acid and lactic acid, cause minimal systemic toxicity.

Another polymer which is used for drug delivery is PLA. This is also biodegradable polymer, degrades to monomeric lactic acid after hydrolysis under physiological conditions and does not show any systemic toxicity. However, their clinical application is limited by its poor aqueous solubility and low therapeutic effectiveness [32, 33]. PCL is another polymer which has gained attention for use in drug delivery. It undergoes slower degradation than PLA and can incorporate drugs such as vinblastine, tamoxifen, docetaxel and PTX [34].

1.3.3. Protein based nanoparticles

Human and bovine albumins are most widely used proteins for the production of Nps. [35]. Albumin is non-toxic, non-immunogenic, biocompatible, biodegradable and easily metabolizable under *in vivo* [36, 37]. Further, amine and carboxylic groups present on surface of albumin particles can be used for covalent modification and attachment of drugs or other proteins [38]. Abraxane®, albumin-PTX is the first water-soluble Nps which were approved by the FDA for

the treatment of cancer (metastatic breast) all over the world [35]. This nanocarrier is safe, have good efficacy and significantly higher response rates compared with standard PTX (33% vs. 19%). Since it is a protein based Np, it is prone to contamination by microbes.

1.3.4. Dendrimers

Dendrimers are highly branched macro molecules. The core of the dendrimers is symmetric. These have three dimensional spherical morphology with multiple targeting sites. Dendrimers which have functional groups can selectively bind drug molecules and deliver them to the target sites [39, 40]. For example, polyamidoamine dendrimers is the most common type of dendrimer which can selectively host chemotherapeutic drug like methotrexate [41]. However, the main concern in use of dendrimers is that undegraded Np produces lot of side effects [39, 42] therefore it is less biocompatible than other biopolymers [23]. Chemical compositions of dendrimers need to be modified to prevent their accumulation in the liver and also to inhibit its nonspecific toxicity.

1.3.5. Metallic nanoparticles

Gold and iron oxide Nps are widely investigated for cancer therapy as well as in diagnosis. These Nps are used mostly with combination of other biomolecules [43]. The advantage of using gold Np is that they release drugs in controlled manner upon absorption of heat on exposure to NIR. Iron oxide Nps release drugs in controlled manner under influence of an external magnetic field. For gold Nps, the cost is the main concern, also accumulation of the particles within the bloodstream can hinder the blood flow and excretion of gold Nps is also not well understood [44].

1.4. Silica nanoparticles

Among the inorganic Nps, Silica Nps have gained lot of attention for tumor imaging and therapy [45, 46]. Since these Nps are inert and have hydrophilic properties, they are useful carriers for bioimaging as well as for therapeutic applications. Compared to other metal oxides such as titania and iron oxide, silica has better biocompatibility. These particles can be taken up by cells due to presence of silanol groups (Si-O-H) which have good affinity to phospholipids. Si-O bonds present in the silica Nps can overcome mechanical stress and degradation and are more stable compared to liposomes and dendrimers [47]. Additionally, these Nps can be synthesized in large scale at low cost. Ultra small nonporous silica Np has been approved by US (FDA) for clinical trial of molecular imaging of cancer [48].

Silica Nps used for drug delivery can be classified as nonporous or mesoporous silica nanoparticles (MSNs). Nonporous silica Nps are solid and drugs are conjugated to these Nps. MSNs have a porous structure with pores size ranging from 2–10 nm , large pore volume (> 0.9 cm^3/g) and high surface area (> 900 m^2/g), due to which their drug loading capacity is high. By modifying the environment of pores drug loading can be enhanced and the surface of particles can be functionalized for targeted delivery [49]. The most notable property of MSNs is their controlled drug release. Drugs can be carried to targeted cells or tissues precisely without leaching by blocking the pore entrances with caps or stimuli responsive agents. In addition, silica Nps are hydrophilic, also they do not show any swelling or porosity changes with changes in pH which is very important for *in vivo* application [50-52]. These Nps are also resistant to microbial attack and have long storage life.

1.4.1. Preparation of MSNs

MSN's are synthesized by Stober or micro-emulsion method using silica precursors. In Stober method, silica precursors (eg. tetraethyl orthosilicate) undergo hydrolysis and condensation in a micellar solution in the presence of catalyst such as ammonium hydroxide at ambient temperature. Precursor polymerizes around the micelles which act as a template. Porous structure is formed after the removal of micelles. Any dye/drug molecules can be either covalently attached or encapsulated in these Nps formed [53]. The density, pore size, structure of the silica matrix and size of particles can be varied by changing concentration of precursors [54]. MSNs can also be prepared by direct microemulsion (oil in water) or reverse microemulsion (water in oil) method, which uses surfactants. Reverse microemulsion gives smaller Nps [55, 56]. MSNs can be prepared using hybrid materials like organotrialkoxysilanes or organotrichlorosilanes that possess specific functions for drug delivery, or organosilanes are condensed along with the silica precursors in the presence of surfactant templates [55-59].

1.4.2. Release of drugs from MSNs

Release of drugs loaded in MSNs can be controlled by various stimuli such as organic molecules, pH, temperature and light [60]. Gold, quantum dots and iron oxide Nps have also been investigated as gate keepers and release drugs in controlled manner. Advantage of stimuli-responsive drug delivery systems is that drugs incorporated in MSNs can be delivered specifically to cancer cells and tissues under both *in vitro* and *in vivo* conditions. For example, pores in the MSN encapsulated with drug molecules have been capped using cadmium sulfide to physically block the drugs loaded in MSNs from leaching out [61]. Drug loaded MSNs have been coated with polymers which release drugs in response to proteases present in tumor cells

[62]. Self-complementary duplex DNA has been used as the gatekeeper to control the release of drugs. Studies have shown that the drugs entrapped in MSNs whose surfaces are modified using self-complementary duplex DNA can induce release of drugs, when DNA is denatured by heating or hydrolyzed by endonucleases in cancer cells [63]. pH can also be used as another triggering factor for drug release from MSNs for tumor therapy. Meng et al [64] developed pH responsive β-cyclodextrin coated MSNs for DOX delivery into cancer cells. Their studies showed that under acidic condition, DOX in the MSNs could be released into nuclei of cancer cells.

Redox potential is another accepted stimulus for triggering drug release. Nps linked to disulfide have been designed to trigger the release of drugs by GSH which is 4-fold higher in tumor cells [65]. Lin et al developed a redox-responsive nanoparticle in which MSNs and the CdS Nps joined by disulfide linkages, could be cleaved by GSH leading to the subsequent drug release from the MSNs [61]. Light is also used as stimuli to release drugs from MSNs. It has been shown that when thymine coated MSNs are exposed to 365 nm UV light, cyclobutane dimers are formed in the pore entrances which blocks the pores. When these Nps are exposed to 240 nm UV light, cyclobutane dimmers are cleaved and drug is released. The advantage of this MSN is drug release occurs at specified location [66].

1.4.3. Uptake of MSNs by cells

Cellular uptake and subcellular distribution of MSN is dependent on its size, surface charge and targeting moiety. Studies have shown that Nps of size between 50-200 nm is efficiently taken up by non-phagocytic cells, whereas large particles of size > 300 nm are easily captured by

phagocytotic cells [67, 68]. Surface property of MSNs is another important parameter which influences cellular uptake. It has been shown that as compared to negatively charged Nps, the uptake of positively charged MSNs is better due to electrostatic interaction with negatively charged surfaces of cells [69].

Studies have shown that uptake of MSNs occurs through endocytosis and efficient uptake of these particles has been demonstrated in several cancer cells such as ovarian, HeLa, as well as normal cells CHO, PANC-1, macrophages, stem cells such as 3TL3, mesenchymal [49, 70]. Mechanisms of endocytosis may involve either clathrin or caveolae mediated pathway. Pathway followed depends on cell type and particle size. A study carried out in human ovarian cancer cells has shown that MSNs of sizes 10 nm and 50 nm are internalized in the lysosomes via caveolae-mediated endocytosis. While, 10 nm Nps was shown to get relocated to cytoplasm with increase in time, 50 nm Nps were permanently retained within these organelles [70]. In another study, it has been shown that MSNs of size ~110 nm were internalized by clathrin dependent endocytosis in human mesenchymal stem cells [71].

Cellular uptake of Nps can be enhanced by attaching a ligand which binds specifically to membrane bound receptors. Studies have shown that when chemotherapeutic drug or PS loaded MSNs are conjugated with ligands like folic acid, HA, their uptake efficacy increases remarkably in cells which over express receptors for folic and CD44 [72, 73]. It has also been demonstrated that in addition to targeting, both folic acid and HA anchored to the pore outlets act as capping agents thus eliminate premature drug leakage and release drugs only within the cytoplasm of targeted cells [74].

1.4.4. Biocompatibility of MSNs

The biocompatibility of MSN with and without surface functionalization has been evaluated in different cells. It has been shown that viability, proliferation of cells is not affected if MSN concentrations is below 100 μg/mL and in cells treated with MSNs, morphology, membrane integrity and mitochondrial activity is conserved and the growth rate of MSN internalized cells are similar to the cells not treated with MSNs [49].

1.4.5. Drug delivery applications

1.4.5.1. Chemotherapeutic drugs

Studies have shown that MSNs are good carriers for many chemotherapeutic drugs. Drugs such as paclitaxel, camptothecin (CPT), doxorubicin, methotrexate, colchicine including curcumin have been successfully loaded in MSNs or covalently conjugated to MSN [75, 76]. Efficacy of MSN loaded CPT has been tested under *in vitro* as well as *in vivo* conditions and therapeutic efficiency of MSNs/CPT tested in nude mice having xenografts of human breast cancer cell (MCF7) is reported to be higher than animals treated with CPT alone group [77, 78]. In another study, it was reported that killing efficacy of doxorubicin delivered by TAT peptide-modified MSNs was enhanced than drug delivered by unmodified MSN [79].

1.4.5.2. Photosensitizers

MSNs have been encapsulated with hydrophobic PS like protoporphyrin IX (PpIX), hypocrellin B, silica phthalocyanine. The photodynamic efficacy of these PS has been demonstrated to be

better than the free drugs [80-82]. Lipid, poly (ethylene glycol) (PEG) and polyethylenimine (PEI), galactose coated and DNA capped MSN's loaded with PS have been prepared for targeted release [75, 83-85]. To improve the penetration depth of visible light required for PS activation, PS loaded MSNs have been coated with up conversion fluorescent Nps. These particles have shown improved phototoxicity both under *in vitro* and *in vivo* conditions [86].

1.5. Organically modified silica (ORMOSIL) nanoparticles

ORMOSIL nanoparticles (SiNp) are another silica based mesoporus Nps which have gained importance as agents for delivery of genes, peptides and PS for PDT [45]. SiNp are prepared using organosilanes precursors such as methyltrimethoxysilane, phenyltrimethoxysilane, 3-aminopropyltriethoxysilane, triethoxyvinylsilane [87]. Due to presence of high density of organic groups in SiNps, hydrophobic drugs can be incorporated in them effectively. SiNp can be synthesized by the alkaline condensation and polymerization of organosilane precursors within the microemulsion of oil-in-water (normal) or water-in-oil (reverse) phase [88]. These methods do not require any complex purification steps such as ultracentrifugation, solvent evaporation or use of any corrosive solvent like cyclohexane. The presence of both hydrophobic and hydrophilic groups on the organosilane precursor helps them to self-assemble as normal micelles or reverse micelles under appropriate conditions.

The presence of the organic group imparts flexibility and silica matrix provides rigidity and enhances the stability by preventing precipitation in aqueous conditions. The biomolecules like proteins as well as drugs can be entrapped in micellar (and reverse micellar) cores [89, 90]. They can also be loaded with either hydrophilic or hydrophobic drugs/dyes after the Np preparation or conjugated through surface functionalization. Their organic groups can be modified further by

attaching targeting molecules [89]. Like MSNs, these Nps are resistant to pH, do not shows any swelling or porosity changes, their sizes can be tuned by varying precursor and surfactant concentrations [88].

1.5.1. Applications of ORMOSIL

1.5.1.1. Photodynamic therapy

SiNps are widely explored as carriers for PS used in therapy as well as in photodiagnosis of cancer. For these applications, the PS can be either entrapped in them or conjugated to surface functionalized groups of Np. Advantage of using SiNp for PDT compared to other carriers is that these are light transparent. Therefore, PS need not be released from the Nps at the tumor site before light exposure for initiating photochemical reactions. Roy et al [88] were the first to demonstrate the efficacy of SiNp for PDT use. They synthesized SiNp of diameter ~ 30 nm, entrapped with water insoluble PS, 2-devinyl-2-(1-hexyloxyethyl) pyropheophorbide (HPPH), using triethoxyvinylsilane as precursors. These Nps were stable in aqueous conditions. Drug entrapped Nps on exposure to light, generated $^1O_2$ which diffused through the porous matrix. Their studies also showed that HPPH doped SiNp were taken by tumor cells efficiently and were more phototoxic compared to free PS [88]. Subsequently, Qian et al. [80] prepared SiNp encapsulating protoporphyrin IX following Prasad's method and demonstrated their improved photodynamic efficacy in HeLa cells. In another study, it was reported that photodynamic efficacy of hydrophobic silicon phthalocyanine (Pc4) improved significantly when it was entrapped in SiNp as compared to free drug [91]. This study also showed that localization and mechanism of cell death induced by Pc4-SiNp was different as compared to free Pc4. A study carried out by Reddi et al [92] showed that SiNp was more stable in presence of FBS (3%), in

aqueous media with high salt concentrations SiNp underwent aggregation and precipitation. In another study, it was shown that uptake of meta-tetra (hydroxyphenyl) chlorine (mTHPC), a hydrophobic PS formulated in SiNp reduced by about 50% in human esophageal cancer cells in comparison to standard solvent. However, photokilling activity of mTHPC in both the formulation was similar. In this study, it was also demonstrated by using fluorescence resonance energy transfer approach, mTHPC is transferred from the SiNp to serum proteins in the medium. By coating the surfaces of Nps doped with PS with poly (ethylene glycol) the transfer of PS to proteins could be prevented [92].

It is also been reported that the $^1O_2$ generation efficacy of HPPH doped SiNp enhanced considerably when heavy atom like iodine was conjugated to SiNp as compared to non iodinated Nps. The enhanced efficacy was attributed due to increase in rate of intersystem crossing of HPPH which increased its triplet yield. Phototoxic efficacy of these iodinated nanoformulation tested in cancer cells was indeed higher than the non iodinated nanoformulation [93]. To overcome the possibility of premature release of the physically entrapped PS during systemic circulation, PSs have been covalently conjugated to SiNp. It has been shown that iodobenzyl pyropheophorbide covalently conjugated to SiNp retains its photophysical and photochemical properties and also exhibit efficient phototoxicity in tumor cells [87]. Phototoxic effects of Rose Bengal, an anionic PS conjugated to SiNp either by covalent or electrostatic interaction have also studied in oral (4451) and breast (MCF-7) cancer cell lines. This study shows that both complexes are more phototoxic than free Rose Bengal. Observed enhancement in phototoxicity of complexes is reported to be due to increased uptake, enhanced photo stability of Rose Bengal and $^1O_2$ generation [94].

1.5.1.2. Bioimaging

Since SiNp is optically transparent, it can be loaded with fluorophores of interest and used for bioimaging studies. It has been shown that SiNp encapsulating Nile red, conjugated with biomolecules like folic acid or apotrasferrin selectively bind to cancer cells which over express folate and transferrin receptors [95]. For improving bioimaging efficacies, SiNp have been doped with two photon absorbing PS/fluorophore. These can be excited using near infrared wavelength of light which penetrate deeper than visible light in the tissue. Kim et al [93] encapsulated a, HPPH, and a fluorescent two-photon absorbing dye, 9,10-bis [4'-(4''-aminostyryl)styryl]-anthracenein (BDSA) in SiNp (≤30 nm) for two-photon PDT. Their studies showed BDSA aggregates in SiNp matrix, up converted the energy of near infrared light and transferred it to the co-encapsulated HPPH molecules. This resulted in enhanced two photon generation of $^1O_2$ in water. They also demonstrated the photodynamic efficacy of co-encapsulating Nps in tumor cells and their potential for two photon PDT applications. Use of PpIX doped SiNps for two photon fluorescence imaging and PDT of tumor cells were also demonstrated by Qian et al 2012 [96]. They also showed the use of PEG modified IR-820 doped SiNps for *in vivo* brain imaging in mice. This study showed that NIR fluorescence signal could be detected at 4 mm depth in animals injected with IR-820 doped SiNps which is useful for noninvasive detection of metastatic cancer cells localized through lymphatic drainage from a primary tumor. This study showed that intravenously injected NIR Nps selectively accumulated in subcutaneously xenografted tumor of a mouse through EPR [96]. SiNp have also been demonstrated to be ideal nanocarriers for multimodal imaging probes such as magnetic resonance imaging and positron emission tomography [97].

1.5.1.3. Gene delivery

Gene delivery is another major application of SiNp besides the delivery of PS and fluorophores. The use of silica Nps for gene delivery has been extensively explored because silica is biocompatible and less toxic than commonly used cationic polymers for gene delivery, and more stable than liposomes. Also negatively charged nucleotides can be conjugated to silica Nps easily by modifying their surfaces with cationic molecules [98]. It has been shown that DNA binds efficiently to SiNp through their surface functionalized amino groups. DNA bound to Nps has been shown to evade DNAse digestion. Cellular studies showed that these Nps could deliver DNA to the nucleus efficiently after it was uptaken by cells and expression of GFP provided evidence for efficient transfection induced by pEGFP plasmid delivered through these Nps [99]. *In vivo* efficacy of gene delivery using these particles was also demonstrated by Bharali et al by injections of Nps complexed with plasmid DNA encoding for EGFP in mice brain. Transfection of neuronal like cells in substantia nigra and the lateral ventricle regions of brain were confirmed by observing GFP fluorescence. It was observed that transfection efficiency of plasmid delivered via Np was comparable to that of using a viral vector. This study also showed that SiNp did not cause any toxicity [100]. It has been demonstrated that SiNp mediated transfection can be used to manipulate the biology of neural stem or progenitor cells as well as studying the poly Q peptides induced neuronal disorders in mice model [100, 101]. These studies suggest that SiNp could be a promising carrier for targeted gene delivery for brain disease.

1.5.2. Toxicity and biosafety

Toxicity and biosafety are important for successful translation of preclinical to clinical studies.

Although SiNp is biocompatible, there is some concern about toxicity [102, 103]. In a recent study, it was reported that toxicity of SiNp was found to depend on cell type [104]. While PEG coated SiNp did not induce any toxicity in normal fibroblasts and non small cell lung adenocarcinoma cells, for A549 carcinoma cells of Alveolar type II these particles were toxic in the concentration range 0.3-0.5 mg/ml. Studies also indicate that size, shape, surface properties, aggregation behaviors of silica Np in cellular environment and body fluids influence toxicity [105, 106]. The precise role of these factors influencing toxicity is still lacking. However, *in vivo* studies carried by using SiNp are encouraging. The study carried out by Kumar et al, 2010 [107] on biodistribution of the SiNp conjugated with the NIR fluorophore DY776 and SiNp conjugated with radioactive Iodine in mice model has shown that although SiNp accumulates in the RES, these Nps do not induce any toxicity to the organs of the RES system and are excreted from this with time [107]. Effect of SiNp on development of Drosophila larvae has also been studied. This study showed that feeding of SiNp to Drosophila larvae at concentration 0.2 to 1 mg/ml did not induce any adverse effect on locomotion or survival of larvae. Although these Nps penetrated brain and did not cause any developmental defects. These studies show that silica based Nps are biocompatible and not toxic to whole organisms, and has potential for the development of long term applications [108].

1.6. Curcumin

Curcumin (diferuloylmethane; (1E, 6E)-1,7-bis(4-hydroxy-3-methoxyphenyl)-1,6-heptadiene-3,5-dione (IUPAC); C21H20O6) is a hydrophobic polyphenol derived from Curcuma longa (turmeric), a rhizomatous plant belonging to the ginger family. Dried turmeric powder is used as spice in India and other Asian countries. Turmeric powder has several curcuminoids that include

curcumin (77%), demethoxycurcumin (17%), and bisdemethoxycurcumin (3%). Curcumin is the most active constituent of turmeric and comprises approximately 2-5% of turmeric; it is responsible for the yellow color of the spice. Majority of turmeric's therapeutic effects are due to curcumin and this is accepted as safe by the Food and Drug Administration [109].

1.6.1. Background of Curcumin

Vogel and Pelletier discovered curcumin from the rhizomes of C. longa about two centuries ago. They first extracted curcumin in impure form in 1815 and it was purified in 1842. The chemical structure of curcumin was reported by Milobedzka in 1910. However, the biological properties of curcumin were studied systematically only in the mid-twentieth century [110].

1.6.2. Physicochemical Properties

The chemical structure of curcumin is shown in Figure 1.1. Curcumin is a diferuloylmethane and it has two methoxyl groups, two phenolic hydroxyl groups and a beta-diketone moiety. Curcumin exhibits keto-enol tautomerism, having a predominant keto form in acidic and neutral solutions and a stable enol form in alkaline media [111]. Curcumin is poorly soluble in water at neutral pH but has good solubility in polar solvents like dimethyl sulfoxide (DMSO), ethanol, methanol, acetonitrile, chloroform and ethyl acetate. In methanol, its molar extinction coefficient is ~ 48000 $M^{-1}cm^{-1}$ at 428 nm [112].

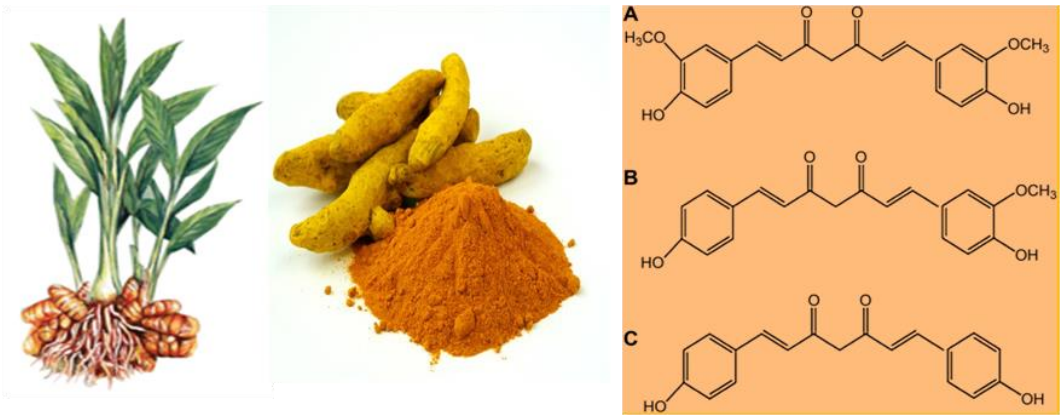

Figure 1.1: Turmeric and chemical structure of different components of curcuminoids (A) curcumin, (B) demethoxycurcumin and (C) bisdemethoxycurcumin.

1.6.3. Therapeutic potential of curcumin

Curcumin is extensively used in Ayurveda for the management of various diseases. Curcumin exhibits a wide range of pharmacological activities against many diseases (Figure 1.2). It has been shown that curcumin is effective against many chronic diseases including type II diabetes, rheumatoid arthritis, multiple sclerosis, atherosclerosis and prevent Alzheimer's disease by suppressing the amyloid-induced inflammation and has also shown protection against liver injury, cataract formation, pulmonary toxicity and fibrosis [113-115]. It is also a good wound healing agent, has been used for treating various skin disorders. Curcumin has also shown to inhibit human immunodeficiency virus replication, platelet aggregation, suppression of thrombosis and also has good antimicrobial, anti-malarial activities [116-118]. Anti-cancer activity of curcumin (Figure 1.3) has been extensively investigated and has been suggested a potential anticancer agent for both prevention and treatment of different cancers, including

gastrointestinal, melanoma, genitourinary, breast, lung, hematological, head and neck, neurological and sarcoma [119, 120]. Additionaly, it has been shown to possess chemotherapeutic as well as photosensitiztion activities [120-123] and improves the efficacy of conventional chemotherapeutic drugs when used synergistically.

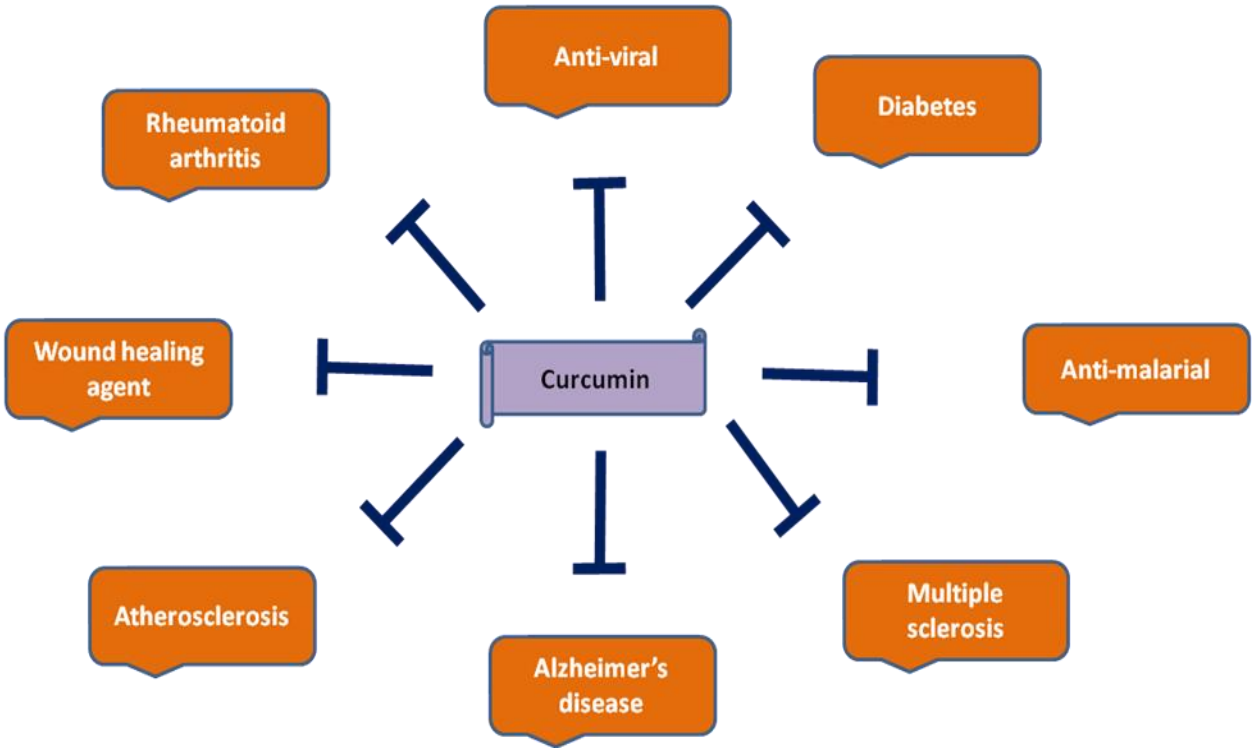

Figure 1.2: Pharmacological activities of curcumin on different diseases.

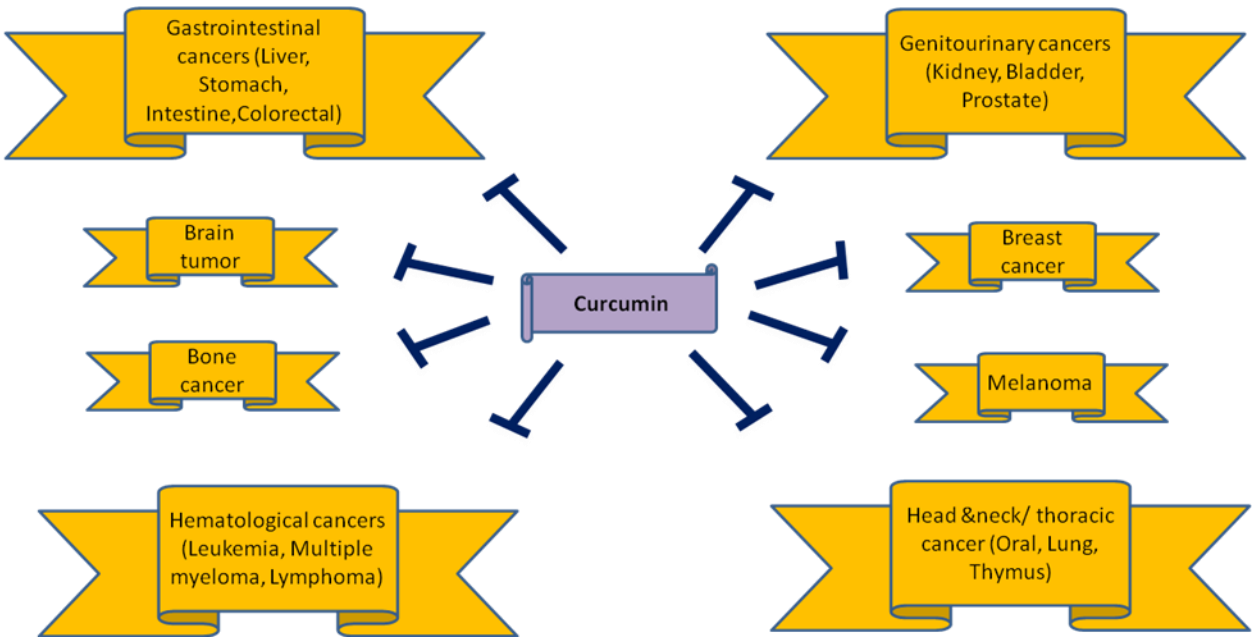

Figure 1.3: Anti-cancer activities of curcumin.

1.6.4. Molecular targets of curcumin for anticancer activity

Curcumin modulates growth of tumor cells through regulation of multiple cell signaling pathways including cell proliferation (cyclin D1 which is deregulated in a wide variety of tumors, c-myc). It also induces apoptosis by modulating several pro-inflammatory cytokines like tumor necrosis factor-α (TNF-α), interleukin (IL)-1, IL-1b, IL-12, and interferon (INF)-g, growth factors (epidermal growth factor, hepatic growth factor and platelet-derived growth factor, human epidermal growth factor receptor (HER)-2, IL-8R and Fas-R), transcription factors (signal transducer and activator of transcription (STAT) 3, nuclear factor (NF)-kB, Wilms' tumor (WT-1) and peroxisome proliferator-activated receptor and protein kinases (e.g. extracellular signal-regulated kinases, mitogen-activated protein kinases, protein kinase A, B and C) [124-

128]. It modulates the expression of early growth response protein 1 (Egr-1), β-catenin, and Nrf-2. It also inhibits cyclooxygenase 2 (COX-2), genes involved in metastasis (matrix metalloproteinase (MMP-9) and angiogenesis and the adhesion molecules [128]. Studies have shown that curcumin inhibits various pathways such as cell survival (Bcl-2, Bcl-xL, cFLIP, XIAP, c-IAP), caspase activation (caspase-8, 3, 9), tumor suppressor (p53, p21), death receptor (DR4, DR5), mitochondrial, and protein kinase (JNK, Akt, and AMPK) pathways [119]. Because of this multi-targeted nature, curcumin has a wide range of actions and therefore better than conventional therapeutic drugs which have only one target and are removed from cells if they do not bind the right target [129].

1.6.5. Curcumin bioavailability

The pharmacological studies done in animals and humans have shown that curcumin is safe and causes negligible systemic toxicity even after administration of high doses orally. Studies carried out in human healthy subjects administered with oral dose of curcumin ranging from 500 to 12000 mg as well as cancer patients taking oral curcumin (500 to 8000 mg/day) for three months did not show any adverse effects [130, 131]. Despite curcumin's superior properties as an anti-cancer agent and safety, its therapeutic applications are limited which is due to its low aqueous solubility (only 0.6 mg/ml), high susceptibility to degradation particularly under alkaline conditions [132-134]. In addition, bioavailability of curcumin within the body is very less because of its poor absorption and it gets metabolized in the liver fast and is eliminated from the body rapidly. These effects are confirmed from many studies carried out in animals and humans. For instance, in a study carried out in rats when 10 mg/kg of curcumin was intravenously injected, a maximum serum concentration was found to be 0.36 ± 0.05 mg/ml, whereas 500

mg/kg of orally administered curcumin gave a maximum plasma concentration of 0.06 ± 0.01 mg/ml, indicating that oral bioavailability was only 1% [135]. In an another study, when curcumin was given orally at a dose of 2 g/kg to rats, a maximum serum concentration of 1.35±0.23 μg/ml was observed after 0.83 h, whereas in humans the same dose of curcumin resulted in either undetectable or extremely low (0.006±0.005 μg/ml at 1 hour) serum levels [136]. Similarly, studies carried in a rat model it was demonstrated that when 1 g/kg of curcumin was orally administered more than 75% was excreted in feces due to its rapid intestinal and hepatic metabolism and negligible amount of curcumin was detected in urine [137]. In another pharmacokinetic study carried out in healthy humans showed presence of only 1.73 ± 0.19 and 2.30 ± 0.26 μg/ml of curcumin in serum even after administration of 10 and 20 g curcumin orally. This suggested that curcumin undergoes extensive metabolic changes in the intestine and liver [138]. Additionally, a clinical study carried out in 15 patients with colorectal cancer showed that administration of 3.6 g of curcumin for 4 months did not show any favorable response [139]. All these studies indicate that concentration of curcumin at the tumor site is insufficient for exhibiting anti-cancer effects.

1.6.6. Formulation for curcumin delivery

For overcoming low bioavailability problems of curcumin several approaches are being explored such as modulation of route of administration, blocking of metabolic pathways, co administration of curcumin with other agents (use of black pepper alkaloid - piperine for inhibition for curcumin metabolism) [136, 140]. Another strategy is the conjugation or structural modifications of curcumin with amino acids or polymers. Some of the conjugates of curcumin and their stability are shown in Table 1.1.

Conjugates of curcumin	Efficacy
Proline, glycine, leucine, isoleucine, alanine, phenylalanine, phenyl glycine, valine, serine and cysteine were coupled to curcumin	Conjugation increased curcumin aqueous solubility 1to10 mg/ml [141]
Conjugation of hyaluronic acid (high molecular weight: polymer) and curcumin	Curcumin in conjugate was intact (90%) in aqueous solution at pH 7.4 for 8h whereas free curcumin showed 60% degradation within 25 min [142]
Curcumin-oligo (ethylene glycol) conjugate	Conjugate showed high loading content (25.3 wt %) and cytotoxic efficacy of conjugate was high [143]

Table 1.1: Conjugates of curcumin and their stability.

1.6.7. Nanotechnology approaches for curcumin

Nanotechnology based drug delivery systems (nanocarriers, nanoparticles) have shown good potential for improving bioavailability of curcumin as these delivery vehicles possess several attractive features: improved encapsulation or solubilization, protect curcumin from degradation, also delivery of curcumin can be targeted by using ligands which bind specifically to receptors on cancer cells and therefore expected to have superior pharmacokinetics under *in vivo* conditions.

1.6.8. Curcumin nanoformulations

Liposomes, polymeric Nps, micelles, nanogels, cyclodextrins, dendrimers and solid lipids have been shown to enhance solubility, stability of curcumin by preventing hydrolysis and also improve its bioavailability by increasing circulation, permeability, and stronger resistance to

metabolic processes and targeted delivery. However, the amount of curcumin encapsulated, size of particle and the amount of curcumin released in its active form for the therapeutic effect depends on nature of Nps. *In vitro* cytotoxicity and *in vivo* stability of different curcumin nanoformulations are shown in Table 1.2 and 1.3.

1.6.8.1. *In vitro* cytotoxicity of different curcumin nanoformulation

Curcumin Nanoformulations	***In Vitro* Cytotoxicity**	**Molecular Mechanism**
β-cyclodextrin self-assembly	Significant enhancement in uptake and cytotoxicity of self-assemblies compared to free curcumin (Inhibitory concentration (IC_{50}) was 17.6 μM and16.8 μM for DU145 cells and C4-2 cells)	Increased cleaved poly ADP ribose polymerase (PARP) expression [144]
poly(butyl cyanoacrylate) nanoparticles	IC $_{50}$(~15 μg/mL) for Huh7 cells, and HepG2 was less compared to free curcumin	Down regulation of VEGF and COX-2 expression [145]
Thermo-sensitive nanocarrier	Shows better selectivity compared to free curcumin. Cytotoxicity is high for cancer cells (KB, MCF-7, and PC-3) and non toxic to normal cell line (L929).	Loss of mitochondrial membrane potential and increased apoptosis [146]
Dendrosome	2-fold reduction of IC_{50} value for A431 and in WEHI-164 cancer cells (14.3 and 7.5 μM) after 48 h.	Higher PARP, increased apoptosis [147]

PLGA (Single-emulsion/solvent-evaporation method)	Cytotoxicity of PLGA nanoparticle was comparable to free curcumin against A549 cells, SKBr3 and HeLa cells	Down regulation of NF-κB, increased annexin V staining PARP induced apoptosis [148]
PLGA (Nanoprecipitation method)	IC_{50} for PLGA curcumin nanoparticles was less than free curcumin in breast (MDA-MB-231), prostate (DU145), esophageal (SEG-1) and colon (HCT116) cancer cells	Downregulation of cyclin D1, NF-κB, MMP-9, VEGF Expression [149]
NanoCurc™	IC_{50} ranged between 10–15 μM for ASPC-1, BxPC3, XPA-1 and PL-11 cell lines, 0.5% of the injected nanoparticle was localized in the brain	Downregulation of of NF-κB and multiple pro-inflammatory cytokines [150]
Amphiphilic mPEG-palmitic acid Polymer	Cytotoxicity of nanoformulation was comparable to free curcumin in HeLa cells	Drug release catalyzed by lipase enzyme enhances the anticancer activity [151]
Folate-modified self micro emulsifying drug delivery system	Cytotoxicity of Folate CUR nanoemulsion, CUR-emulsion and free curcumin were 20.57, 38.59, 25.62 μM in HT-29 cancer cells respectively.	Not available [152]
Curcumin-loaded cationic liposome	cytotoxicity increased ~1.3 times in HeLa and SiHa cell line as compared to free curcumin	apoptosis induced by nanoformulation was ~9 times more than free curcumin [153]
Hyaluronic acid-cur conjugated gold nanoparticle (HA–Cur@AuNPs)	cytotoxicity of nano formulated curcumin was ~3.4, ~2.6 and ~2.7 fold higher than native curcumin in HeLa, glioma and coco-2 cells at similar concentration of curcumin (0.63 μg/0.1 mL) after 24h	Enhanced cellular uptake by endocytic process [154]

Table 1.2: *In vitro* studies on cytotoxicity of different curcumin nanoformulations.

1.6.8.2. *In vivo* studies of curcumin nanoformulation

Curcumin Formulation	***In vivo* curcumin Administration**		**Bioavailability of nanoformulation**
	Dose	**Route**	
PLGA-CUR	7.5 mg/kg body weight of rat	Intravenous	Enhanced compared to native curcumin [155]
PLGA-poly(ethylene glycol) (PEG)	50 mg/kg body weight of rat	Oral	Improved by 55.4-fold [156]
Low (L)and High(H) molecular weight (Mw) PLGA-CUR nanoformulations	50 mg (nanocurcumin formulations) /kg body weight for rat	Oral	~1.67 (LMw) and 40-fold (HMw) higher compared to free curcumin [157]
Curcumin loaded poly(lactide-*co*-glycolide) (PLGA) NPs	100 mg /kg (PLGA NPs) along with 10 mg/ kg (piperine), Body weight of rat	Oral	9-fold higher for nanoformulation +piperine compared to free curcumin+piperine [158]
Solid lipid NPs	400 mg/kg body weight of mice	Intraperitoneal	Improved by ~ 83 fold, compared to free curcumin [159]
Silica-coated flexible liposomes nanohybrid	50 mg/kg body weight of rat	Oral	Improved by 7.76 fold, compared to free curcumin [160]
Lipid based oral formulation	250 mg/kg rat	Oral	Improved the area under the curve ($AUC_{0-\infty}$) by 35.8 fold compared to free curcumin [161]
Nanocur™ (polymeric nanoparticles prepared from isopropyl acrylamide, vinyl pyrrolidone and acrylic acid	25 mg/kg body weight of mice	Intraperitoneal	Improved by ~345 fold compared to free curcumin [150]
Organogel-based nanoemulsion	240 mg/kg body weight of mice	Oral	~ 9.8 fold increase in bioavailability of curcumin [162]

Glycerol monooleate-poly(vinyl alcohol) with pluronic (F127) polymer NPs	30 mg/kg body weight of mice	Intravenous	Improved by ~87.5 fold compared to free within 24 h [163]
Triblock copolymer NPs Poly(ε–caprolactone)-b-poly(ethylene glycol)-b-poly(ε–caprolactone)	15 mg/kg body weight of rat	Intravenous	Increased ~4.2fold [164]
Nanoemulsion (NE-Cur), Amorphous solid dispersion (ASD-Cur), Nanocrystal solid dispersion (CSD-Cur),	20 mg (NE-CUR, ASD-CUR and CSD-CUR) /kg body weight of rat	Oral	Increased by 7.9, 10.7 and 14.3%, for NE-CUR, ASD-CUR and CSD-CUR, respectively compared to free curcumin [165]
Curcumin nanosuspension in combination with D-α-tocopheryl polyethylene glycol 1000 succinate (TPGS)	15 mg/kg body weight of rabbit	Intravenous	Improvement by ~ 3.8-fold than free curcumin [166]

Table 1.3: Bioavialability of curcumin nanoformulation - *In vivo* studies.

1.6.9. Curcumin as photosensitizer

Curcumin has been shown to exhibit photosensitizing effects in bacteria and mammalian cells when irradiated with visible or ultraviolet light (UVA) [167, 168]. The phototoxic effects of curcumin have been shown to involve both oxygen dependent and independent mechanism. When irradiated with visible light, curcumin gets excited to singlet state from ground state, through intersystem crossing it goes to triplet state where it reacts with molecular oxygen and

contributes to formation of reactive oxygen free radicals such as superoxide radicals ($O_2^{\bullet-}$) and $^1O_2$ [169, 170]. Effect of photosensitizing property of curcumin has been studied in both mammalian cells and bacteria. Dahl et al. [171, 172] demonstrated the phototoxic effect of curcumin on mammalian cells (rat basophilic leukemia cell) and bacterial system in presence of oxygen. Studies of Koon et al showed that the cytotoxicity of curcumin was enhanced in nasopharyngeal carcinoma cell line (NPC/CNE2) when irradiated with visible light [173]. It was also reported that combination of light (UVA and Visible light) in presence of low concentrations of curcumin can induce apoptosis in human keratinocytes by inhibiting NF-kB, growth/survival kinases PKB/Akt, ERK1/2 and increase IKB-α expression [167]. Later same group demonstrated that combination of curcumin treatment with visible light could induce significant inhibition of tumor growth under *in vivo* conditions compared to curcumin alone [174]. Bruzell et al 2005 studied the photocytotoxicity of curcumin prepared in 5% DMSO, non-ionic micelles, cyclodextrin, liposomes, or a hydrophilic polymer on salivary gland acinar cells (SM 10-12) and showed that among the different nanoformulations studied, liposome was found to be the most efficient vehicle [175]. These studies show that combination of curcumin and light can overcome the limitations of oral administration of high concentration curcumin required for therapeutic purpose. These studies indicate that curcumin can be exploited as a potential PS especially for superficial cancer.

1.7. Photodynamic therapy

As discussed earlier, PDT is a promising approach for treatment of tumor. It involves the administration of PS which preferentially gets accumulated in tumor. When PS localized in

tumor is excited with light of specific wavelength it leads to generation of ROS which is cytotoxic to cancer cells [176, 177].

A major advantage of PDT over conventional therapies is that only target tissue which has accumulated PS is exposed to light, PS itself is not toxic in the absence of light and hence accumulation of PS in nonspecific tissues does not cause any toxicity. The efficacy of the PDT depends on the chemical nature of the PS, PDT dose, i.e. PS concentration and light fluence, localization of PS in target cells [177].

1.7.1. Basics principle of photodynamic reactions

The basic photophysical processes involved in PDT is illustrated in Figure 1.4. Upon absorption of light of appropriate wavelength, the PS which in the ground electronic state (S_0) gets excited to the short-lived excited singlet-state (S_1) [178, 179]. The excited PS can return to the ground state by emitting the absorbed energy as fluorescence or by internal conversion. Alternatively, the excited PS (S_1) can move to the lower energy triplet state (T_1) by intersystem crossing. The T_1-state of PS is long-lived and therefore can initiate photochemical reactions by reacting with other molecules and generate ROS or the PS (T_1) can also return to the S_0-state by emitting phosphorescence. Excited PS in triplet state can produce ROS through two mechanisms, Type I and Type II processes. In Type I processes, transfer of electron or hydrogen occurs between the excited PS (T_1) and other molecules giving rise to free radicals like superoxide anion, hydroxyl radical or hydrogen peroxide. In Type II processes, the excited PS interacts directly with molecular oxygen by transferring energy to produce $^1O_2$. Reaction products of both Type I and Type II induce oxidation of biological molecules such as lipids, proteins in cells which ultimately causes cell death either by apoptosis or necrosis. The mechanism of cell death induced

by PDT is dependent upon the localization of the PS within the cell and the amount of $^1O_2$ or free radicals generated.

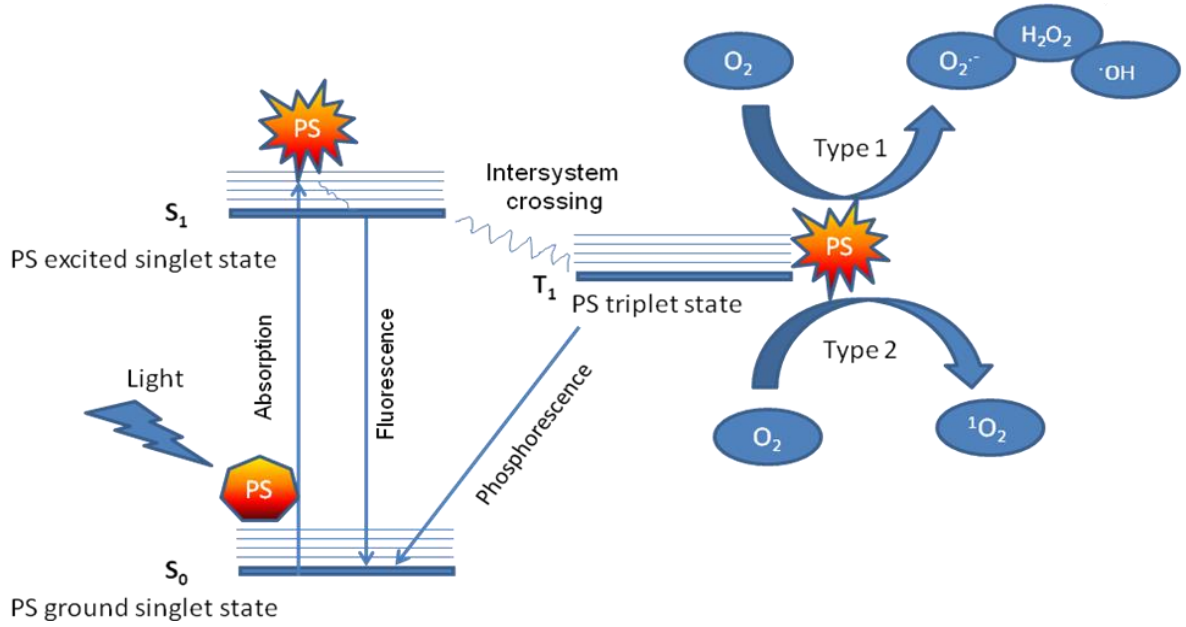

Figure 1.4: Photophysical process involved in photodynamic therapy.

1.7.2. Characteristics of an ideal photosensitizer

Photophysical characteristics of PS determine the efficacy of PDT. Ideal PS should have the following characteristics [180, 181].

- Should have high quantum yield of the triplet formation so that generation of $^1O_2$ is high.
- Should be a pure compound with known composition.
- Should not be toxic in absence of light, should be eliminated from normal tissues rapidly to avoid systemic toxicity.

- Should have strong absorption in the long wavelength of visible light (> 650 nm), so that the deep seated tumors can be treated effectively.
- Should have high molar extinction (~ 50,000–100,000 M^{-1} cm^{-1}).
- Should preferentially localize in tumor tissues compared to healthy tissues.
- Should have ampihilic nature, it should be water soluble so that it can be easily administered in the body and also have sufficient lipophilicity to penetrate tumor cells for inducing photodynamic reaction.
- Synthesis of the PS should be relatively easy and cost effective

1.7.3. Classification of Photosensitizers

PSs are classified as first and second generations based on their characteristics. Photofrin and hematoporphyrin derivative are the first generation PSs. Photofrin is approved by FDA (US) for treating esophageal cancer, lung cancer, and Barrett's esophagus [182, 183]. It is a porphyrin based PS, and is a complex mixture of monomeric, dimeric, and oligomeric structures. Maximum wavelength of absorption of Photofrin is at 630 nm and at this wavelength ε max is ~ 3000 M^{-1} cm^{-1}which is lower than ideal PS. Also, at 630 nm, the penetration of light in tissue is limited to 2–3 mm. This limits its application to treatment of surface tumors. Toxicity of photofrin to skin is high and lasts for long durations (about three weeks).

To improve PDT, second-generation PSs have been developed. These are either synthetic or prepared from natural precursors. Most of these PS have strong absorbance in the longer wavelength region (630 - 850 nm range), good ability to generate $^1O_2$ and good retention at tumor site. The second generation PS belongs to the groups of porphyrins, phthalocyanines, texaphyrins, chlorins, and bacteriochlorins. Some of the PSs under clinical trial are 2-(1-

Hexyloxyethyl)-2-devinyl pyropheophorbide (HPPH), Palladium bacteriopheophorbide, Tin ethyl etiopurpurin, Motexafin lutetium (Lu-Tex) and Silicon phthalocyanine (Pc4). Aluminum phthalocyanine tetrasulfonate (AlPcS4), N-aspartyl chlorin e6 (NPe6) and 5-Aminolevulinic acid (ALA) are already approved for ceratin cancers [184].

1.8. Chlorophyll derivatives

Second generation PSs derived from plant pigment chlorophyll-a (Chl-a) have considerable interest for PDT applications due certain advantages over the synthetic PS. They are easily prepared from natural precursors like chlorophylls and protoheme which are available in abundance and are therefore more economical. [180]. Chlorophyll-a shows very good absorption in the wavelength range 660 to 800 nm (good tissue penetration). However, because of presence of lipophilic phytyl group, it is highly hydrophobic and can not be used in its natural form [180, 185]. For PDT applications different hydrophilic derivatives of Chl-a such as chlorin e_6 and chlorine p_6 and hydrophobic derivaties like pheophorbide have been prepared.

1.8.1. Pheophorbide and its derivatives

Pheophorbide-a (Pba), [(3S,4S)-9-ethenyl-14-ethyl-21(methoxycarbonyl)-4,8,13, 18-tetramethyl-20-oxo-3-phorbinepropanoic acid], is a chlorophyll (Chl) derivative prepared from Chlorophyllic mixture (solid Chl a/Chl b prepared from green leaves, such as spinach) using 30% (w/w) aqueous hydrochloric acid and diethyl ether [180]. Pba is an amphiphilic PS has a hydrophilic propionic acid residue but it gets aggregated when dissolved in aqueous solutions. The $^1O_2$ quantum yield ($\Phi\Delta$) of Pba in organic solvent like in ethanol is 0.51 [180, 186].

Pyropheophorbide-a (PPa) is a semisynthetic PS, synthesized from methyl pheophorbide-a (MPa) obtained from algae Spirulina pacifica biomass by a two step chemical procedure including pyrolysis of MPa with 2,4,6-collidine and hydrolysis of methyl pyropheophorbide-a [187]. PPa which has a carboxylic acid group and is more stable than Pba. The structure of PPa is shown in Figure 1.5.

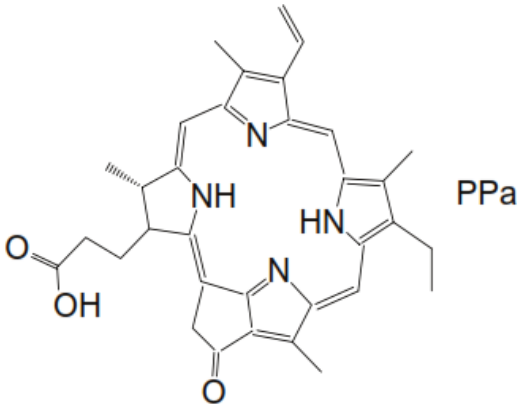

Figure 1.5: The structural formula of pyropheophorbide-a.

1.8.1.1. Photophysical properties

PPa has a strong soret band centered at ~ 410 nm with extinction coefficient (ε) = 1.15 × 10^{7} $(mol/l)^{-1}m^{-1}$ and a strong Q band at 667 nm with ε = 4.96 × 10^{6} $(mol/l)^{-1}$ m^{-1} which is better than 630 nm peak of Photofrin and can penetrate more deeper in the tissue. Therefore PPa is an attractive PS for PDT. In DMF, PPa is in monomeric state [188]. Quantum yield of singlet oxygen for PPa is 0.52 in DMF. Photosensitizing efficacy of PPa either as methyl esters or as carboxylic acids, is found to increase with the length of the alkyl ether side chain. The photosensitizing ability increases with the length of the alkoxy group, being highest for the

hexoxy and heptoxy derivatives [189]. Photodynamic activity of methyl ester of PPa and HPPH are the two pyropheophorbide-a derivatives which have been investigated extensively. HPPH known with brand name Photochlor has been approved for use in clinical trials and has undergone Phase I/II trials for esophageal cancer and Barrett's esophagus basal cell skin cancer, lung cancer, esophageal cancer at precancerous or early stage conditions, dysplasia, carcinoma of the oral cavity, carcinoma of the oropharynx [184].

1.8.2. Pyropheophorbide-a and its conjugates

PPa in native form although has a good photophysical characteristics its bioavailability is poor due to limited solubility in water. To improve its solubility, native PPa has been conjugated with lysine. Conjugated PPa is 13 times more efficient than native PPa [190]. Complexes of PPa and hydrophilic organic amine containing piperazine and imidazole groups have been prepared for improving solubility. These complexes have shown to retain the phototoxic property of native PPa [187]. To improve the selective tumor targeting ability, PPa has been conjugated with tumor specific antigens or biomolecules (inhibitors or antagonists) which specifically bind with the receptors that are overexpressed in cancer cells. Savellano et al [191] conjugated PPa with monoclonal antibodies of HER2 receptors and studied the uptake and phototoxic efficacy of these PPa immune conjugates in HER2-overexpressing breast cancer (SK-BR-3), ovarian cancer (SK-OV-3) and HER2 negative (MDA-MB-468) cells. Their study showed photodynamic action of PPa immunoconjugates were selective and killed only HER2 overexpressing cells although these were less phototoxic than free PPa which did not show any selectivity. Their study also showed that multi epitope targeted photo immunotherapy with a HER50 and HER66 PPa immunoconjugate mixture was significantly more effective than single epitope targeted photo

immunotherapy with a single anti-HER2 photosensitizer [192]. In another study, PPa conjugated to an anti-HER2 scFv containing multiple PS molecules also showed good cellular uptake by HER2-positive, SKOV-3 cells, and negligible uptake in HER2-negative KB cells and significant tumor regression of human breast cancer xenografts than free PS following photodynamic treatment [193]. Studies carried out by Liu et al [194, 195] have also shown that PPa conjugated to inhibitor of prostrate cancer specific membrane antigens (PSMA) accumulate specifically in PSMA positive prostrate cancer (LNCaP) cells but not PSMA (negative) PC-3 cells. Targeted PDT efficacy of PSMA inhibitor conjugate of PPa was confirmed by observation of apoptotic events like cell permeability to HOE33342/PI double staining, appearance of poly-ADP-ribose polymerase (PARP) p85 fragment and terminal deoxynucleotidyltransferase dUTP nick end labeling (TUNEL) assay detected DNA fragmentation, activation of caspase 3 and 8, observed in PSMA+ LNCaP cells.

Conjugation of PPa with estrogen antagonist have proved effective. It has been reported that PPa conjugated to tamoxifenan antagonist for estrogen receptor could specifically bind and selectively kill estrogen sensitive MCF-7 breast cancer upon light exposure [196]. In another study, PPa conjugated to C(17α)-alkynylestradiol has been shown to accumulate selectively in hormone sensitive breast cancer (MCF-7) cells expressing nuclear estrogen receptor and preferentially kill tumor cells upon exposure to visible light [197].

Studies have shown by conjugating PPa with folic acid using peptide sequence as linker, its uptake as well as photodynamic efficacy improved particularly in folate receptor expressing cancer cells (KB cells). Improved efficacy was also observed under *in vivo* condition in mice bearing tumors induced by KB cells. By using a short peptide sequence it was demonstrated that

PPa retention in liver and spleen could be reduced compared to that peptide lacking PPa probe [198].

1.8.3. Pyropheophorbide-a derivatives and nanoparticles

Use of Np for delivery of hydrophobic PS like PPa provides additional advantages compared to traditional conjugation of PS with targeting moiety. These particles can be conjugated with high density of targeting moiety eg. antigens conjugated with more than one PS. They can be made multifunctional. Studies have shown that Nps such as ORMOSIL [88], polymeric micelles of diacylphospholipid-poly (ethylene glycol) (PE-PEG) and magnetic Fe3O4, liposomes, amine functionalized polyacrylamide (AFPAA) drug-doped Nps have shown improved efficacy as compared to native PS. Polymeric micelles and magnetic Fe3O4 loaded with HPPH showed magnetophoretic control of these Np cause efficient cellular uptake, enhanced imaging and phototoxicity of drug loaded Nps [199]. The studies have shown liposomal formulation of PPME improves the cellular uptake by 5 fold than free PPME in a human colon carcinoma cell line (HCT-116) [200]. Studies have shown HPPH post loaded in amine functionalized polyacrylamide (AFPAA) Nps exhibit good phototoxicity compared to free drug [201]. Up conversion Np containing PPa loaded chitosan wrapped NaYF(4):Yb/Er has been prepared for near-infrared PDT. *In vitro* studies showed improved targeting specificity of UCNP-Ppa-RGD to integrin α(v)β(3)-positive in U87-MG cells compared with free drug. UCNP-Ppa-RGD exhibited high phototoxicity against U87-MG cells, after 980 nm laser irradiation [202]. While all these studies have shown the use of different Nps for improving cellular uptake of PPa derivatives like HPPH, there are very few studies on effect of tumor environment such as pH on uptake of passive or actively targeted Nps entrapping PPa on cancer cells.

1.9. Aim & objective of study

Although liposomes, polymeric Nps, drug polymer conjugates particularly for curcumin, have shown improved water solubility, stability and bioavailability, many of these systems requires elaborate preparations, have short storage life as these are prone to biofouling and also drugs get aggregated in some of these nanoformulations. For photodynamic applications, drugs entrapped in Nps need to be released at the target site before light exposure. Compared to polymeric Nps, ORMOSIL (SiNps) are optically transparent, resistant to pH changes, have hydrophobic core and porous structure, therefore allows easy encapsulation of hydrophobic drugs and protect them from degradation. Also selectivity of drug delivery of these NPs can be enhanced by covalently conjugating ligands of interest with their surface functionalized groups.

In this thesis, use of SiNp for improving delivery of curcumin and pyropheophorbide-a has been evaluated. To improve tumor targeting efficacy, drugs loaded in SiNps have been conjugated with ligands that bind to receptors over expressed on cancer cells. Since pH surrounding the tumor strongly influences the outcome of anticancer drugs, effect of pH on uptake and photodynamic efficacy of passive and actively targeted SiNp entrapping PS on different tumor cells have also been studied.

The main objectives of this study are as follows:

1. To evaluate the uptake and phototoxic efficacy of curcumin loaded in SiNp on oral cancer cells and tumor spheroids.

2. To evaluate the cytotoxic efficacy of Hyaluronic acid conjugated SiNp loaded with curcumin on CD44 expressing cancer cells.

3. To study the photodynamic efficacy of plain (Np-PPa) and folate receptor targeted SiNp encapsulating pyropheophorbide-a (FR-Np-PPa) on cancer cells at different pH.

4. To assess biodistribution and *in vivo* toxicity of Np-PPa and FR-Np-PPa.

CHAPTER 2

MATERIALS AND METHODS

2.1. Materials

Dulbecco's modified essential media (DMEM), Roswell Park Memorial Institute media (RPMI 1640), N-2-hydroxyethylpiperazine-N'-2-ethanesulphonic acid (HEPES), aerosol-OT (AOT), vinyl-trimethoxysilane (VTMS), vinyl-triethoxysilane (VTES), 3-aminopropyl-triethoxysilane (APTES), curcumin, hyaluronic acid (HA, oligomers-HA4), hyaluronidase, reduced glutathione (GSH), bicinchoninic Acid (BCA), dimethylsulfoxide (DMSO), thiobarbituric acid (TBA), bovine serum albumin, folic acid, propidium iodide (PI) and hoechst were purchased from Sigma, St.Louis, MO, USA. 3-(4,5-dimethylthiazol-2-yl)-2,5-diphenyltetrazolium bromide (MTT), nystatin, streptomycin, penicillin, fetal bovine serum (FBS), phosphate buffered saline (PBS), trypsin, and 5,5'-Dithiobis-(2-Nitrobenzoic Acid) (DTNB) were purchased from Himedia, Mumbai, India. Ethyl-3-(3-dimethylamino) propyl carbodiimide hydrochloride (EDC) was obtained from Merk, India. N-hydroxysuccinimide (NHS) was obtained from Fluka, pyropheophorbide-a (PPa) was purchased from Frontier Scientific, Inc., Logan, UT. LIVE/DEAD viability/cytotoxicity kit and 2,7'-dichlorodihydrofluorescein diacetate (H2DCFDA) were purchased from Invitrogen Molecular Probes, Eugene, Oregon. All antibodies MMP-9 (sc-6840), VEGF (SC1881), TNF-α (SC1348), NF-kB (SC1190) and horseradish peroxidase (HRP)-conjugated secondary antibodies and detection reagents were obtained from Santa Cruz Biotechnology (Santa Cruz, CA). All other chemicals were of highest purity and procured locally.

Cell line 4451, was obtained from Institute of Nuclear Medicine and Allied Sciences, Delhi, India. Human squamous cell carcinoma cell line (Nt-8e) was obtained from Advanced Centre for Treatment Research and Education in Cancer (ACTREC), Mumbai, India. Human breast carcinoma (MCF-7) cells, colo-205 cells (colon carcinoma) and mouse mammary carcinoma

(C127I) were purchased from National Centre for Cell Sciences (NCCS), Pune, India. Cell culture wares i.e. culture flask, petri plates, multiwell plates were obtained from Tarson, India.

2.2. Preparation of NPs

2.2.1. ORMOSIL (SiNp) Nanoparticles

SiNp were prepared by microemulsion method under alkaline condition by condensation polymerization of organosilane precursors [88]. Precursors used for making SiNp were APTES, VTES and VTMS. Dioctyl sodium sulfosuccinate (Aerosol OT) and 1-Butanol were used as surfactant and cosurfactant respectively. SiNp were synthesized at room temperature in the nonpolar core of Aerosol-OT (AOT)/1-butanol/water micellar system. Micelles were prepared by dissolving 0.44 g AOT and 800 µl of 1-butanol in 20 ml of water by vigorous magnetic stirring. VTES was added to the micellar system, and the resulting solution was stirred for about ~1 h until it became clear. To this, 20 µl of APTES was added and stirred for about 20 h till the solution turned bluish white. This indicated the formation of Nps. This solution was dialysed against double distilled water for about 48 h using a cellulose membrane (cut off 20 kDa) to remove unreacted AOT and 1-butanol. Colloidal solution of SiNp was sterilized using 0.2µ membrane filter and stored at 4 ^{0}C till further use. To determine concentration of SiNp, an aliquot (1ml) of the colloidal solution was transferred to microfuge tube and lyophilised. The weight of the lyophilized powder was determined and expressed as mg/ml.

2.2.2. Curcumin loading in SiNp

For preparing curcumin SiNp complex (cur-SiNp), a known volume of curcumin from stock solution (10 mM curcumin in DMSO) was added to SiNp (100 µg/ml or 150 µg/ml) dispersed in aqueous medium and stirred for ~30 min. The absorption and the fluorescence spectra of cur–SiNp complexes in water was measured and compared with free curcumin under similar conditions to ensure loading. Absorption spectra of curcumin and its complex with SiNp in water were recorded from 350 to 600 nm using Cintra 20 absorption spectrophotometer (GBC, Australia). Fluorescence spectra of free curcumin and cur–SiNp in water were recorded in the wavelength range 450 to 700 nm using Fluorolog-2 spectrofluorometer (Spex USA).

For determining the loading capacity, different concentrations of curcumin was mixed with known concentration of SiNp (100 µg/ml or 150 µg/ml). Changes in the fluorescence spectra of the complex were measured. A concentration dependent enhancement in fluorescence of curcumin was observed upto 25 µM of curcumin loaded in 150 µg/ml of SiNp. Beyond this concentration, fluorescence of cur-SiNp decreased with red shift in peak position.

2.2.3. Preparation of HA-SiNp and HA-SiNp-curcumin complexes

Preparation of HA conjugated SiNp-curcumin complexes (HA-SiNp-cur) is shown in scheme 2.1. SiNp was prepared as described above. HA was conjugated to amine modified SiNp (void/drug loaded) following the procedure described in Ref. [203]. Prior to conjugating, carboxylic groups of HA was activated. For this, 0.2 mg of HA was dissolved in 10 ml HEPES buffer (10 mM, pH 6.0) and stirred for 30–60 min, to this 20 mM EDC and 10 mM of NHS prepared in water was added, and the mixture was stirred at room temperature for 30 min.

Curcumin loaded SiNp was prepared by adding 0.6 mM of curcumin to SiNp (1 mg/ml) in aqueous solution and stirred for 30 min and then unbound curcumin was dialyzed in water containing 5% methanol using cellulose membrane (cut off 20 kDa). This solution was divided into two parts. To one part of the solution, 3 ml of activated HA (Oligomer) was added and stirred continuously overnight. Solution was dialyzed for 48 h against water to remove unbound reactants. Other part was used as HA free (untargeted) SiNp-cur. Similarly, void SiNp was conjugated with HA except that in this SiNp did not contain any curcumin. To determine the concentration of bound curcumin, 100 µl of HA conjugated or HA free SiNp-cur complex was added to 1 ml of DMSO. Mixture was stirred for 30 min and absorbance of curcumin was measured. Concentration was determined by comparing with the standard curve obtained by measuring the absorbance of known concentration of curcumin in DMSO.

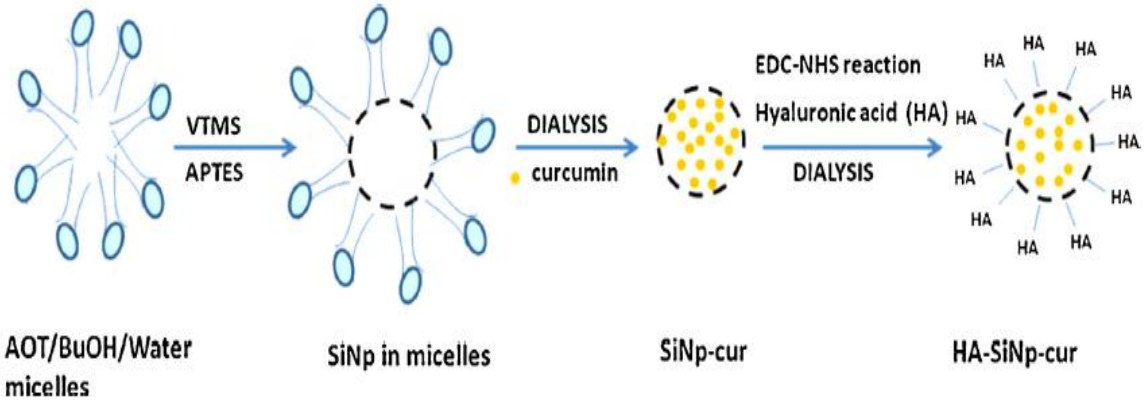

Scheme 2.1: Hyaluronic acid conjugated SiNp loaded with curcumin (HA-SiNp-cur) preparation.

2.2.4. Curcumin content in the SiNp

Curcumin content in the SiNp and HA-SiNp was determined by encapsulation efficiency (EE) and drug Loading content (DL) was determined by the following equations:

EE (%) = 100 × (Total amount of curcumin − Free curcumin)/ Total amount of curcumin

DL (%) = 100 × Weight of curcumin in Np/ (Weight of the curcumin in Np + Weight of Np)

2.2.5. Quantitation of HA

HA density on nanoparticles was estimated by cetyltrimethylammonium bromide (CTAB) turbidimetric method as described in Ref. [204]. In this method, the CTAB reagent (2.5 g) was dissolved in 100 ml of 2% (w/v) NaOH. For standard, HA (1mg/ml) was dissolved in water. A 50 µl of sample (HA-SiNp, curcumin free) and different concentrations of standard HA (25 – 200 µg/ml) were placed in different wells of 96-well plates. To this, 50 µl of 0.1 M phosphate buffer (pH 7.0) was added. After incubating for 15 min at 37 ºC, 100 µl of CTAB reagent was added to each well and the plate was again incubated for 10 min. Absorbance of well contents was read at 600 nm after shaking the plate for 10 s using ELISA microplate reader (Biotech Instrument, US). Absorbance of the blank (water (50 µl) + phosphate buffer (50 µl) + CTAB (100 µl) was subtracted from the standard solutions of HA and plotted against HA concentrations. Concentration of the HA in sample (HA-SiNp) was determined from the standard graph. Conjugation efficiency of HA bound to surface of SiNp was determined by estimating the amount of HA bound to SiNp before and after dialysis.

2.2.6. Curcumin release in presence of hyaluronidase enzyme

To study the release of curcumin from HA-SiNp-cur complex, a known volume of sample was taken in two different dialysis bags (MW cutoff 20 kDa). In one 120 U/ml of hyaluronidase enzyme was added. To the other sample, equal volume of water was added. The bags were placed in different beakers containing 20 ml of distilled water having 5% methanol. Samples were incubated at 37 ^{0}C under shaking condition. At a specified time interval, 2 ml of sink media was withdrawn from each of the beaker containing complex with and without enzyme. Fluorescence spectra of samples were measured to evaluate the curcumin released from the nanocomplex. To maintain a constant volume, similar volume of sink media was added to the beakers. The concentration of curcumin released was determined from the standard curve of free curcumin generated under similar condition.

2.2.7. Pyropheophorbide-a entrapped SiNp

Preparation of pyropheophorbide-a doped SiNp (Np-PPa) and folic acid conjugated Np-PPa is shown in Scheme 2.2. SiNp was synthesized following procedure described by Roy et al [88] except that VTMS was used as precursor instead of VTES. Nonpolar core of Aerosol-OT (AOT) ⁄1-butanol⁄water micellar system was prepared at room temperature. Micelles were prepared by dissolving 0.44 g AOT and 800 µl of 1-butanol in 20 ml of water by vigorous magnetic stirring. About 30 µl of PPa dissolved in DMF (stock 15 mM) was added to the above solution. For void (drug free) Nps similar volume of DMF without PPa was added. 300 µl of VTMS was added to the micellar system and the resulting system was stirred for about 1 h until solution was clear. After this procedure, 5 µl of APTES was added and stirred for about 20 h till the solution turned

bluish white. This indicated formation of Nps. Unreacted AOT, PPa and 1-butanol were removed by dialysis for about 72 h using a cellulose membrane (cut off 20 kDa).

For determining the concentration of the PPa entrapped in the SiNp, a 50 µl PPa doped SiNp was dissolved in 1.0 ml of DMF and after thorough mixing the absorbance of the sample was measured at 668 nm. The concentration was determined by comparison with standard curve obtained by measuring absorbance of known concentrations of free PPa in DMF.

2.2.8. Conjugation of SiNp with folic acid

To a 5 ml portion of stock solution of amine-terminated Np PPa-doped or void Nps, 200 µl of EDC (10 mM) and NHS (10 mM) solution was added, and the mixture was stirred at room temperature for 30 min. Then, folic acid (2 mg) dissolved in distilled water containing 1mM NaOH (20 ml) was added to Np, and the reaction between folic acid and amino groups was allowed to proceed for 18-20 h. The reaction mixture was dialyzed against deionized water for 50 h to remove unreacted molecules. Finally, all the samples were filtered through a 0.2 µ cutoff membrane filter and stored at 4 °C for later use.

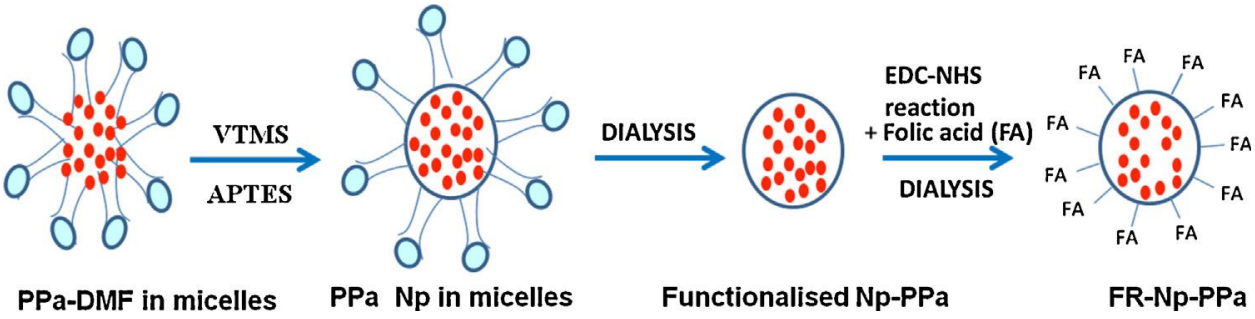

Scheme 2.2: Folate conjugated SiNp loaded with pyropheophorbide-a (FR-Np-PPa) preparation.

2.3. Characterization of SiNp

The morphology of SiNps was determined by Atomic force microscopy (AFM) imaging. Size (hydrodynamic radii) of SiNp (void, drug free), post loaded with drug or entrapped with PS) conjugated with and without bioligands were measured by dynamic light scattering (DLS). Surface charge of the different SiNps was characterized by measuring their zeta potential.

2.3.1. Atomic force microscopy

The AFM consists of a cantilever which has a sharp tip (probe) made of silicon or silicon nitride of nanometers radius. When the tip is brought into proximity of a sample surface, forces between the tip and the sample lead to a deflection of the cantilever which is measured using a laser spot reflected from the top surface of the cantilever into an array of photodiodes.

For measuring the morphology of Np by AFM, SiNp was spread on clean coverslips and air dried at room temperature. AFM measurements were carried out in a contact mode using silicon cantilever tips. Tip used for measurement had spring constant of 5.5 N/m and radius of curvature around 10 nm with resonance frequency 190 KHz. The topographic image (Figure 2.1) of SiNps was measured by imaging software (SOLVER-PRO, Russia).

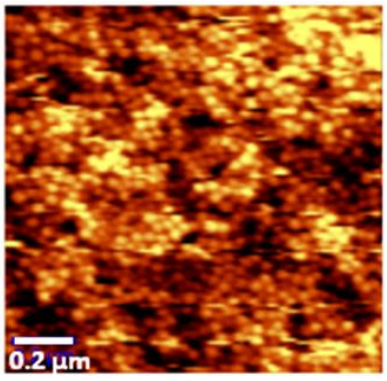

Figure 2.1: Atomic force microscopic image of SiNp (scale bar, 0.2 µm).

2.3.2. Hydrodynamic radius measurement

Size of SiNp was measured by particle size analyzer Brookhaven 90Plus particle analyzer (USA). The particle size analyzer determines the average hydrodynamic diameter of Nps by DLS. This technique is based on the measurement of diffusion of particles in solution. In this technique Brownian motion (random) of the particle due to forces from the solvent molecules that surrounded them is measured. Movement of particle in fluid is determined by its hydrodynamic diameter i.e. the particle surrounded by the counter ions. The smaller particle moves faster whereas movement of larger particle is slower.

The principle of this technique is that the sample materials or Nps will scatter incoming laser light. The scattered light intensity fluctuates with time due to the random motion of these particles. Processing the fluctuating signal gives the particle's diffusion coefficient, from which the equivalent spherical particle size is calculated.

The size of a particle is calculated from the translational diffusion coefficient by using the Stokes-Einstein equation.

$$D=kBT/6\pi\eta a$$

Where

D = Diffusion constant

a = Radius of the Nps

kB = Boltzmann constant

T = Temperature in Kelvin degrees

η = Viscosity of the solvent

Particle size analyzer 90 plus, Brookhaven used in this study can measure particle size ranging from ~1 nm to 6 μm with an accuracy of ±5%. The light source in this instrument is equipped with diode laser of 35 mW power output. For measurements Nps are diluted in distilled water (2 ml). The scattered light is collected at 90º (right angle). This instrument gives the average size as well as polydispersity of the Nps. The size distribution of SiNp measured by DLS is shown in Figure 2.2.

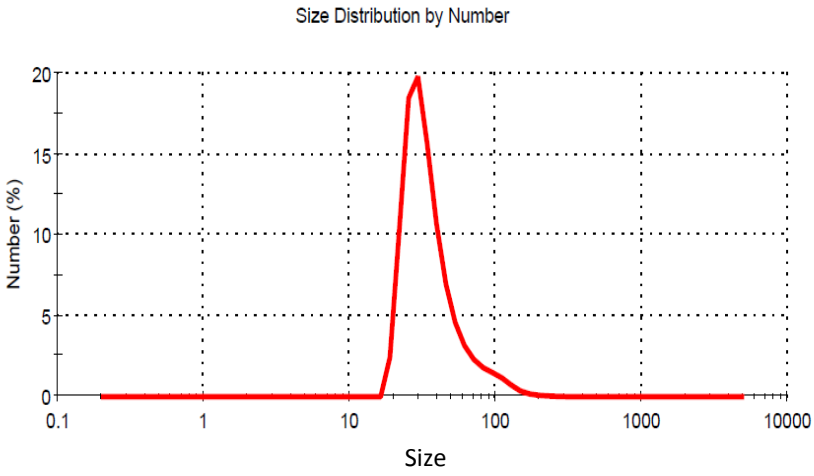

Figure 2.2: Measurement of size (nm) of SiNp by dynamic light scattering.

2.3.3. Zeta potential measurements

Zeta (ζ) potential is the potential difference between the stationary layer of fluid attached to the particle and solution in which it is dispersed. The particle is surrounded by strongly associated counter ions (Stern layer) and in the outer region, ions are loosely bound. The potential difference between the boundary of diffuse layer and strongly associated ions to particles is the zeta potential (Figure 2.3). The ζ potential is a measure for the degree of stability of a colloidal

system. If all particles in suspension have a high negative or positive ζ potential, they repel each other. In contrast, if the particles have a low ζ potential, they are unstable and aggregate.

For measuring the Zeta potential, SiNp (void) or drug loaded ligand free and ligand attached were diluted appropriately in water and placed in sample holder and potential was recorded.

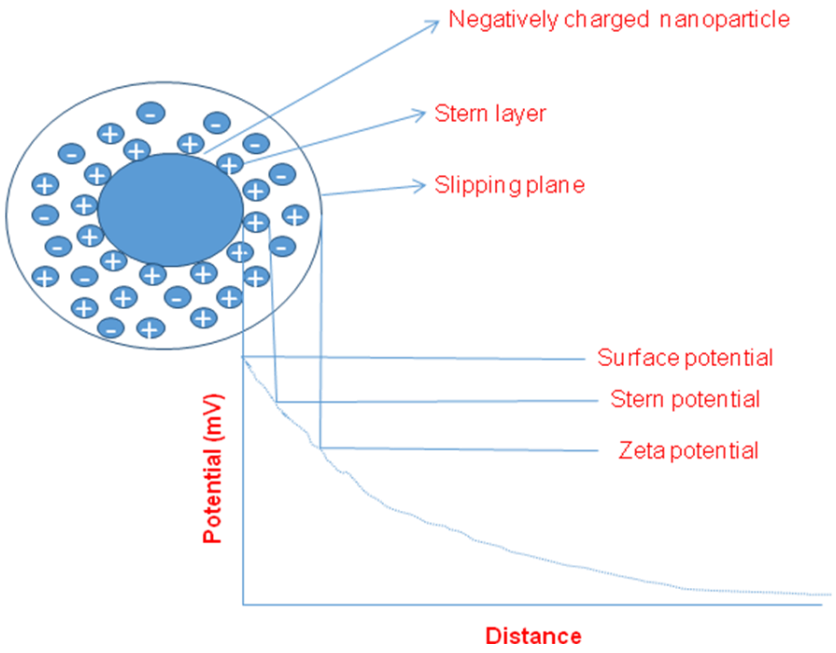

Figure 2.3: Illustration of the zeta potential measurement (modified from Malvern Technical Note).

2.4. Cell lines

The cell lines used are MCF-7 (human breast adenocarcinoma), Nt-8e (human squamous cell carcinoma derived from upper aero-digestive tract [205], colo-205 (human colon carcinoma), 4451 cells (human squamous cell carcinoma) established from carcinoma of oral cavity [206] and C127I a mouse mammary carcinoma.

2.5. Cell culture

2.5.1. Monolayer

Nt-8e, MCF-7, C127I and 4451 cells were grown in Dulbecco's minimum essential medium (DMEM), for MCF-7, medium was supplied with 1 mM pyruvic acid. Colon carcinoma cells (colo-205) were grown in RPMI-1640 medium. All the media used contained HEPES (25 mM), $NaHCO_3$ (2.2 gm/l), 10% FBS and antibiotics penicillin (10,000 IU), streptomycin (10,000 µg/ml) and nystatin (100 U/ml). The cells were incubated at 37 °C in a humidified atmosphere containing 5 % CO_2.

2.5.2. Spheroid

Spheroids of Nt-8e and colo-205 cells were generated by modified hanging drop method [207]. Single cell suspensions were prepared by using 1% and 0.25% trypsin (w/v) for Nt-8e and colo-205 cells grown in monolayers respectively. Cell count was determined using hemocytometer. Cell suspensions were diluted in growth media so as to have ~ 2 X 10^6 cells ml^{-1} for colo-205 or ~4 X 10^6 cells ml^{-1} for Nt-8e. For generating cellular aggregates, 10 µl cell suspension containing either ~20,000 cells (colo-205) or ~40,000 cells (Nt-8e) was placed as drops on the lids of 60 mm Petri dishes. The lids with drops were inverted over the dishes containing 2 ml growth medium and then incubated at 37 ^{0}C in 5% (v/v) CO_2 incubator. After 24 h, cellular aggregates formed were picked up using a Pasture pipette. These were transferred to non-adherent (agar coated (0.4% agar in distilled water) 96-well culture plates. A single aggregate was placed in each well and grown for 4 to 7 days. Growth was monitored by measuring the size

of spheroids using inverted microscope (Leica, Olympus). Thickness of spheroids was confirmed by optical coherence tomography as described in ref. [207].

2.6. Animal model

All animal experiments were performed following the protocols approved by the Animal Ethical Committee. Female Swiss albino mice (weight ~25 g, 8 weeks of age) were used in all experiments. All animals were housed in individual cages under constant temperature (20 ± 4^0C) with a 12 h light /dark cycle, and had free access to food and water.

For generating tumor in mouse models, C127I cells grown for 96 h in tissue culture flasks were harvested by trypsinizing. Cells were centrifuged and pellet was resuspended in sterile PBS (pH; 7.4) and the cell number was determined. Cells (~3.0 X 10^7) suspended in 250 µl of sterile PBS containing 5% glucose was injected subcutaneously on dorsal side of mouse. After 10 days, tumors of size ~0.9 to 1cm^3 were developed.

2.7. Cellular uptake

2.7.1. Curcumin uptake in monolayer

The uptake of curcumin by 4451 (oral cancer cells) was evaluated following the protocol of Kunwar et al [208]. About 5×10^6 cells were seeded in each well of a 24-well plate (Tarsons, India). For each measurement, cells were plated in two wells. One well was used for extraction of curcumin from cells using methanol other well was trypsinized to determine cell count. After 24h of incubation, the medium in wells was replaced with a fresh growth medium containing a specific concentration of either nanoformulated or free drug. Plates were incubated at 37 °C.

After specified time of incubation, cells were washed twice with PBS and 1 ml of methanol was added into each well. Curcumin extracted in methanol was collected from each well after 30 min of incubation at room temperature, and extracts were centrifuged at 10,000 rpm for 10 min at 4°C to remove the cell debris. The fluorescence of curcumin from supernatant was measured using a Fluorolog-2 fluorometer by exciting samples at a wavelength of 420 nm. The concentration of the drug extracted from cells was determined by a standard graph obtained with known concentration of curcumin in methanol and values were normalized with the cell number determined from wells treated with similar concentration of curcumin.

2.7.2. Curcumin uptake in spheroids

To study the uptake of the curcumin and its nanoformulation, 3 and 7 days grown spheroids (Nt-8e) were incubated in growth medium containing a containing 25 µM of either free curcumin or cur-SiNp complex with equivalent concentration of curcumin for 4 and 24 h. For each treatment three spheroids were used. Concentration of SiNp (150 µg/ml) used for drug loading was not cytotoxic. After specified time, spheroids were washed 3-4 times in PBS and transferred to microfuge tubes. About 300 µl of methanol were added for extracting cell bound curcumin and tubes were incubated at room temperature for 60 min. Methanol extracts were centrifuged at 10,000 rpm for 10 min at 4 ºC to remove cell debris. 200 µl of the extract was transferred to 96–well plates and absorbance was read at 420 nm using microplate reader (Biotech Instrument Power Wave 340). The total concentration of drug extracted from spheroids was determined by standard graph obtained from absorbance of known concentration of curcumin in methanol. The uptake of curcumin per spheroid was estimated and represented as nanomoles per spheroid. To

normalize uptake with cell number, small and big spheroids were dissociated using sterile accutase and the cell suspensions were counted microscopically.

2.7.3. Quantitation of curcumin uptake from HA free and HA-SiNp

To study the uptake of curcumin from HA free and HA-SiNp, colo-205 cells were grown in monolayer in 24 well plates. After 24 h, these cells were incubated with 25 µM free curcumin, or cur-SiNp or HA-SiNp-cur for 4 h. Cells were harvested by trypsinization after washing with PBS and cells were suspended in PBS. An aliquot of this suspension was used for cell counting. To the rest of cell suspension, 500 µl of methanol was added and incubated for 60 min at room temperature for extracting cell bound curcumin. Curcumin extracted in methanol was collected from each well and centrifuged at 10,000 rpm for 10 min at 4 ºC to remove the cell debris. 200 µl of extract was transferred to 96-well plates and absorbance was read 420 nm using microplate reader. To study the uptake of curcumin, spheroids grown for 120 h were incubated upto 96 h in growth medium containing either 25 µM curcumin (free) or in different nanoformulations. For each treatment three spheroids were used. After specified time of incubation, spheroids from different wells were pooled, washed 3–4 times in PBS, incubated with 200 µl accutase enzyme (37 ºC, 20 min) for dissociation of cells. Dissociated cells were centrifuged and the pellet was resuspended in PBS. An aliquot of this cell suspension was used for cell counting. Curcumin was extracted from the rest of the cell suspension as mentioned above. The concentration of drug extracted from cells was determined by standard graph obtained with known curcumin concentration in methanol containing PBS and normalized with the cell number.

2.7.4. Uptake of pyropheophorbide-a

For studying the pH dependent uptake of Np-PPa and FR-Np-PPa, Nt-8e (~0.6×10^6) and MCF-7 (~0.4×10^6) cells were grown in 24 well plastic dishes at 37 ºC. After 24 h of incubation, the medium was replaced with fresh HEPES buffered growth media of pH 7.4 or pH adjusted to 6.5. After incubating for 1 h in a medium of specific pH, a known volume of the two nanoformulations containing 0.5 µM of PPa was added into each well and cells were incubated for different durations. Each experiment included untreated (not treated with nanoformulated PPa) controls. After changing the growth media of pH 6.5 or 7.4, cells were incubated in CO_2 free atmosphere to avoid fluctuations in the pH. In some experiments, for studying the role of folate receptors, cells were incubated with 1 mM free folic acid for 30 min and then PPa loaded Nps were added to culture media of pH 6.5 or 7.4 and incubated for 4 h in the dark. Subsequent to incubation with drug loaded Nps, the culture medium containing the sensitizer was removed and the monolayer was washed three times with cold PBS with pH adjusted to 5.0 to remove loosely attached folate drug conjugates. Cells were harvested using 0.25% trypsin and resuspended in PBS (pH 7.4). About 10 µl of cell suspension was used for determining cell count. Rest of the cell suspension was solubilized using 2% SDS in 0.1 M NaOH, as described by [209]. Solubilized cells from drug treated and untreated controls were centrifuged to remove cell debris, supernatant was mixed with 1 ml of PBS and the fluorescence intensity of the PPa in the diluted supernatant was measured using spectrofluorometer. Samples were excited at 410 nm wavelength and emission was recorded from 550 to 700 nm. Fluorescence peak intensity of each sample measured at 677 nm was compared with standard curve to determine the concentration of PPa and values were normalized with the cell count of each sample. For quantifying the uptake, the background fluorescence of the untreated control was subtracted. For standard curve,

different volumes of known concentration of PPa (stock) were added into a 0.1 M NaOH 2% SDS (1 ml) and diluted with 1 ml of PBS. Samples were mixed thoroughly; the fluorescence emission peak intensity of each sample was recorded at 677 nm after exciting the samples at 410 nm. Standard graph was generated by plotting concentration of PPa against fluorescence intensities.

2.7.5. PPa uptake in C127I in presence of free folic acid

In order to verify the involvement of folate receptors in uptake of FR-Np-PPa, a competitive binding assay was performed. Cells (C127I) were plated on poly-lysine coated cover slip at a density of 1×10^5 cells. After overnight incubation, medium was replaced with growth medium containing 0.5 mM folic acid. After 2 h of incubation, FR-Np-PPa or Np-PPa containing PPa at a concentration 0.5 µM was added into petridishes containing cells incubated further for 2 h in dark at 37 ^{0}C. Cells were washed thrice with PBS and then observed under fluorescence microscope. PPa fluorescence was observed using 405 nm excitation filter.

2.8. In vivo biodistribution of free and nanoformulated PPa

To study biodistribution of different formulations of PPa, about ~250 µl of free PPa (5.0 µM) and the two nanoformulated PPa (Np-PPa and FR-Np-PPa) containing similar concentration of PPa were injected intraperitonially into mice. The concentration of SiNp injected was 3 mg/kg weight. Mice were anesthetized by intraperitoneal injection of ketamine (80 mg/kg) and xylazine (10 mg/kg) before injecting drug. After 4, 24, 72 and 120 h (post injection of Np), animals were euthanized and different organs were dissected and weight of the organs were determined.

Tissues of different organs were homogenized using homogenizer (3500 rpm, Remi, India). Homogenates were mixed with tissue extraction solvent containing perchloric acid, methanol, DMF in the ratio (1:1:1) left overnight for extraction of PPa from the tissue. Then the samples were centrifuged at 10,000 rpm for 10 min and supernatants were collected. Fluorescence of PPa from the supernatant was measured using SPEX fluorolog fluorometer by exciting at wavelength 410 nm. The fluorescence intensity was compared with standard graph obtained using known concentration of PPa in tissue extraction solvent to determine the PPa in tissue and values were normalized with the weight of tissue and expressed as (PPa in n moles/gm). Tissues of some organs (liver, kidney) was used for histology or biochemical assays.

2.9. Fluorescence microscopic study

2.9.1. Monolayer

To study the intracellular accumulation of free curcumin, cur-SiNp and HA-SiNp-cur, 4451cells or colo-205 cells were grown on poly-lysin coated glass coverslips placed in petridishes and incubated in CO_2 incubator at 37 °C. After 24 h, cells were treated with a specific concentration of free curcumin and equivalent dose of nanoformulated curcumin. After a specified time of incubations, the cells from different groups were washed twice with PBS (pH 7.4) and examined under a fluorescence microscope (Olympus, Japan). Curcumin fluorescence was monitored by using blue excitation filter. The images of sample were recorded using a CCD Camera Model 'ProgRes CF scan' and a ProgRes Capture Pro software (Jenoptik, Germany).

To confirm involvement of HA receptors in uptake, colo-205 cells were incubated with 0.5 mg/ml HA for 1 h before treating with free curcumin, SiNp-cur and HA-SiNp-cur. After

specified time of incubations, the cells treated with different formulations of curcumin washed with growth medium then twice with PBS (pH 7.4) and examined under fluorescence microscope.

2.9.2. Spheroids

Spheroids treated with free curcumin or its SiNp complex were washed with PBS to remove unbound curcumin and placed on coverslip and observed under fluorescence microscope. In some experiments to study the distribution of different formulations of SiNp within spheroids, spheroids were disrupted with accutase and single cell suspension was prepared. These were transferred to uncoated coverslips examined under fluorescence microscope.

2.9.3. Confocal microscopy

Confocal fluorescence microscopy was used to study the localization of PPa in Nt-8e and MCF-7 cells incubated with the two Np formulations containing PPa in a medium of pH 6.5 and 7.4 respectively. Cells were plated on poly-lysine coated glass coverslips contained in 35 mm Petri dishes. After overnight incubation, medium contained in the Petri dishes was replaced with fresh medium and required volumes of the nanoformulated PPa was added, plates were incubated at 37 ºC in the dark for specific duration. Cells were then washed with PBS and fixed using formaldehyde (4 %) for 15 min. Cells were imaged using near field scanning optical microscope (WiTec alpha 300SR, WiTec GmbH Germany) in confocal fluorescence mode. Argon ion laser of wavelength 488 nm was used for fluorescence excitation. All measurements were done using 60×, 1.22 NA water immersion objectives. Fluorescence was collected using the same objective

and directed to the detector through a 100 µm core multimode optical fiber that also served as pinhole. A stack of 15 images were acquired at the interval of 0.5 µm in depth direction with each XY scan comprising 256×256 pixel image acquired over 50 µm ×50 µm area. Images were processed WiTec Project 2.10 software. Changes in cell morphology due to incubation in media of different pH were studied by phase contrast microscopy (Olympus Japan).

2.10. Cytotoxicity

2.10.1. Toxicity of void nanoparticles

To determine the safe concentration of SiNp to be used for drug loading, cytotoxicity of void SiNp (drug free) was assessed. For this, 200 µl of growth medium containing 5×10^4 cells was seeded in each well of a 96-well tissue culture plate. After 24 h, cells were incubated in growth medium containing different concentrations of SiNp. After a specified time period of incubation, the growth medium containing SiNp was removed, wells were washed once, and 100 µl of medium containing 10 µl of MTT (3-[4,5-dimethylthiazole-2-yl]-2,5- diphenyl tetrazolium bromide) (5.0 mg/ml) was added into each well and incubated for 4 h as described by Mosmann [210]. Subsequently, MTT was removed and formazan crystals formed were dissolved by adding 150 µl of DMSO into each well. The absorbance of the resulting solution was recorded immediately at 570 nm using a microplate reader (BioTek Instruments, Vermont, USA).

2.10.2. Phototoxicity of nanoformulated curcumin

2.10.2.1. Monolayer

For assessing phototoxicity, 4451 cells grown on 96 -well plates were incubated in a growth medium containing free curcumin and cur-SiNp complex containing equivalent concentration of

curcumin. After a specified time, the medium containing free and nanoformulated curcumin was replaced with a fresh medium (not containing phenol red) and then exposed to white light. The light source used for irradiation was a halogen lamp equipped with a multimode fiber (Applied Optical Technologies, India) which is emitting in the wavelength range of 400–700 nm. Power output measured by a power meter (Ophir) at the cell surface was 200 mW. Following exposure to light, cells were incubated for 20 h and then MTT assay was performed as described above. All experiments included cells treated with free curcumin or curcumin in nanoformulation in dark and cells treated void SiNp as well as cells not treated with either curcumin or light (untreated control).

2.10.2.2. Spheroids

To study the phototoxicity of curcumin, spheroids were incubated in growth medium containing a specified concentration of either free curcumin or SiNp loaded with equivalent concentration of curcumin (cur-SiNp) at 37 ^{0}C. After a specific duration, wells containing spheroids were washed with PBS to remove unbound curcumin and 200 µl of fresh medium (not containing phenol red) was added into each well and then exposed to blue light. The light source used for irradiation was a LED (Applied optical technologies, India) emitting light of wavelength ~ 460 nm. Power output measured by a power meter at the cell surface was 36 mW. After irradiation spheroids were further incubated for 24 h in dark. Each experiment included untreated spheroids, spheroids treated with SiNp 150 µg/ml (void) or spheroids treated with either free curcumin or cur-SiNp complex in dark. After specified time period of incubation, growth medium was removed, wells containing spheroids were washed twice using PBS and each of the treated and untreated

spheroids were transferred to wells without agarose base in fresh micro-well plate to avoid its interference in absorbance. MTT assay was performed as described above.

2.10.3. Phototoxicity of pyropheophorbide-a

Cells were inoculated at the concentration of 2×10^4 cells per well in a 96-well microplate. After overnight incubation, medium in wells was replaced with growth medium of different pH. Specified quantities of Nps containing PPa was added and incubated for 2 h in the dark. Subsequently, the medium containing PPa doped Np was removed, the monolayer was washed with medium without serum, and fresh growth medium of the required pH was added. Cells were irradiated with red light (660 ± 25 nm). Source used for irradiation was LC-122A (Ci-Tec, US) which was coupled to an optical fiber probe (diameter 1.2 cm, length 1 m) with a built in narrow band pass filter. The intensity of light at the cell surface was ~ 39 mW/cm^2. The power output was measured by a power meter. Following irradiation of the cells, the media in all the wells were replaced with fresh growth medium at pH 7.4. After 24 h, MTT assay was performed to determine the cell survival as described above. All experiments included dark controls in which cells were treated with PPa containing Nps but not exposed to light, and untreated cells (neither treated with light or PPa containing Nps).

2.11. Post treatment growth of spheroids

To study the effect of curcumin treatment on growth of tumor spheroids (Nt-8e, colo-205), spheroids were incubated with a particular concentration of either free curcumin or its nanoformulation for a specified time. Following which spheroids were washed with PBS and individual spheroid was placed in well (coated with agarose) filled with 200 µl of fresh growth

medium in a 96-well plate and the plates were incubated in the dark at 37 °C in CO_2 incubator. Morphological changes and growth of treated and untreated spheroids were monitored upto 7 days by measuring the diameter using a phase contrast microscope (olympus, Japan). The culture medium were changed every after 48 h.

2.12. Migration of cells from spheroids

Spheroids (Nt-8e) treated with curcumin and its SiNp complex in dark as well as spheroids exposed to light in presence or absence of Glutathione (GSH) were washed with PBS and then transferred to 24-well plates without agarose coating and incubated at 37 °C. Migration of cells from spheroids subjected to different treatments was assessed microscopically by measuring the total distance (diameter) covered by the cells after different durations as described in ref. [211].

2.13. Live and dead assay

The LIVE/DEAD viability/cytotoxicity kit (Invitrogen Molecular Probes, Eugene, OR) was used to determine the live and dead cells based on membrane integrity and esterase activity. This assay uses calcein and ethidium homodimer. Calcein, is a polyanionic fluorescent dye that is retained within live cells and produces an intense uniform green fluorescence. Ethidium homodimer enters cells with damaged membrane and upon binding to nucleic acids it produces a bright red fluorescence but in live cells with intact plasma membranes ethidium homodimer do not permeate.

4451 cells (1×10^6 ml^{-1}) grown in 24-well plates were treated with either free or nanoformulated curcumin for a specific duration and then exposed to light as described above. After 3 h of

irradiation, cells were washed with PBS and incubated with the working solution containing 2 µM calcein AM and 4 µM ethidium homodimer prepared according to the protocol described by the manufactures and were incubated for 30 min at room temperature. Cells were then washed twice with PBS to remove unbound dyes, and stained cells were examined under a microscope (Olympus, Japan).

2.14. Estimation of intracellular ROS

ROS generation in spheroids (Nt-8e) treated with different formulations of curcumin was monitored by using 2',7'–dichlorofluoresceindiacetate (DCFDA). This is a non-polar compound that is converted into a polar derivative by cellular esterase after incorporation into cells, and is rapidly oxidized to highly fluorescent 2′,7′-dichlorofluorescein (DCF) by intracellular ROS. After photodynamic treatment, spheroids were incubated with 500 µl of PBS containing 10 µM H2DCFDA for 30 min at 37 ºC. Spheroids were then washed in plain medium (without serum), to remove the extracellular dye. The fluorescence of DCF was monitored by fluorescence microscopy using 480 nm and 530 nm excitation and emission filters respectively.

2.15. Assessment of apoptosis and necrosis

Spheroids (Nt-8e) treated with free curcumin and its SiNp complex after irradiation with light were washed with PBS twice and incubated with PBS containing Propidium iodide, PI (10 µg/ml) and hoechst (20 µg/ml) for 30 min at 37 °C. Spheroids were then washed twice with PBS and observed under fluorescence microscope by exciting with 360 and 510 nm band-pass filters for hoechst. PI stained cells were viewed using 546 nm excitation and 590 nm emission filters.

Red fluorescence in cells due to uptake of PI indicated membrane damage associated with necrotic death. In some experiments, treated and untreated spheroids stained with fluorescent probes were dissociated and single cell suspension was observed under microscope. Cells showing fragmented nuclear morphology were scored as apoptotic. Images were captured using fluorescence microscope as described above.

2.16. Biochemical test

2.16.1. BCA assay

Protein concentration of cell / tissue lysates was measured by BCA method. Principal of this assay is the peptide bonds in protein reduce Cu2+ ions from the copper (II) sulfate to Cu+ which is temperature dependent reaction. The amount of Cu2+ reduced is proportional to the amount of protein present in the sample. Reduced Cu forms a complex with BCA which is a purple-colored product that strongly absorbs light at a wavelength of 562 nm.

Following reagents were used for the assay, reagent A, B and C. Reagent A comprises of sodium carbonate monohydrate (8 gm), sodium tartarate (1.6 gm), dissolved in 100 ml of distilled water. pH of solution is adjusted to 11.25 using 10 M NaOH. Reagent B comprises of 4 gm BCA dissolved in 100 ml distilled water and Reagent C consists of 0.4 gm cupric sulfate (5 x hydrated) in 10 ml water). Working solution of reagents was prepared by mixing 1 volume of reagent C with 25 volumes of reagent B, to this 26 volumes of reagent A is added. For protein detection, an aliquot (50 µl) of the sample was mixed with 500 µl of working solution. Samples were heated at 60 ºC for 60 min and absorbance was read at 562 nm after cooling the samples.

The concentration of the protein was determined from the standard calibration curve prepared using different concentration of BSA.

2.16.2. Western blot analysis

Effect of photodynamic stress induced by free and nanoformulated curcumin on protein expressions (NF-κB and related proteins) were studied by western blot following procedure described in ref. [212]. Oral cancer cells (4451) were collected by scrapping petridishes following treatment with free curcumin or cur-SiNp in dark for 4 h or after irradiation with light. After washing once, cells were lysed using lysis buffer (100 mM NaCl, 500 mM Tris, pH 8.0, 10% SDS (wt/vol) and protease inhibitors, AEBSF, Aprotinin, Pepstatin and Leupeptin). The protein concentration of cell lysate was determined by the BCA protein assay. Protein (50 μg) of each treated sample was solubilized in 2× sample buffer and electrophoresed on SDS PAGE. Separated proteins were transferred onto a nitrocellulose membrane and detected by incubating with primary antibodies against NF-κB p50, VEGF, TNF-α, and MMP-9 for 2 h and with HRP conjugated secondary antibody for 1 h; a conjugated antigen–antibody complex was detected by DAB reagent. The bands obtained were quantified using the GeneTools software (Syngene, UK).

2.16.3. Estimation of lipid peroxidation in tissue homogenate

Lipid peroxidation was estimated by determining the level of TBARS following the method of Placer et al [213]. After 72 h of injection of void SiNp (3 mg/kg weight) in mice, animals were sacrificed. Liver tissues were weighed. Tissues were suspended in phosphate buffer (0.1 M, pH 7.4) homogenized for 10 min. Homogenized samples were centrifuged and then homogenate

(200 µl) was deproteinised by adding 500 µL of 5% (w/v) chilled TCA. Samples were incubated for 30 min at room temperature. To this mixture 500 µL of 0.67% TBA was added and the mixture was centrifuged at 5000 rpm for 15 min. The supernatant was collected and placed in a boiling water bath for 20 min. The absorbance of the pink colour developed was measured at 532 nm by using a UV–visible spectrophotometer. The concentrations of TBARS were calculated by using the molar extinction coefficient 1.56 X 10^5 $M^{-1}cm^{-1}$. Protein content from same cell homogenate was determined by BCA method. The lipid peroxides detected were expressed in nmoles/mg of protein.

2.16.4. Measurement of GSH in tissue homogenate

The reduced glutathione (GSH) in the liver tissue homogenates were determined using DTNB method following method reported in ref. [214]. This method is based on a chemical reaction between GSH and DTNB which generates a yellow colored product formed due to glutathione disulfide (GSSG) and 5-nitro-thiobenzoic acid. Liver tissue homogenates (oragans resected after 72 h from mice injected with different formulations of PPa) prepared and deproteinised as described in section 2.16.3**.** The protein precipitate was removed by centrifugation at 5000 rpm for 10 min. To 100 µl of supernatant, 100 µl of PBS and 50 µl DTNB (10 mM) were added and the mixture was incubated for 30 min at room temperature and the absorbance of the mixture was read at 412 nm by using a spectrophotometer. GSH content was determined and normalized with the protein content as (mM/mg of protein).

2.17. Histological analysis

2.17.1. Spheroid

Spheroids subjected to different treatments (free curcumin, cur-SiNp in dark as well as on exposure to light) were fixed with 4 % formaldehyde for 24 h. The samples were dehydrated in ethanol gradients up to 100 % ethanol for 1-2 h followed by xylene (100%) and then xylene: ethanol (1:1) for 30 min then again by 100% xylene for 30 min twice. Spheroids were transferred to mixture of xylene, liquid paraffin and bee wax in ratio of (1:1:1) for 1 hour at 80 °C temperature. Then mixture was transferred to mixture of paraffin wax and bee wax (1:1) at 80 °C for 30 min. Spheroids was then embedded in paraffin wax. Sections of 4 μm were cut using a microtome. Subsequently, these sections were stained with hematoxylin and eosin according to the standard protocol. The section were stained with alum hematoxylin then rinsed with running water, and then stained with eosin for 2 min, sections were dehydrated, mounted. Images of sections were observed by optical microscopy.

2.17.2. Tissue

Liver and kidney tissues resected at 72 h or 360 h after mice were injected with void Np or FR-Np and untreated mice were fixed in 10% neutral buffered formalin after dissection. Tissue sample processed as described above and stained by Hematoxylin and eosin (H&E) and observed under an optical microscope.

CHAPTER 3

EVALUATION OF PHOTOTOXICITY OF CURCUMIN LOADED IN ORGANICALLY MODIFIED SILICA NANOPARTICLES ON HUMAN ORAL CANCER CELLS

3.1. Introduction

As discussed in Chapter 1, curcumin is well known for its antioxidant, anti-inflammatory, cancer preventive and chemotherapeutic properties [215, 216]. In addition, curcumin also exhibits photosensitizing activity [173]. This property has been explored for enhancing its anticancer effects and antibacterial activity [173, 217]. Nevertheless, the therapeutic effectiveness of curcumin is hampered due to its low bioavailability under *in vivo* conditions. The reasons for this include poor solubility in water, lack of stability at physiological pH and rapid metabolism when taken orally [112, 131].

For superficial cancers like cancer of the oral cavity, since curcumin can be applied locally, its photosensitizing effect may be explored for improving its therapeutic effect. However, curcumin being hydrophobic in nature, it needs to be suitably formulated for local application. To enhance the aqueous solubility of curcumin, it has been encapsulated in liposomes [218], polymeric nanocarriers [219] and lipid-based nanoparticles [158, 220]. Among the different nanoformulations of curcumin such as non-ionic micelles, cyclodextrin, liposomes and alginate tested for photodynamic application in mammalian cells, liposomal preparation has been reported to be the most efficient [175]. Although, liposomes are good carriers, drug loading in these particles is poor [221] and also these are prone to microbial attack. To overcome these drawbacks, biocompatible inert Nps are being explored as drug carriers.

As reported in chapter 1, organically modified silica nanoparticles (SiNp) are emerging as promising delivery systems for genes and photodynamic drugs that are investigated in therapy and diagnosis [96, 222]. These offer several advantages such as aqueous solubility, resistance to pH changes, stability under *in vivo* conditions, [108]. These have hydrophobic core because of

which hydrophobic drugs can be entrapped inside these particles, targeting biomolecules like antibodies to receptors can be conjugated to these through surface functionalized chemical groups [88] or drugs can be covalently conjugated to functional groups. Also these are optically transparent [94]. In addition, these particles have excellent storage stability and are resistant to contamination. Since SiNp have hydrophobic core, it is expected that water insoluble drugs like curcumin form stable complexes with these particles.

In this chapter, we have presented results of our investigation on the efficacy of SiNp for delivery of curcumin (cur-SiNp) in squamous cell carcinoma cells derived from oral cavity (4451). The cytotoxicity, uptake, and photodynamic efficacy of cur–SiNp complexes and the effect of photodynamic stress induced by these complexes on the expression of transcriptional factors in oral cancer cells have been compared with free curcumin.

3.2. Experimental methods

3.2.1. Nanoparticle and curcumin loading in SiNp

Details of procedure used for preparing SiNp and cur-SiNp complex are described in chapter 2. Concentration of SiNp used for loading curcumin was 100 µg/ml. Concentration of curcumin used is 25 µM.

3.2.2. Cellular uptake of curcumin

The cell line used in this study is human squamous cell carcinoma (4451). Cells grown on 24-well plates were incubated with 25 µM of either free curcumin or its SiNp complex for 1, 2, 4

and 20 h in dark. Curcumin from cells was extracted using methanol after washing the unbound curcumin and quantitated by fluorescence spectroscopy. Details are described in chapter 2.

3.2.3. Fluorescence microscopy

Intracellular accumulation of curcumin was studied by incubating cells grown on cover slips with either 10 or 25 µM of free curcumin and its SiNp complex for 1 h. Fluorescence of curcumin was monitored using fluorescence microscope using blue excitation filter. The detailed procedure is described in chapter 2.

3.2.4. Cytotoxicity

3.2.4.1. Toxicity of SiNp

To determine the safe concentration of SiNp to be used for loading curcumin for cellular studies, cytotoxicity of void SiNp (drug free) was assessed. Cells grown in 96-well culture plate were incubated with SiNp (50 µg/ml-150 µg/ml). After 24 h, growth medium containing SiNp was removed, wells were washed once with PBS and the MTT assay was performed as described chapter 2.

3.2.4.2. Toxicity of curcumin in dark and light

For assessing dark as well as phototoxicity of curcumin, $5X10^4$ cells were seeded in each well of 96-well culture plates. After 24 h, cells were incubated in a growth medium containing 25 µM of free curcumin and equivalent concentration of curcumin mixed with SiNp (100 µg/ml). After a specified time (1 or 4 h), the medium containing free and cur-SiNp was replaced with a fresh medium (not containing phenol red) and then exposed to white light for different durations. For

studying dark toxicity cells were treated with either 25 µM of free curcumin or its SiNp complex (1 or 4 h) but not exposed to light. Control cells were neither treated with curcumin nor exposed to light. Microplates were incubated for 20 h after treatment and then MTT assay was performed. Details of light source and procedure of MTT assay followed is described in chapter 2.

3.2.5. Live and Dead Assay

Cells (1×10^6) grown in 24 well plates for 24 h were treated with 25 µM free curcumin or its SiNp complex for 4h and then exposed to light (20 J/cm^2). After 3 h of post irradiation, live/ dead assay was performed to study membrane integrity. Cells fluorescing green (viable) and cells which showed red fluorescence (dead) due uptake of PI were counted separately in different microscopic fields. The details of the procedure followed are described in the chapter 2.

3.2.6. Western blot analysis

Western blot analysis was done to study the effect of photodynamic stress induced by free and nanoformulated curcumin on NF-kB and related gene products (MMP-9, VEGF and TNF-α) in 4451 cells following procedure described in chapter 2.

3.2.7. Statistical analysis

All the experiments were repeated at least three times. Data was represented as mean ± standard error of the mean (SEM) of three experiments. A t-test was used to compare the statistical difference among the groups. P value <0.05 was considered as statistically significant.

3.3. Results

3.3.1. Cytotoxicity of void SiNp

In order to determine the safe concentrations of SiNp to be used for curcumin loading for cellular experiments, concentration and incubation time dependent effect of SiNp (void) on cell viability was studied. Viability of cells treated with SiNp upto 100 µg/ml for 72 h did not change significantly. However, reduction in viability (35%) was observed when cells were treated with 150 µg/ml of SiNp (Table 3.1).

SiNp (µg/ml)	Viability (% untreated control)
0	100
50	93.07±2.72*
100	92.27±2.73*
150	65.07±6.33

Table 3.1: Viability of 4451 cells treated with different concentrations of SiNp for 24 h. Viability was measured by MTT assay following treatment *$p<0.05$, with respect to untreated control.

3.3.2. Physicochemical characterization of curcumin-SiNp complex

Absorption and fluorescence spectra of curcumin post loaded in SiNp (cur–SiNp complex) and free curcumin in aqueous solution are shown in Figure 3.1 (a & b). The nature of absorption spectra of cur–SiNp was similar to free curcumin except that the absorbance at peak (426 nm) was higher. However, fluorescence spectra of cur–SiNp complex showed a blue shift (~45 nm) in the fluorescence peak with ~5 times enhancement in intensity as compared to free curcumin. The size and surface charge determined by dynamic light scattering and zeta potential measurements of drug free (void) SiNp were ~32 nm and −39 ± 1.0 mV, respectively. No significant change in zeta potential was noted when curcumin was post loaded.

(a)

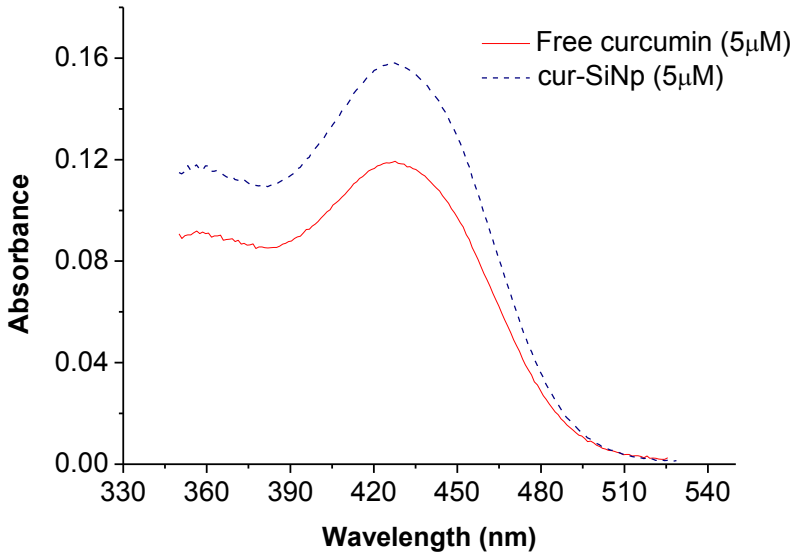

(b)

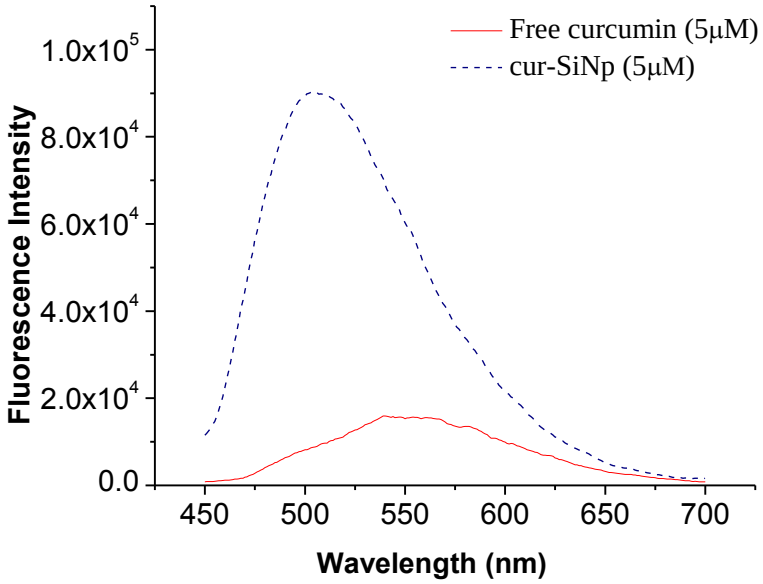

Figure 3.1: (a) Absorption and **(b)** fluorescence emission spectra of free curcumin and cur–SiNp complex in aqueous solution.

3.3.3. Cellular accumulation of curcumin

3.3.3.1. Fluorescence microscopic study

It is important to determine the cellular uptake of curcumin to assess the efficacy of delivery vehicle. Therefore, incubation time and concentration dependent uptake of free and cur-SiNp complex by cells was studied by fluorescence microscopy. Cells were incubated with SiNp (100 μg/ml) containing different concentrations of curcumin and equivalent concentrations of free curcumin. Within 1 h of incubation, curcumin fluorescence was observed in cells treated with either free curcumin or cur–SiNp complex at concentrations 10 and 25 μM respectively. Cells treated with 10 μM cur-SiNp complex showed stronger fluorescence after 1h of incubation

(Figure 3.2 c) as compared to cells incubated with free curcumin (Figure 3.2 a). At higher concentration of curcumin (25 μM), stronger fluorescence of curcumin was observed throughout the cells whereas in cells treated with free curcumin, fluorescence was weaker (Figure 3.2 b). This indicated that the uptake of curcumin from SiNp complex is higher than the free curcumin.

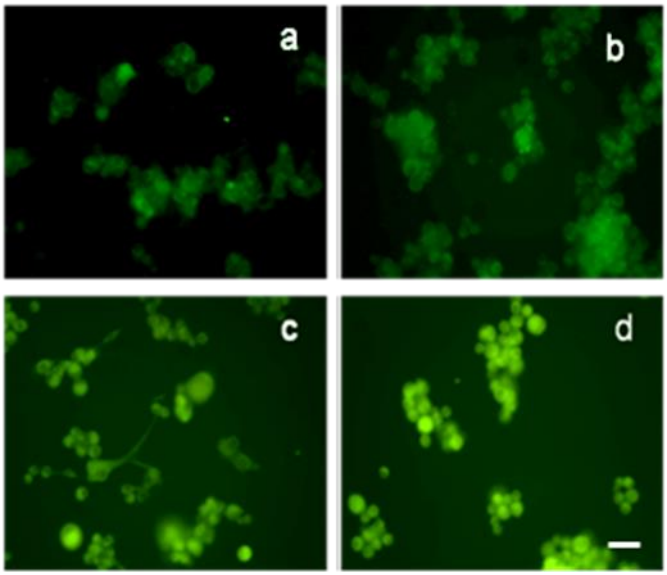

Figure 3.2: Fluorescence microscopic images of 4451 cells treated for 1 h with (a) 10 μM and (b) 25 μM of free curcumin and (c) 10 μM and (d) 25 μM of cur–SiNp complex. Scale bar: 50 μm**.**

3.3.3.2. Quantitation of uptake

To quantify the time-dependent uptake, curcumin was extracted from cells incubated with 25 μM of free curcumin or its SiNp complex (25 μM) for different time durations using methanol. Curcumin fluorescence from the methanol extracts was measured by fluorescence spectroscopy (Figure 3.3). As compared to free curcumin, in cells incubated with cur-SiNp, the drug uptake increased with incubation time (up to 4 h), and at this time point, the uptake of curcumin complexed with SiNp was ~5 times higher. However, the uptake of both free curcumin and cur–

SiNp decreased at longer incubation time (20 h). To check the stability of free and nanoformulated drug, free curcumin and cur–SiNp complex incubated in PBS at pH 7.4 for different durations were examined by measuring absorption of curcumin. As seen in (Figure 3.3, inset), compared to free drug, degradation of curcumin in SiNp complex was slower; however, at longer incubation time, difference in rate of degradation was much less.

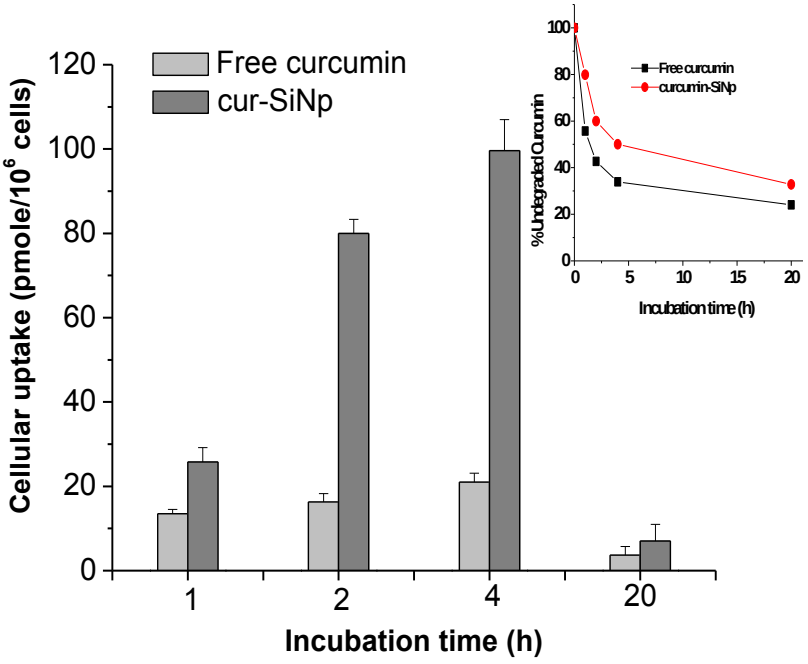

Figure 3.3: Uptake of curcumin in 4451 cells incubated with 25 μM of free curcumin or cur–SiNp complex containing equivalent concentration of curcumin for different durations. The inset shows stability of 10 μM of free curcumin and cur–SiNp complex containing equivalent concentration of curcumin in PBS (pH 7.4) at different time points.

3.3.4. Cytotoxicity of curcumin with and without light treatment

Figure 3.4 shows the cytotoxic effect of free curcumin (25 μM) and cur–SiNp complex with and without exposure to visible light on 4451 cells. Cells were incubated for 1 and 4 h in dark before exposing to light. In all the experiments, 100 μg/ml of SiNp was used for curcumin loading. Incubating cells with only SiNp, free curcumin or cur–SiNp complex in the dark for 1 h did not lead to any significant change in viability. Dark toxicity of cells incubated with cur-SiNp complex for 1 h was about ~10 %. However, exposure of these cells to light (12 J/cm^2) reduced the viability to ~58 %. On the other hand, at similar light dose in cells treated with free curcumin, viability reduced only by ~13 %. Exposure of cells to light without any treatment did not reduce the viability. We also investigated the effect of varying incubation time of nanoformulated curcumin on cytotoxicity with and without exposure to light. As expected, dark toxicity of cur-SiNp complex increased with increase in incubation time (Figure 3.4). About ~40% cell death was observed in cells treated with 25 μM cur-SiNp complex for 4h. Exposure of these cells to light (~12 J/cm^2) increased the cell death to more than 80%. On the other hand, increasing incubation time did not have significant influence on the viability of cells pretreated with similar concentration of free curcumin. On exposure to light, cell death in free curcumin treated cells enhanced only by ~20%. Increasing the light dose did not enhance death in cells pretreated with either free or cur-SiNp complex significantly at both the incubation time points (1 and 4 h). This may be due to photobleaching of curcumin.

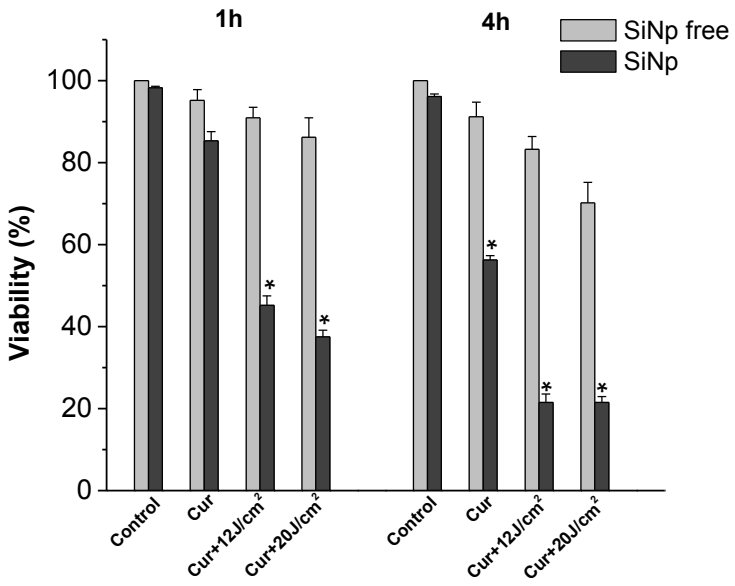

Figure 3.4: Viability of 4451 cells treated with 25 μM of free curcumin and equivalent concentration of cur–SiNp complex for 1 and 4 h in the dark and then exposed to light. Viability of cells after different treatments was compared with untreated controls. *$p<0.05$, with respect to free curcumin.

3.3.5. Phototoxicity of curcumin on membrane integrity

To study the effect of treatment of free and its SiNp complex on cell membrane, Live/Dead assay was performed (Figure 3.5). Cells incubated with free curcumin for 4 h in the absence of light showed predominantly green fluorescent cells (~97 %), indicating more number of viable cells with intact membrane (left: upper panel). In cells treated with cur–SiNp complex in the dark some cells (~15 %) showed red fluorescence (nonviable). On the other hand, cells exposed to light (20 J/cm^2) after 4 h of incubation with cur–SiNp complex showed predominantly red fluorescent cells (~70 %) as compared to cells treated with a similar concentration of free

curcumin and light dose (~20 %) and to cells exposed to cur–SiNp complex in the dark. This indicated extensive plasma membrane damage in this group. Addition to this, phase-contrast images showed extensive morphological alterations in cur–SiNp treated cells following photodynamic treatment, indicating necrotic cell death due to membrane damage.

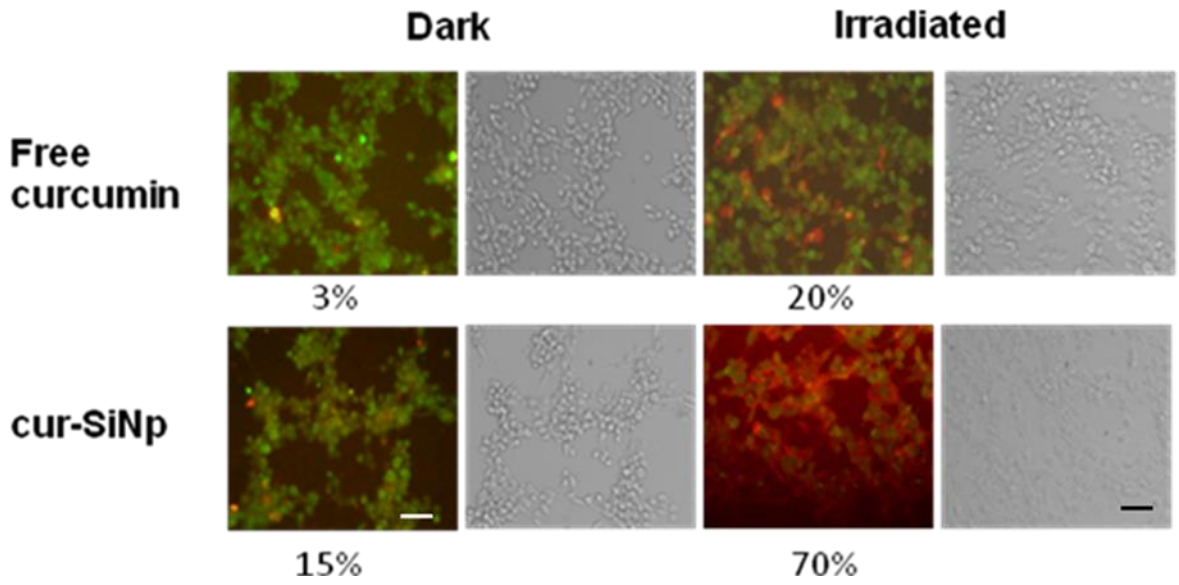

Figure 3.5: Fluorescence and phase-contrast images of 4451 cells stained with Live/Dead stain after incubation with 25 μM of free curcumin and cur–SiNp complex containing equivalent concentration of curcumin in dark for 4 h and then irradiated with light (20 J/cm^2). Nonviable cells (in percent) observed due to treatments are shown below each fluorescence image. (Scale bar: 50 μm).

3.3.6. Effect of photodynamic action of curcumin on transcriptional factor

NF-kB, a transcription factor regulates the expression of genes involved in cellular proliferation, inflammation, tumor metastasis, angiogenesis and stressful stimuli such as oxidative stress [223]. To understand the cellular responses to photodynamic stress, NF-kB and its related gene

products were studied in cells treated with 25µM of free curcumin and its SiNp complex after exposure to 20 J/cm^2 light dose.

The results presented in Figure 3.6, show strong intensity of NF-kB in extracts of whole cells not treated with curcumin. Band intensity of NF-kB reduced by ~25% in cells treated with free curcumin as compared to untreated controls and much higher (~50%) inhibition was observed in cells treated with cur-SiNp complex.

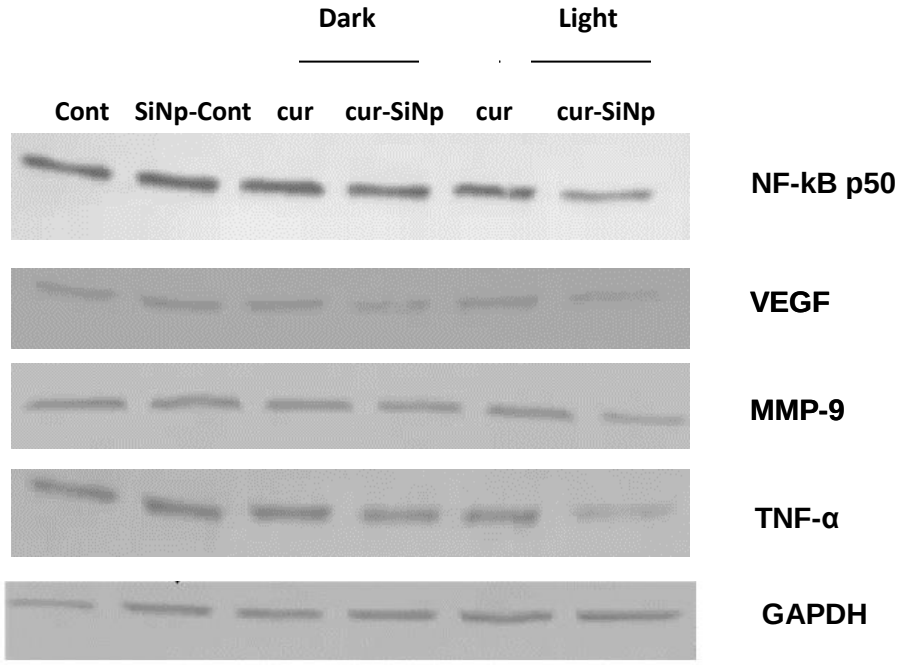

Figure 3.6: Effect of treatment of 4451 cells with free curcumin or cur–SiNp complex in dark and after irradiation on NF-kB, VEGF, MMP-9 and TNF-α. Cells were irradiated (20 J/cm^2) after incubating cells with 25 µM of free curcumin and cur–SiNp for 4 h in the dark.

On exposure to light, in both free curcumin and its SiNp complex treated cells, NF-kB band intensity reduced further. The decrease was more (~66% reduction) in cells treated with

nanoformulated curcumin. We also examined the effect of free curcumin and its SiNp complex before and after light exposure on NF-kB regulated gene products VEGF, MMP-9 and TNF-α which are involved in angiogenesis, metastasis and inflammation. We observed less intense bands of VEGF, MMP-9 and TNF-α in light exposed cells pretreated with cur–SiNp complex as compared to cells exposed to free curcumin and light.

3.4. Discussion

In this chapter, we have described use of SiNp for improving the uptake and phototoxicity of curcumin in oral cancer cells. The porous matrix of SiNp facilitated post loading of curcumin. Results presented in Figure 3.1, show that whereas free curcumin, gets aggregated in aqueous media as evidenced by reduction in fluorescence peak intensity and red shift, curcumin in nanoformulation, remain uniformly dispersed. This is confirmed by the blue shift and enhancement in the fluorescence peak intensity of curcumin. Similar spectral changes have been noted when curcumin is bound to hydrophobic domains in phosphatidylcholine, liposome, human serum albumin [208] and in glycerol monooleate based nanoparticle [212]. It should be noted that no significant change in zeta potential and size was observed when curcumin was post loaded in SiNp. This confirms that curcumin is in hydrophobic core of SiNp and do not influence the charge of SiNp.

Our data on cytotoxicity (Table 3.1) indicates that drug free SiNp at concentrations below 150μg/ml do not cause toxicity in oral cancer cells which implies that these nanoparticles do not interfere with cell survival when used at 100 μg/ml concentration. Indeed, no toxicity was

observed in larvae of Drosophila melanogaster fed with SiNp (ORMOSIL) upto 0.2, 0.4 and 1 mg/ml although particles were shown to get incorporated into living neuronal cells [108].

Higher uptake of curcumin observed in cells incubated with nanoformulated curcumin at shorter durations could be due to enhanced permeation of cur-SiNp complex (Figure 3.3). Curcumin being in hydrophobic environment in SiNp is protected from rapid degradation (Figure 3.3; inset). Also due to small size, cur-SiNp complex is expected to get internalized in cells faster. Previous studies have shown that silica nanoparticles are internalized rapidly by cells [224] as compared to studies reported in curcumin entrapped in polymeric nanoparticles [219]. Additionally, since curcumin is hydrophobic it may get released rapidly from SiNp through its porous matrix when internalized nanocomplexes are localized in membranes of subcellular organelles. This contention is consistent with strong fluorescence of curcumin observed in cells incubated with cur-SiNp complex (Figure 3.2; panels c & d). The observed decrease in uptake at longer incubation time (20 h) is attributed to higher loss of cell viability as compared to free curcumin. The results presented in Figure 3.4, show that incubation time dependent increase in dark toxicity observed is consistent with higher uptake of curcumin from nanoformulation (Figure 3.3) as compared to free drug which could have inhibited cell proliferation and induced cell death. It has been shown that curcumin inhibits cell proliferation and survival associated kinases, such as phosphatidylinositol-3-kinase/AKT signaling [225, 226] and epidermal growth factor receptor (EGFR) signaling [227] and induces apoptosis in a variety of cells. Manifestation of these effects depends on concentration, incubation time and also cell sensitivity. High uptake of curcumin could have caused excess of oxidative stress on exposure to visible light in presence of oxygen via formation of highly reactive singlet molecular oxygen ($^1O_2$), and superoxide (O_2^-) and curcumin radicals [169, 228]. This could have contributed to increased cell death in cur-

SiNp treated cells as compared to free curcumin. In contrast to our results, other studies have reported phototoxicity of curcumin at much lower concentration than used in this study. A study carried out in Rat submandibular salivary gland acinar cells has shown that curcumin at 0.4 µM and 0.7-13.5µM in liposomal and cyclodextrin formulation respectively are effective in inducing cell death at a light dose of 6 J/cm^2 [175]. In another study, significant reduction in viability of human epidermoid carcinoma cell line (A431) was reported when cells are treated with 2 µg/ml curcumin dissolved in DMSO and exposed to 1 J/cm^2 visible light [174]. However, in these studies cells were exposed to light and curcumin simultaneously in PBS along with cell unbound drug. In this irradiation procedure, reactive intermediates such as curcumin radicals formed in the bulk phase would also contribute to toxicity [169]. However, for localized photodynamic therapy it may be more appropriate to remove the unbound drug to avoid the possible cell damage to surrounding normal cells. It should be noted that in our study since unbound curcumin was removed before irradiation, the intracellular concentration of curcumin which contributed to phototoxicity was only in picomolar range.

The reason for observed necrosis in cur-SiNp treated cells in the dark and due to photodynamic treatment (Figure 3.5) could be due to localization of curcumin in the hydrophobic pockets of membranous structure in cells [112, 218] which might have led to alterations in membrane functions. Studies on curcumin in model membranes (micelles) have shown formation of curcumin radicals and its ability to chelate cations even in absence of light [229]. These properties may affect functions of membrane bound enzymes and also augment sensitivity of cells towards light induced reactions. In addition, short lived ROS such as $^1O_2$ generated on exposure to light in these regions could have caused structural damage to membrane resulting in necrosis. Extensive necrosis observed in cur-SiNp complex treated cells is attributed due to

increase in concentration of reactive oxygen species generated due to enhanced accumulation of curcumin in cells.

Results presented in Figure 3.6 show that in oral cancer cells (untreated) active NF-kB is expressed constitutively and consistent with other studies reported in head and neck squamous cell carcinoma [230]. Decrease in NF-kB expression in cells treated with cur-SiNp in dark could be due to loss of cell survival. Curcumin, at high concentrations in dark has been shown to inhibit the expression of prosurvival transcription factor NF-kB in various cell types by blocking phosphorylation of IkB and p65 and subsequent translocation of NF-kB into nucleolus [231]. However, ROS generation has been shown to activate NF-kB that lead to inflammatory response [232]. In contrast to these findings, results of this study showed that exposure of curcumin treated cells on exposure of light down regulated the NF-kB expression further as compared to cells treated with curcumin in dark (Figure 3.6). This observation is in agreement with results reported on inhibition of NF-kB activity in HaCaT cells subjected photodynamic treatment using 0.2 µg/ml curcumin and light. However, in these cells NF-kB inhibition facilitated apoptosis [167]. Nevertheless, necrosis observed in curcumin treated cells after light exposure in this study implies the reduced expression of NF-kB is more likely due to damage of NF-kB transcriptional factor which might have occurred due to excess oxidative stress generated during light irradiation as result of increased drug uptake from cur-SiNp complex. The induction of necrosis together with down regulation of NF-kB gene products confirmed the damage to NF-kB due to higher uptake of curcumin. This correlated with enhanced cytotoxicity induced by nanoformulated drug.

3.5. Conclusion

In summary, we have shown that uptake and cytotoxic effects of curcumin loaded in SiNp is higher for oral cancer cells as compared to free curcumin which is due to its increase in aqueous solubility and stability at physiological pH. In addition, photodynamic activity of curcumin in nanoformulation is enhanced as indicated by increase in cell killing, and down regulation of NF-kB activity. Enhanced accumulation of nanoformulated curcumin in oral cancer cells and its increased photodynamic activity suggest that SiNp could be a useful delivery vehicle especially for topical application of curcumin for photodynamic treatment of oral malignancies.

CHAPTER 4

EVALUATION OF PHOTOTOXIC EFFECTS OF CURCUMIN LOADED IN ORGANICALLY MODIFIED SILICA NANOPARTICLES ON TUMOR SPHEROIDS OF ORAL CANCER CELLS

4.1. Introduction

Although nanocarriers have been demonstrated to improve efficacy of chemotherapeutic and photosensitizing drugs used in cancer therapy by offering several advantages such as targeted delivery [233], protection against degradation of drugs under physiological conditions, facilitate delivery of insoluble agents [234], accumulation of nanocarriers under *in vivo* conditions remains a concern due to limited penetration into avascular tumor compartments. Studies suggest that size of the Nps plays a critical role in their penetration and retention within the tumor tissue [235-237]. Generally monolayer cultures (2-D cultures) are used for testing the efficacy of nanocarriers. Although many of the Nps including gold and SiNps of sizes upto ~50 nm have been shown to be internalized efficiently in monolayer cells, results observed in two dimensional culture models do not translate similar results *in vivo* [238-241]. This is due to the inherent limitations of monolayer cultures such as absence of three dimensional organization, extracellular matrix (ECM), phenotypic differences, complex biochemical and biomechanical environment as present *in vivo* [242]. To more accurately predict the *in vivo* efficacy, nanocarriers need to be screened by using three dimensional culture systems. Multicellular tumor spheroids models reflect the *in vivo* situation as these have closely packed cells with extracellular matrix, gradients of nutrients, oxygen, and wastes. As a result, spheroids contain heterogeneous regions of tumor cell growth, including a proliferating region, a quiescent region, and a necrotic core which may have different responses to drugs [242, 243].

In the previous chapter, we have presented results on evaluation of efficacy of SiNp for delivery of curcumin in oral carcinoma cells (4451) grown in monolayer [244]. Our study showed that the phototoxic effect of curcumin could be improved significantly when drug was loaded in SiNp

due to lower degradation of curcumin and higher uptake as compared to free curcumin. Also cells treated with nanoformulated curcumin showed reduced expression of NF-kB, a key transcription factor related to growth and invasiveness of cancer. However, since the size of nanoformulated curcumin is larger than the free curcumin, efficacy of its accumulation and cytotoxicity induced in tumor which has complex environment may therefore vary. In this chapter, results of investigations on uptake and phototoxic efficacy of cur-SiNp complex in tumor spheroids of oral cancer (Squamous cell carcinoma, Nt-8e) cells which mimic avascular tumors are presented. Effect of free curcumin and nanoformulated curcumin on growth, migration of cells in spheroids was also investigated as gradients of oxygen and nutrient concentration results in changes in gene and protein expression involved in proliferation and migration [242].

4.2. Experimental methods

4.2.1. Preparation of cur-SiNp complex

SiNps and cur-SiNp complex were prepared and characterized as reported in chapter 2.

4.2.2. Curcumin uptake in spheroids

Nt-8e cells (human squamous cell carcinoma derived from upper aero-digestive tract) were grown in monolayer and as spheroids. Small (195 ±10 µm thick) and big (365 ±10 µm thick) spheroids were incubated in growth medium containing 25 µM of either free curcumin or cur-SiNp complex with equivalent concentration of curcumin for 4 and 24 h. Curcumin accumulated in the spheroids was extracted by using methanol and quantitated by measuring its absorbance at 420 nm using a microplate reader (Biotech Instrument Power Wave 340, USA). Detailed procedure used is described in chapter 2.

4.2.3. Phototoxicity of free and nanoformulated curcumin

Spheroids grown for 3 or 7 days were incubated in a growth medium containing either 25 μM of free curcumin or SiNp loaded with similar concentration of curcumin at 37 ^{0}C for 24 h. Wells containing spheroids were replaced with fresh medium without phenol red after washing with PBS and exposed to blue light (~460 nm) for different durations. To study if ROS was involved in the phototoxicity, in some experiments spheroids were irradiated in presence of GSH (1 mM), a ROS scavenger. Spheroids were incubated with GSH for 4 h prior to light exposure. Viability of cells in spheroids subjected to different treatments was assessed after 24 h by MTT assay. Details of light source used for irradiation and the procedure of MTT assay followed are described in chapter 2.

4.2.4. Detection of ROS generation

For evaluating ROS generation induced by curcumin and light treatment, spheroids treated with 25 μM of either free curcumin or cur-SiNp complex for 24 h in the dark or exposed to light (10 J/cm^2) after incubation with different formulations of curcumin were incubated in growth medium containing 10 μM H2DCFDA for 30 min at room temperature. Fluorescence of DCF was monitored by fluorescence microscopy. Detailed procedure used is described in chapter 2.

4.2.5. Mode of cell death

Spheroids treated with 25 μM of either free curcumin or cur-SiNp complex for 24 h in the dark or exposed to blue light (10 J/cm^2) after incubation with different formulations of curcumin were stained with PI (10 μg/ml) and hoechst (20 μg/ml) for 15 min at 37 °C. Stained spheroids (intact)

or after dissociation were examined under fluorescence microscope (Olympus, Japan) using appropriate emission filters. Details are described in chapter 2.

4.2.6. Post treatment growth and migration

For studying post treatment growth, spheroids treated with 25 μM of free curcumin or its SiNp complex in dark (24 h) or subjected photodynamic treatment (light dose 20 J/cm^2) in presence or absence of GSH were placed in agarose coated 96-well plate again after washing with PBS. Single spheroid was placed in individual well. Growth of spheroid was monitored upto 7 days using a phase contrast microscope.

To study migration of cells subjected to different treatments, spheroids were transferred to 24 well plates without agarose coating and incubated at 37 °C. Migration of cells from spheroids was assessed microscopically. All procedures are described in detail in chapter 2.

4.2.7. Histology

Spheroids treated with 25 μM of free curcumin or its cur-SiNp complex in dark or irradiated with light (10 J/cm^2) were fixed with 4% formaldehyde for 24 h and processed for histology. Morphology of cells in the spheroids was observed under microscope. Detailed procedure followed for histology is described in chapter 2.

4.2.8. Statistical analysis

All the experiments were repeated at least three times. In each experiment at least three spheroids (n=3) for each data point. Data was represented as mean ± SEM of three experiments. A t -test

was used to compare the statistical difference among the groups. P value <0.05 was considered as statistically significant.

4.3. Results

4.3.1. Uptake of free curcumin and its complex by spheroid

In Figure 4.1 A, we show the quantity of curcumin accumulated in small and big spheroids after incubation with free curcumin or its SiNp complex for different durations. This was determined by measuring the absorbance of methanol extracted curcumin from spheroids. Uptake of curcumin in small spheroids increased with an increase in incubation time for both free as well as nanoformulated curcumin. Compared to free curcumin, the uptake of nanoformulated curcumin was ~1.5 and ~1.7 times higher at 4 and 24 h respectively. In big spheroids uptake of nanoformulated curcumin increased by ~ 1.4 times as compared to free curcumin after 24h of incubation. Between small and big spheroids, no significant difference ($p>0.05$) in the uptake of both the formulations of curcumin was noted. However, when normalized with respect to cell number, uptake of nanoformulated curcumin by small spheroids was significantly ($p<0.05$) higher (~3.9 times, 6.8 nmole/10^6 cells) as compared to big spheroids (1.75 nmol/10^6 cells). In Figure 4.1 B, we show the fluorescence microscopic images of spheroids (small) incubated with either free curcumin or its nanocomplex for 24 h. For 4h incubation time, fluorescence of curcumin from spheroids was similar for both free curcumin and nanocurcumin. However, at 24 h, curcumin fluorescence was stronger in spheroids (small) incubated with nanoformulated curcumin as compared to free curcumin. In agreement with this, the cells dissociated from the spheroids incubated with cur-SiNp complex for 24 h also showed strong fluorescence (Figure 4.1B (d) as compared to free curcumin treated cells.

A)

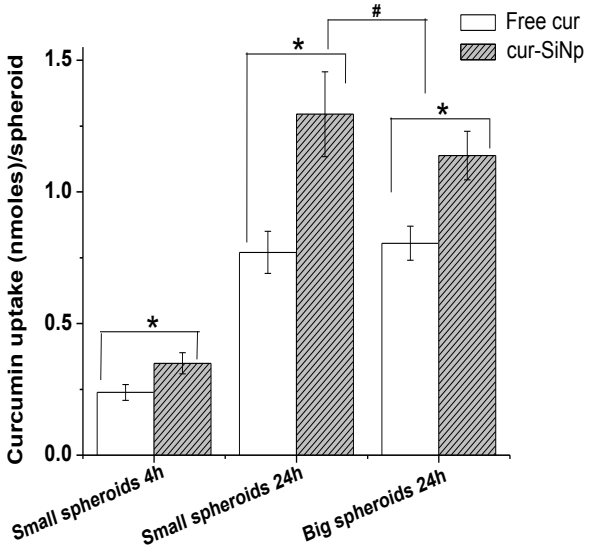

B)

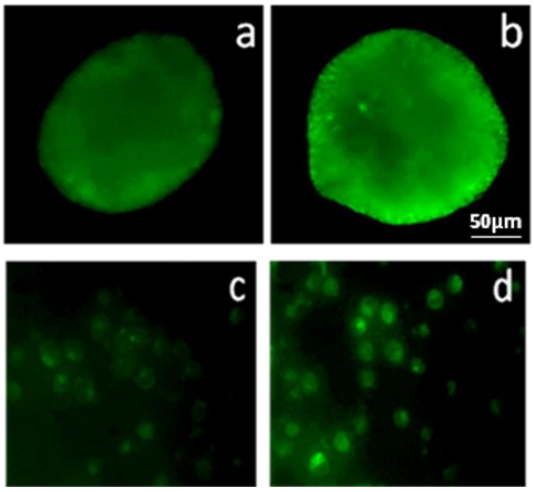

Figure 4.1: (A) Uptake of curcumin in small and big spheroids. Spheroids were incubated with either 25 µM of free curcumin or its SiNp complex for different incubation times. *P < 0.05 & # P > 0.05. **(B)** Fluorescence microscopic images of intact spheroids incubated for 24 h with 25 µM of **(a)** free curcumin, **(b)** cur–SiNp complex; Curcumin fluorescence in cells dissociated from spheroids incubated with 25 µM for 24 h **(c)** free curcumin and **(d)** cur–SiNp complex.

4.3.2. Phototoxicity of free and nanoformulated curcumin

Effect of light exposure on viability of monolayer Nt-8e cells treated with free curcumin (25 μM) or its SiNp complex (25 μM curcumin equivalent) is shown in Figure 4.2 A. The data are compared with the viability of cells in small and big spheroids treated with similar concentration of free curcumin and its SiNp complex for 24 h and then irradiated with light (Figure 4.2 B and C). For monolayer cells incubated with either free curcumin or nanocurcumin in dark, viability reduced by ~30 and ~50 %. After exposure to light (20 J/cm^2), less than ~10% of nanocurcumin treated cells were viable as against ~40% viability observed in free curcumin treated cells under similar conditions. On the other hand, treatment of small spheroids with either free curcumin or its SiNp complex in dark reduced the cell viability by ~14% and ~22% respectively. Significant reduction in cell viability was observed in spheroids treated with either free or nanoformulated curcumin following exposure to blue light. While the cell death was about ~78% in nanocurcumin treated spheroids irradiated at a light dose of 20 J/cm^2, in free curcumin treated spheroids viability reduced by ~39% under similar irradiation condition. Although viability of cells in big spheroids treated with cur-SiNp complex was significantly ($p<0.05$) lower as compared to free curcumin, surviving fraction was much higher in nanocurcumin treated (~58 %) or free curcumin (~69.5 %) treated spheroids as compared to small spheroids. It should be noted that no significant change in viability of cells was observed in spheroids treated with void SiNp (150 μg/ml) as compared to spheroids incubated with either curcumin or void nanoparticles (untreated control).

A)

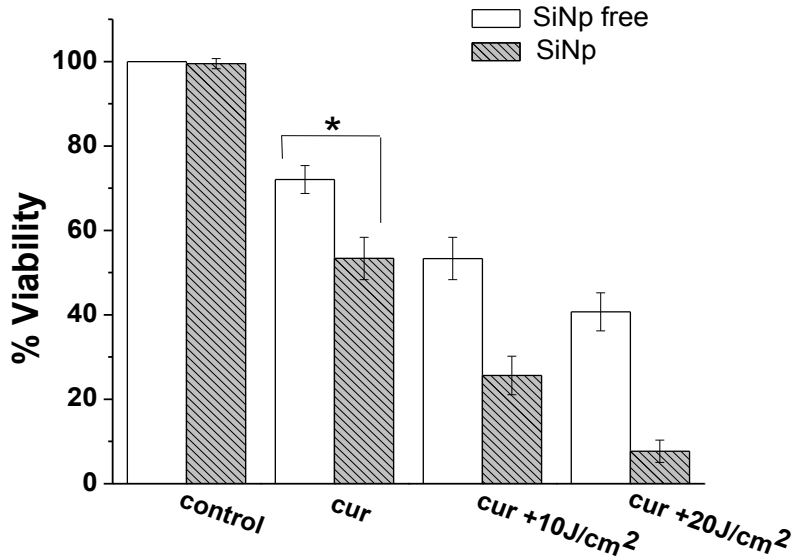
SiNp free
SiNp
% Viability
100
80
60
40
20
0
*
control
cur
cur +10J/cm2
cur +20J/cm2

B)

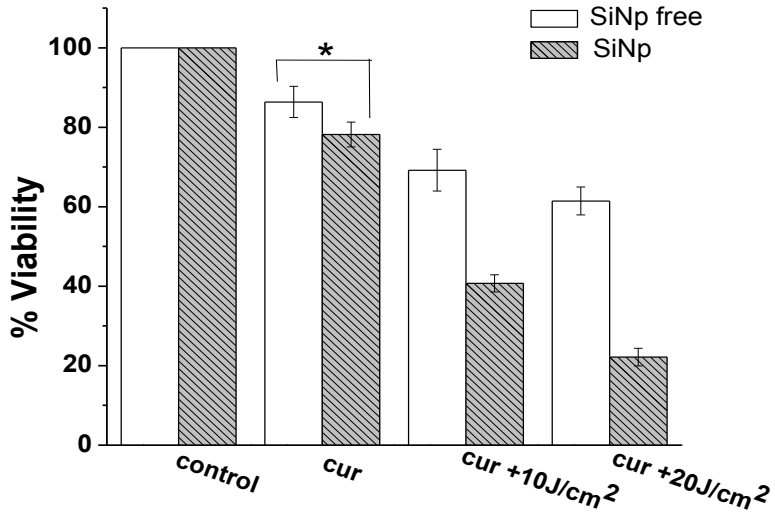
SiNp free
SiNp
% Viability
100
80
60
40
20
0
*
control
cur
cur +10J/cm2
cur +20J/cm2

C)

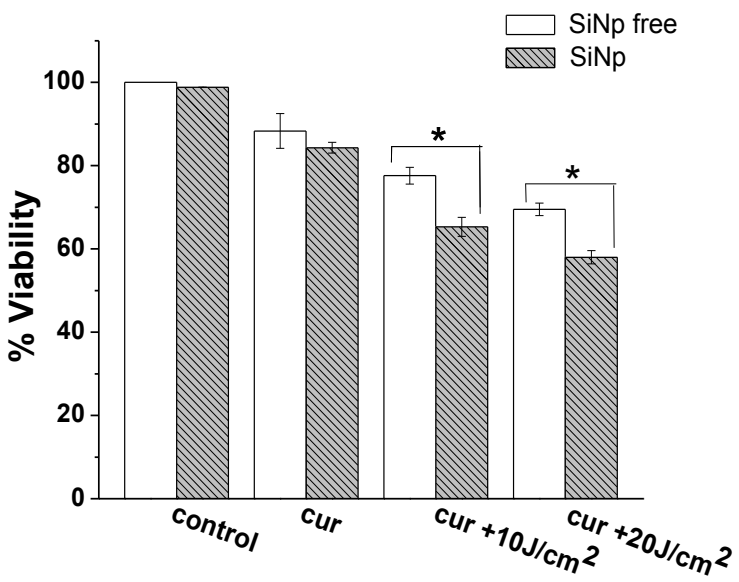

Figure 4.2: Viability of cells treated with 25 μM of free curcumin or equivalent concentration of cur–SiNp complex for 24 h in the dark and then exposed to blue light **(A)** monolayer, **(B)** Small spheroids, **(C)** Big spheroids. Viability of cells assessed by MTT assay in spheroids subjected to different treatments was compared with untreated controls *P < 0.05.

4.3.3. Effect of curcumin and light on ROS generation

To investigate the differences observed in the photodynamic effects of curcumin in two formulations, spheroids (small) subjected to different treatments were stained with H2DCFDA, a probe for detecting ROS (Figure 4.3). In the spheroids treated with free curcumin in dark (25 μM), fluorescence of DCF was weak. This indicated low generation of ROS. Compared to free curcumin, fluorescence of DCF was stronger in nanocurcumin treated spheroids indicating

higher generation of ROS. However, ROS increased remarkably in spheroids treated with cur-SiNp complex after irradiation with blue light (10 J/cm^2) in comparison to free curcumin treated spheroids. We also investigated the effect of two formulations of curcumin and light treatment on ROS generation in big spheroids. ROS was quantitated by measuring the fluorescence of DCF in cells dissociated from the spheroids spectroscopically. The fluorescence intensity of DCF in nanocurcumin treated spheroids after exposure to light (10 J/cm^2) was found to be ~1.24 times higher than the free curcumin treated spheroids under similar conditions.

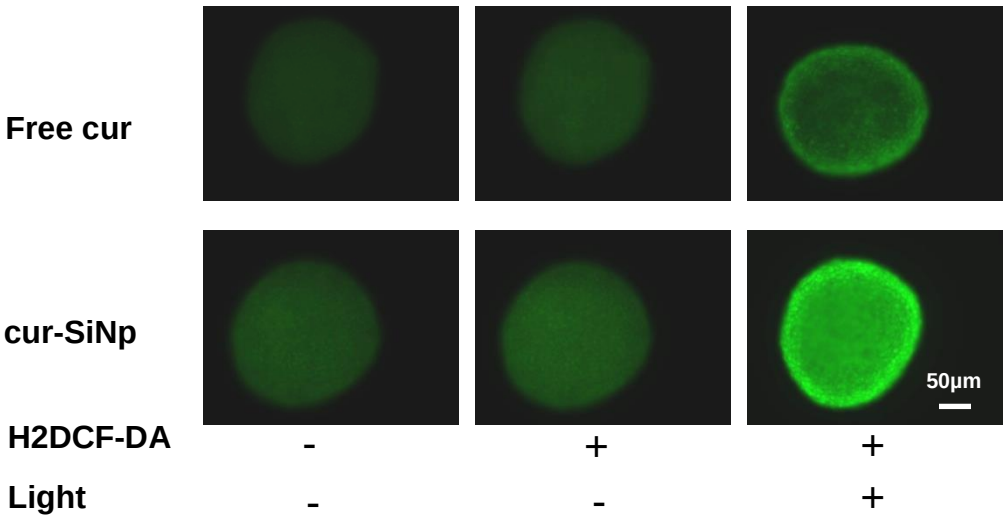

Figure 4.3: Fluorescence images of spheroids stained with H2DCFDA after treatment with curcumin or its nanoformulation in dark and subsequent to light exposure. Spheroids were incubated with 25 µM of either free curcumin or cur–SiNp complex for 24 h in the dark and then exposed to blue light (10 J/cm^2). Treated and untreated spheroids were stained with H2DCFDA (10 µM) for 30 min for evaluating ROS generation.

4.3.4. Phototoxicity in presence of ROS scavenger

To confirm the involvement of ROS in the phototoxic effect induced by different formulations of curcumin, spheroids (small) incubated with either free curcumin or its silica complex were irradiated in presence of GSH (1mM). GSH was chosen because it is a water soluble low molecular weight antioxidant present in cellular compartments and has been used widely to study the involvement of ROS generated in the photochemical reactions of photosensitizers [245-247]. In Figure 4.4, we show the effect of irradiation (20 J/cm^2) of small spheroids treated with different formulations of curcumin in presence of GSH on cell viability.

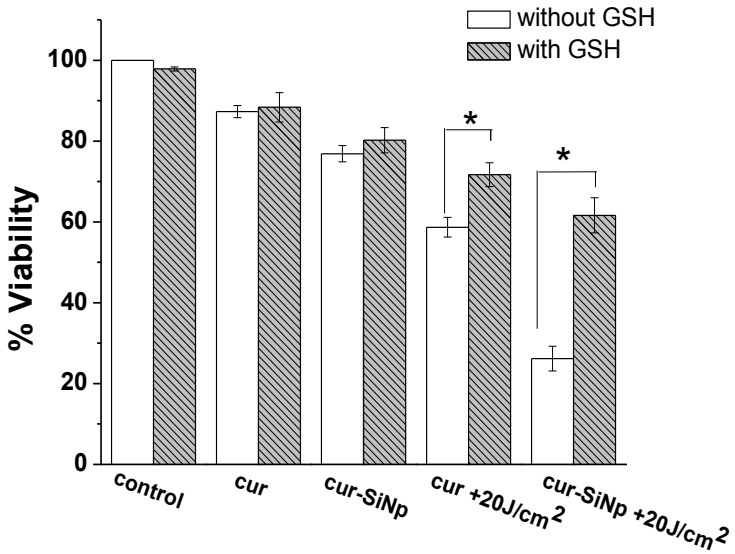

Figure 4.4: Phototoxicity of different formulations of curcumin on spheroids irradiated in presence and absence of GSH. Spheroids treated with 25 μM of free curcumin or equivalent concentration of cur–SiNp complex for 24 h in the dark and then irradiated with blue light (20 J/cm^2) in presence and absence of GSH. Spheroids were incubated with GSH (1 mM) for 4 h prior to irradiation. Viability of cells assessed by MTT assay in spheroids subjected to different treatments was compared with untreated controls *$P < 0.05$.

Viability of cells was higher in spheroids irradiated in presence of GSH after treatment with either free curcumin or cur-SiNp than the spheroids irradiated without GSH. In cur-SiNp treated spheroids, a remarkable difference in cell viability was observed between GSH treated and untreated (without GSH) groups. When cur-SiNp spheroids were irradiated in presence of GSH cell death reduced by ~2 times as compared to spheroids irradiated without GSH. These results indicated involvement of ROS.

4.3.5. Effect of curcumin and light on mode of cell death

Figure 4.5 A shows the spheroids stained with PI and hoechst following photodynamic treatment with either free or cur-SiNp complex. As seen in Figure 4.5 A, compared to untreated and spheroids treated with free curcumin in dark, fluorescence of PI from the surface of spheroids treated with cur-SiNp complex (right panel) was higher. When nanocurcumin treated spheroids were irradiated with light, significant enhancement in PI fluorescence was observed (lower right panel) as compared to spheroids treated with nanoformulated curcumin in dark. These results indicated that nanocurcumin induces extensive membrane damage in cells. To further verify this observation, cells from spheroids subjected to different treatments were dissociated and examined under the microscope. The population of cells with condensed chromosomes (apoptotic) was higher in disaggregated spheroids treated with free curcumin and light, whereas cells with PI uptake was predominant in spheroids treated with nanocurcumin and light after dissociation (Figure 4.5 B).

A)

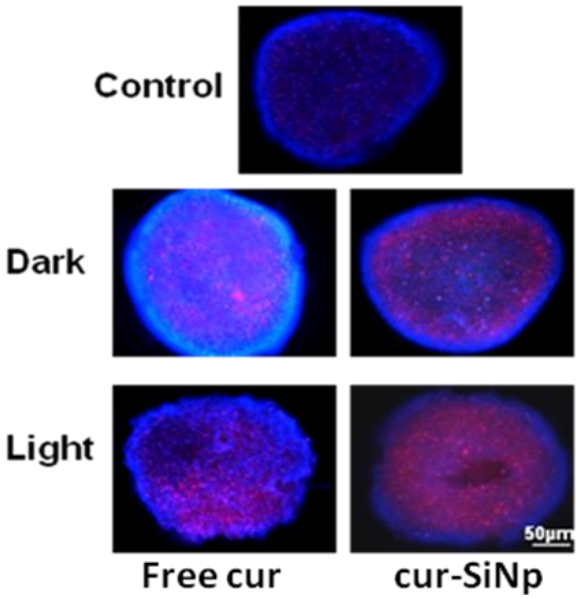

B)

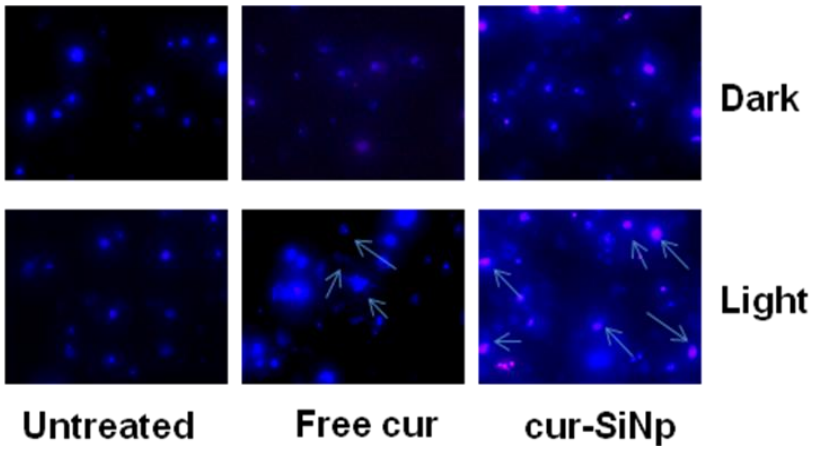

Figure 4.5: Fluorescence images of Hoechst (10 µg/ml) and PI (20 µg/ml) stained **(A)** intact spheroids, **(B)** cells dissociated from spheroids. Spheroids (small) were incubated with 25 µM of either free curcumin or its cur–SiNp complex in dark for 24 h and then irradiated with light (10 J/ cm^2) before staining with hoechst and PI.

4.3.6. Histology of spheroids

Figure 4.6 shows histological sections of spheroids (small) treated with the two formulations of curcumin with and without irradiations. Cells in untreated spheroids appeared normal with well defined nucleus, abundant cytoplasm and intact extracellular matrix (top panel). The spheroids treated with free curcumin and light at 10 J/cm^2 showed large nucleus and a scanty cytoplasm. Apoptotic cells were also abundant. In contrast, cells in spheroids treated with nanocurcumin and light showed irregular nucleus, damaged extracellular matrix, many cells lacked nucleus.

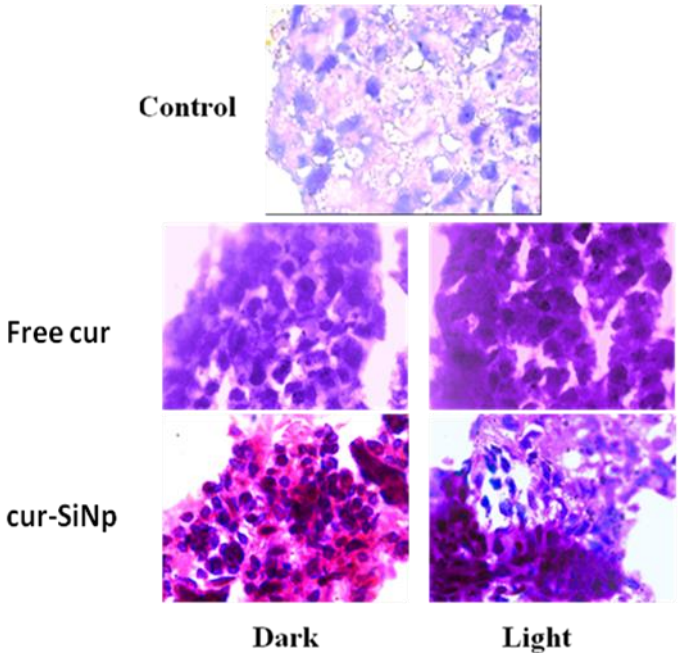

Figure 4.6: Histological analysis of spheroids treated with 25 μM of either free curcumin or its cur–SiNp complex. Spheroids were incubated in dark for 24 h with either free or cur–SiNp complex and then irradiated with light (10 J/ cm^2).

4.3.7. Effect of phototoxicity on growth of spheroids

To study the possible regrowth of cells surviving in spheroids (small) after treatment with two formulations of curcumin in dark and after exposure to light, spheroids were incubated in fresh culture medium on nonadherent surfaces. The morphology and time dependent changes in diameter of the treated and untreated spheroids are shown in Figure 4.7 A & B.

A)

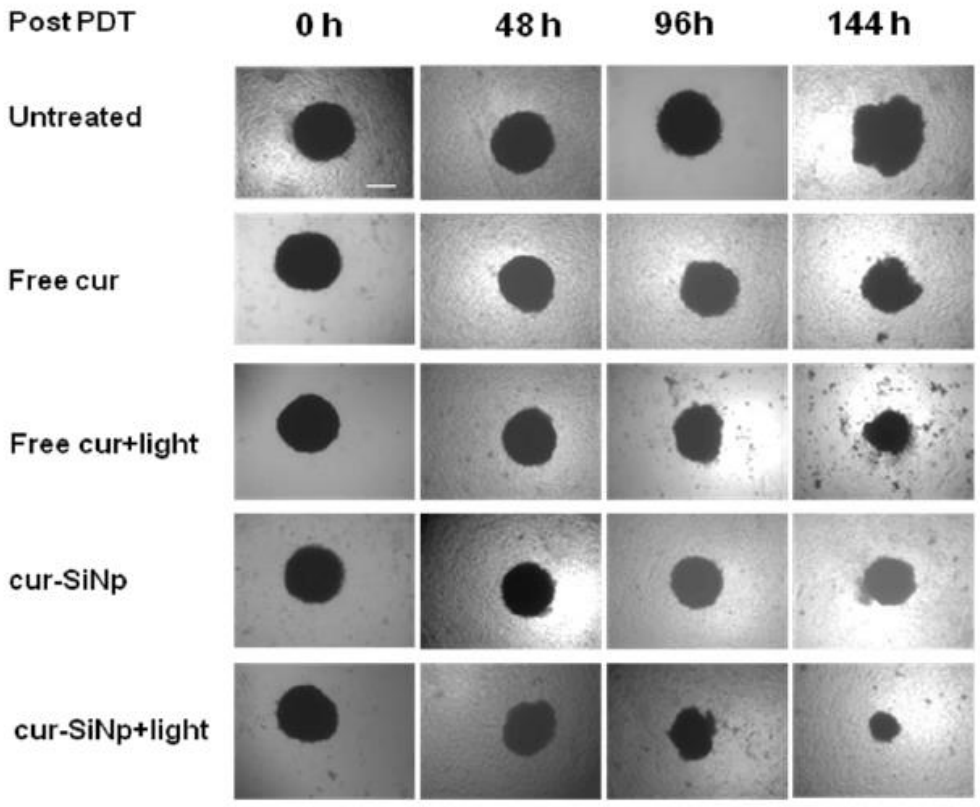

B)

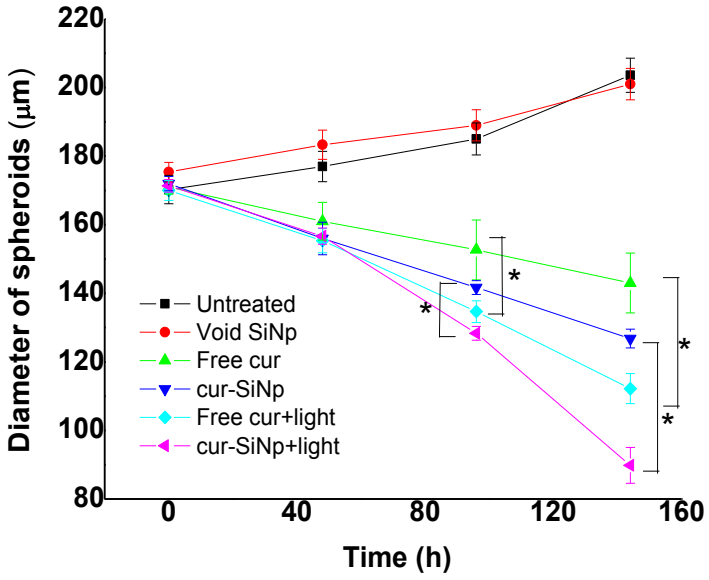

Figure 4.7: Phase-contrast images of spheroids grown for different days after treatment with either 25 µM of free curcumin or its SiNp complex in dark (24 h) and then exposed to light (10 J/ cm^2) Scale bar represented is 100 µm. **(A)**. Changes in diameter of spheroids subjected to different treatments **(B)** *P < 0.05.

With increase in incubation time, diameter of the untreated spheroids increased, from initial 170 µm ± 4.0 to 203 ± 5.0 µm after six days and appeared compact. On the other hand, diameter of spheroids treated with free curcumin or nanoformulated curcumin with and without irradiation decreased with increase in incubation time (Figure 4.7 B). The size of spheroids treated with

nanoformulated curcumin after irradiation decreased from initial 171.3 ± 2.0 µm to 89.8 ± 5.0 µm, whereas for spheroids treated with free curcumin the decrease was from 170.3 ± 3.0 µm to 112.2 ± 4.0 µm after six days of incubation.

4.3.8. Migration of cells from Spheroids

To investigate the effect of free curcumin and its complex on cell dissemination from extra cellular matrix of spheroid, spheroids (small) were transferred to adherent surfaces. Figure 4.8 (A & B) shows the extent of migration of cells from untreated and spheroids treated with either free and nanoformulated curcumin (for 24 h) in dark and after exposure to light (10 J/cm^2). Representative images of untreated spheroids, spheroids treated with either free curcumin, or nanocurcumin on Day 0 and 2 post irradiation are shown in Figure 4.8 (A). Untreated spheroids had a mean diameter of 176.6 ± 5.0 µm. After 4 days (96 h) of incubation, the diameter of spheroids plus cells emigrating from them increased to 672 ± 5.0 µm. Spheroids treated with void nanoparticle showed similar results (Figure 4.8 B).

A)

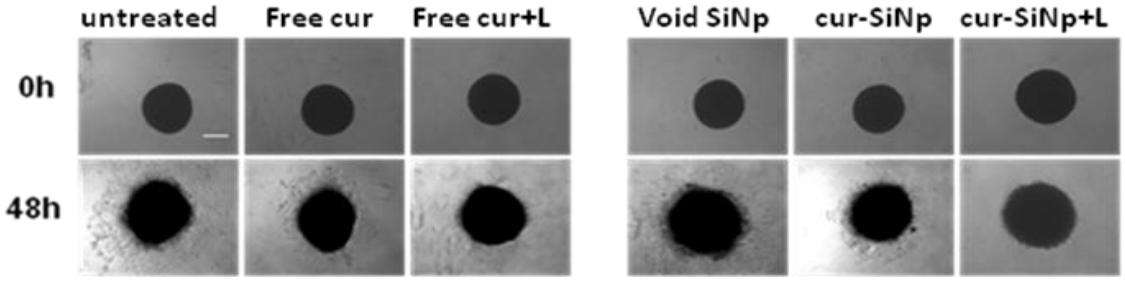

B)

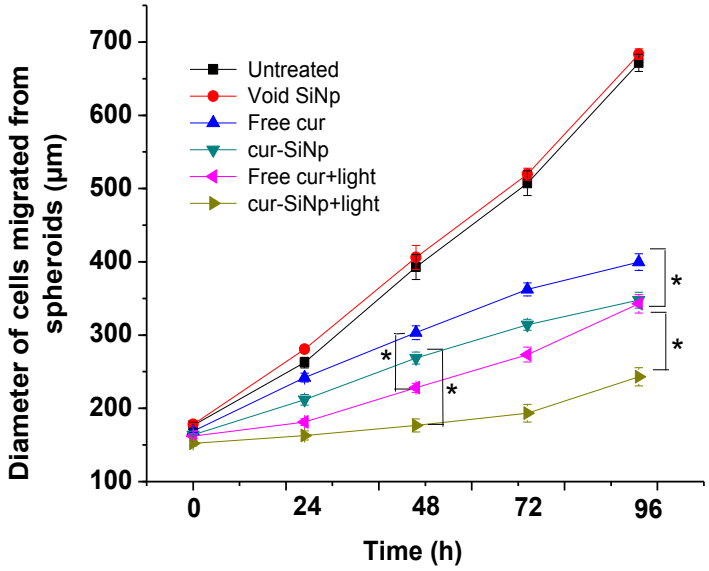

Figure 4.8: **(A)** Phase-contrast images of cells migrating from spheroids subjected to different treatments after transferring to petridishes, Scale bar represented is 100 µm. **(B)** Changes in diameter of cells migrating from spheroids subjected to different treatments. Spheroids were incubated with 25 µM of either free curcumin or its SiNp complex for 24 h in dark before exposing to blue light (10 J/cm^2).

Compared to untreated control, migratory capacity of spheroids incubated with either free curcumin or its complex in dark, reduced by ~1.7 and ~2.0 times respectively (Figure 4.8 A and B). In spheroids treated with nanocurcumin and light, inhibition in cell migration was even more remarkable (~2.7 times than that of untreated control).

4.3.9. Effect of ROS scavenger on regrowth and migration

The effect of irradiation of small spheroids treated with different formulations of curcumin in presence of GSH on regrowth and cell migration is shown in Figure 4.9 (A & B). As seen, post treatment inhibition in growth of spheroids treated with either free or cur-SiNp complex irradiated in presence of GSH was less as compared to spheroids irradiated in absence of GSH at 144 h. However the effect was more for cur-SiNp complex. Similarly, as compared to untreated control, cells spreading (migrating) from spheroids treated with cur-SiNp complex and light was reduced by ~68%, whereas in spheroids irradiated in presence of GSH inhibition in spreading of cells was ~18% at 48 h. While in free curcumin treated spheroids, inhibition was ~48% after light exposure. In presence of GSH, inhibition in migration was only ~23%. These results indicated the involvement of ROS in phototoxicity of curcumin.

A)

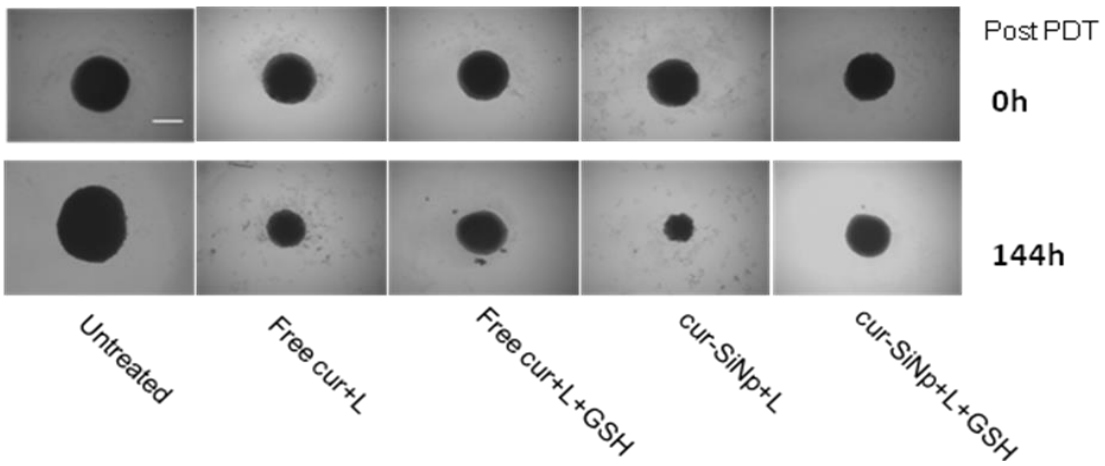

B)

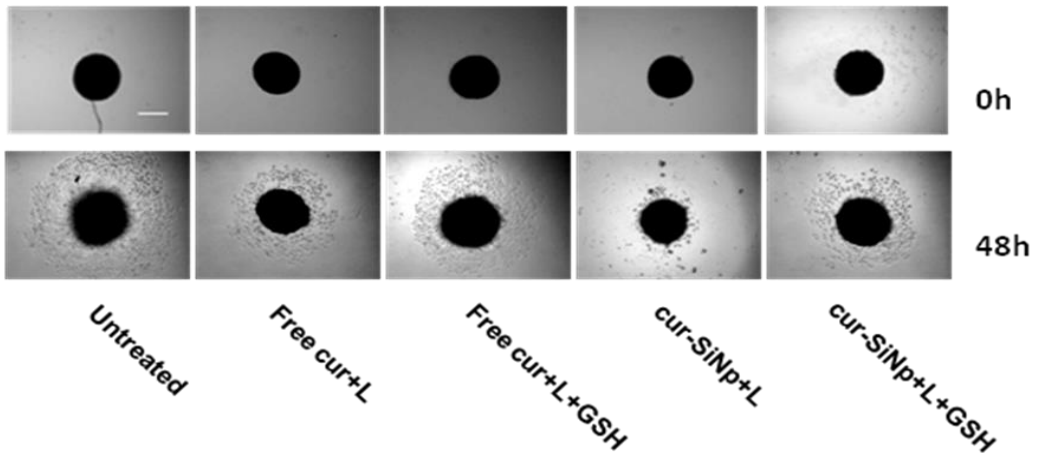

Figure 4.9: **(A)** Relative change in diameter of spheroids, **(B)** Phase-contrast images of cells migrating from spheroids subjected to photodynamic treatment in presence and absence of GSH. Spheroids were incubated with 25 μM of either free curcumin or its SiNp complex for 24 h in dark and then irradiated with blue light (20 J/cm^2) in presence and absence of GSH. Spheroids were incubated with GSH (1 mM) for 4h prior to irradiation.

4.4. Discussion

The objective of the present study was to evaluate the accumulation and phototoxic efficacy of free curcumin and its silica nanoformulations in three dimensional cell culture models (spheroids) of human squamous cell carcinoma cells which have extracellular matrix, complex biochemical and biomechanical environment other phenotypic differences similar to tumors under in vivo conditions. Results of our study presented in Figure 4.1 (A & B) suggests that the uptake of curcumin in nanoformulation in both small (~ 195 μm) and big spheroids (~ 365 μm)

is better than the free curcumin. One of the reasons for high uptake observed is due to higher stability of curcumin in SiNp formulation and lower dark toxicity of curcumin at 24 h in spheroids as compared to monolayer [244]. The strong fluorescence observed from the large number of cells dissociated from spheroids treated with nanoformulated curcumin suggests that nanocarriers are distributed within the spheroids. The differences in the accumulation of two formulations may also arise due to variation in the mechanism of internalization in spheroids. Whereas free curcumin enters cells through diffusion, cur-SiNp complex due to its large size (~30 nm) may be internalized through endocytosis. Penetration of nanocarriers in spheroids is also influenced by surface charge [248, 249]. Since nanocomplex has negative surface potential, it is likely that it diffuses deeper in spheroids due to reduced nonspecific adsorption by negatively charged extracellular matrix components like collagen and proteoglycans present in spheroids [250, 251]. These results are consistent with studies carried out on uptake of gold nanoparticles by tumor cylindroids wherein it has been shown that negatively charged particles diffuse faster and deliver drugs deep into the spheroids as compared to positively charged particles [252]. In addition, our results suggest that the size of spheroid has limitation on uptake of both the formulations of curcumin. Lower uptake of both formulations of curcumin observed in big spheroids as compared to small spheroids when normalized with cell number could be due to variation in distribution of curcumin SiNp complexes in different regions of the spheroids. It has been reported that spheroids have heterogenous population of cells. This arises due to variations in nutrients, oxygen levels, size and cell-cell communications [253, 254]. Rapidly dividing cell population present in the periphery generally show higher uptake of drugs than the quiescent population found in hypoxic regions. As the size of spheroids increases hypoxic regions and necrotic regions (dead cells) also increase contributing to overall reduction in uptake.

Indeed, spheroid size dependent difference in accumulation of photosensitizer has been reported in other studies also [255].

Our data (Figure 4.2) show that nanoformulated curcumin exhibits higher cytotoxicity in dark and after exposure to light in small spheroids as compared to free curcumin which is consistent with the higher uptake of curcumin in nanoformulation. Since cytotoxicity of cur-SiNp complex is comparable with monolayer cells, it confirms that there is little hindrance to penetration of the curcumin nanocomplex. Dark toxicity (~20%) of nanoformulated curcumin observed in spheroids might be due to release of curcumin from the SiNp which may be localized near the hydrophobic pockets. Released curcumin may induce toxicity by interfering with various signaling pathways such as phosphatidylinositol-3-kinase/AKT and epidermal growth factor receptor signaling associated with cell proliferation and survival [226, 227, 256]. However, observed lower dark toxicity and higher resistance to photodynamic damage exhibited by big spheroids as compared to small spheroids is consistent with the lower uptake of cur-SiNp complex (Figure 4.1 A) due to nonuniform distribution of curcumin SiNp complexes in different regions of the spheroids. The existence of hypoxic regions and reduction in the light penetration with increase in thickness also contribute to lower photodynamic efficacy. In spheroids hypoxic cells are found either in the core, or in the rim surrounding the necrotic core with low oxygen tensions typically below 10-mm Hg [257]. It has been shown that photosensitizing effect of curcumin requires the presence of oxygen for generating free radical photoproducts [169, 171]. Therefore, it is likely that if oxygen in the spheroids reduces the phototoxic effect also reduces. It has been reported that within 150 μm radius of spheroids, the light dose is reduced by ~ 20% while the oxygen concentration is reduced by around 15% compared to the periphery [258, 259]. Results of our study are consistent with a study carried out on size dependent photodynamic

sensitivity of human colon carcinoma spheroids wherein it has been shown that the photosensitizer uptake and photodynamic sensitivity reduces sharply in spheroids of size 500 μm as compared to spheroids of sizes 100 and 200 μm [255].

Higher phototoxicity observed in spheroids treated with curcumin complexed with SiNp as compared to free is consistent with the higher generation of ROS (Figure 4.3) which may be due to enhanced stability of curcumin in nanocomplex. It has been shown that curcumin produce ROS such as superoxide and curcumin radicals upon irradiation with visible light of >400 nm. However, the type of species depends upon sensitizer environment [169, 171]. Higher protection of phototoxic damage (reduction in cell death) induced by cur-SiNp complex when irradiated in presence of GSH as compared free curcumin observed in our study (Figure 4.4) further confirm that curcumin entrapped in SiNp generates higher ROS. It should be noted that the ROS levels induced by either free curcumin or its complex in big spheroids after light exposure was almost comparable to reduction in viability of cells in spheroids treated with respective formulations of curcumin in dark. These results confirmed reduced photosensitivity of big spheroids to curcumin.

Increased ROS generation induced in cur-SiNp complex treated spheroids (small) resulted in necrotic cell death (Figure 4.5) and damage to extra cellular matrix as evident in histology (Figure 4.6). Apoptotic death appears to be more predominant in free curcumin treated spheroids (Figure 4.5). This variation could have arisen due to differences in amount of curcumin accumulated within cells and also due to differences in the subcellular localization of the free drug and nanocomplex. While free curcumin may diffuse and get localized in membrane and other subcellular organelles, curcumin associated with nanoparticle may be more likely to be localized in lysosomes as nanocarriers are internalized by cells via endocytosis [260]. ROS

generated due to interaction of curcumin and light in lysosomally located SiNp may destroy lysosomes and release lytic enzymes leading to necrosis. Since the concentration of free curcumin accumulated by spheroids is lower than nanocurcumin, cell death occurs mainly through apoptosis. Induction of apoptosis by curcumin in combination with light has been reported in other studies also [167, 173].

The high phototoxicity induced by cur-SiNp complex and necrotic cell death could have contributed to remarkable growth inhibition in small spheroids (Figure 4.7). It should also be noted that regrowth was not observed even in spheroids treated with curcumin in absence of light. This observation confirms that both forms of curcumin have infiltrated the spheroids and inhibition of cell proliferation due to curcumin leaked out from nanoformulation appears to be sustained and irreversible. Marked differences observed in the sizes of spheroids treated with cur-SiNp complex irradiated with and without GSH is consistent with differences observed in the viability. Larger size of GSH treated spheroids is due to reduced cell death as a result of quenching of ROS by scavenger (Figure 4.4).

Inhibition of migration of cells from irradiated spheroids pretreated with nanocurcumin observed in our study (Figure 4.8) may be due to inhibition of NF-kB, not only due to cell death as at this light dose ~40% cells were still found to be viable. Studies carried out by us and others have shown that curcumin and light treatment inhibits NF-kB which is a key transcription factor that regulates metastasis and invasion of cancer cells [167, 244]. In addition, migration of the cancer cells involves interaction with ECM components, proteases (such as metallomatrix proteases), adhesion molecules and cytoskeletal proteins, curcumin has been reported to inhibit invasiveness of cancer cells [261]. Thus, damage to ECM observed in spheroids treated with light and

nanocurcumin (Figure 4.6) along with reduced NF-kB expression could have contributed to inhibition of migration of cells from spheroids. Increased migration of cells observed in spheroids treated with cur-SiNp after irradiation in presence of GSH as compared to spheroids irradiated in absence of it is due to enhancement of viable cells in spheroids and lower damage to ECM components due ROS scavenging activity of GSH (Figure 4.9).

4.5. Conclusion

This study showed that compared to free curcumin silica nanoparticles loaded with curcumin could penetrate better in oral cancer spheroids and the efficacy of uptake was found to be higher for small (~195µ) spheroids than large spheroids (~365 µ). Due to enhanced uptake of curcumin, cytotoxicity, inhibition in growth and antimetastatic ability were amplified in small spheroids treated with cur-SiNp complex and light profoundly as compared to free curcumin. Further, significant attenuation of phototoxic effect of cur-SiNp observed in presence of GSH vis- a -vis free curcumin treated spheroids confirmed enhanced generation of ROS. These results suggest that cur-SiNp complex and light treatment could be effective in controlling the growth of avascular tumors of oral cancer.

CHAPTER 5

CYTOTOXICITY OF CURCUMIN LOADED IN ORGANICALLY MODIFIED SILICA NANOPARTICLES CONJUGATED WITH HYALURONIC ACID ON COLON CANCER CELLS

5.1. Introduction

As discussed in chapter 1 & 4, Np based drug delivery offers several advantages in cancer therapy as they can encapsulate poorly soluble drugs [262], protect therapeutic molecules from degradation [234], modify their blood circulation and also reduce side effects of drugs [263]. Although nanoscale delivery vehicles increase the local concentrations of drugs in tumors by enhanced permeability and retention (EPR) effect, the distribution of Nps within the tumor cells is still challenging due to limited permeability of Nps within the tumors and lack of inherent affinity between the passively targeted Nps and tumor cells. By conjugating drug loaded Nps with suitable ligands that bind specifically to receptors over expressed on cancer cells (Active targeting) cellular or intracellular targeting can be improved. Receptor targeted drugs delivered through nano carrier systems have shown better pharmacokinetic and internalization of drugs than passive targeting [264, 265].

In our previous studies we showed that the phototoxic effect of curcumin in oral carcinoma cells (4451) could be improved significantly when drug was loaded in SiNp due to enhancement in its stability [244]. However, bioavailability of curcumin to diseased tissue may be enhanced further, if the drug loaded SiNp particles are conjugated with biomolecules which selectively bind to cancer cells. In this context, Hyaluronic acid (HA), a naturally occurring polysaccharide composed of N-acetyl-d-glucosamine and d-glucuronic acid is receiving a lot of attention because it has a strong affinity for cell-specific surface marker CD44 that are over expressed on the surface of malignant cells and HA also interacts with receptors which influences hyaluronan-mediated motility (RHAMM), HARE (HA receptor for endocytosis) and migration [266, 267].

However, biological functions and applications are dependent on molecular mass of HA. It has been reported that HA of molecular weight of about tens of kDa (about 100 disaccharides) and oligosaccharides up to a few kDa (10–15 disaccharides) enhance angiogenesis [266-268], whereas short oligomers (3–9 disaccharide units), exhibit anti carcinogenic effect under both *in vitro* and *in vivo* conditions [269-271]. It is therefore expected that by conjugating the SiNp-cur complex, curcumin delivery can be targeted to CD44 expressing cancer cells.

In the present chapter, we present results of study on evaluation of cellular uptake and cytotoxic potential of curcumin loaded in the SiNp conjugated with short oligomers (HA4). The cellular uptake and cytotoxic efficacy of HA targeted SiNp-cur was compared with untargeted SiNp-cur in colon carcinoma (Colo-205) cells grown in monolayer and multicellular spheroids. The cell line chosen express CD44 receptors [272].

5.2. Experimental methods

5.2.1. Preparation of nanoparticles

Preparation and characterization of SiNp, HA-SiNp, SiNp–cur, HA-SiNp-cur, quantitation of HA in HA-SiNp-cur and procedure used for release of curcumin from SiNp and HA-SiNp-cur have been described in detail in chapter 2.

5.2.2. Fluorescence microscopy

Colo-205 cells (5×10^4) were grown on poly-lysine coated cover slips. After 24 h, the attached cells were treated with 25 μM of either free curcumin or its different nanoformulations. In some experiments, to confirm involvement of HA receptors, colo-205 cells were incubated with 0.5 mg/ml HA for 1 h before treating with different formulations of curcumin. After specified time

of incubations, cells from different groups were washed first with growth medium then with PBS (pH 7.4) and examined under fluorescence microscope (Olympus, Japan) using blue excitation filter. For studying distribution of free curcumin and nanoformulated curcumin in spheroids, after 72 h of incubation with different formulations of curcumin, the spheroids were either disrupted by accutase to prepare single cell suspension or examined as such (intact) under fluorescence microscope after these were transferred to uncoated coverslips. Curcumin fluorescence was monitored.

5.2.3. Quantitation of curcumin uptake in cells

Cells were grown in monolayer for 24 h, were treated with either 25 µM curcumin in free form or in different nanoformulations for 4 h. Cells were harvested and curcumin was extracted from cells using methanol as described in chapter 2. To study the uptake of curcumin in spheroids, 3-4 days grown spheroids were incubated upto 96 h in growth medium containing either 25 µM curcumin (free) or different nanoformulations. After specified time of incubation, spheroids from different wells were pooled, washed 3-4 times in PBS, incubated with 200 µl accutase enzyme (37 ^{o}C, 20 min) for dissociation of cells from spheroids and curcumin was extracted using methanol and quantitated as described in chapter 2.

5.2.4. Cytotoxicity of free and nanoformulated curcumin

5.2.4.1. Monolayer

To evaluate the cytotoxic effect of different nanoformulations of curcumin, cells were seeded at a density of $3X10^4$ cells in 24 well plates and grown for overnight. Subsequently, cells were incubated with 25 µM of curcumin in free or its nanoformulations for different durations (24-96 h). MTT assay was performed after specified time as described in chapter 2.

5.2.4.2. Spheroids

Spheroids grown for 120 h (~250 µm diameter) were incubated with 25 µM of free curcumin, SiNp-cur, and HA-SiNp-cur complex containing equivalent concentration of curcumin in fresh medium (200 µl) for 24 to 96 h at 37 ºC. After specified time of incubation, growth medium was removed, spheroids were washed twice using PBS and spheroids were transferred to uncoated 96 -well plate. MTT Assay was performed as described in chapter 2. Viability of cells in treated spheroids was calculated with respect to untreated spheroids.

5.2.5. Post treatment growth of spheroids

Spheroids incubated with 25 µM of curcumin in free or its nanoformulations for 72 h, were washed twice with PBS, and transferred to agar coated 24 well plate containing 1ml of fresh growth medium and incubated at 37 ^{0}C. Growth of spheroids was followed upto 6 days by measuring the size of spheroids using reticulated eye piece by phase contrast microscope.

5.2.6. Effect of free and nanoformulated curcumin on invasion of cells from spheroids

For studying invasion, 24-well plates were coated with collagen (1 mg/ml). Spheroids incubated with 25 µM of curcumin in free or its nanoformulations for 72 h were washed in PBS and then transferred to collagen coated plates. Culture medium (500 µl) supplemented with 2% (v/v) FBS was added over the spheroid placed in each well. Migration of cells from spheroids through collagen matrix was imaged using phase contrast microscope at 0, 24, 48 and 72 h.

3.2.7. Statistical analysis

All the experiments were repeated at least three times. Data was represented as mean ± SEM of three experiments. In each experiment at least three spheroids (n=3) for each data point was used. A t-test was used to compare the statistical difference among the groups. P value <0.05 was considered as statistically significant.

5.3. Results

5.3.1. Physicochemical characterization of HA functionalized SiNp

In Figure 5.1a, we show the absorption of 25 µM curcumin in different SiNp formulations in aqueous solutions. While the magnitude of absorbance of curcumin in SiNp-cur complexes was higher, no significant change in peak position was observed as compared free curcumin. Both SiNp-cur complexes (HA bound and free) showed a peak around 425 nm and no significant difference was observed in the magnitude of absorbance. The conjugation of HA to SiNp-cur, was ascertained by observation of a peak at ~215 nm which corresponded with peak observed in absorption spectra of free HA (inset). EE% and LC% was found to be ~59 % and ~11.4 %

respectively. In Figure 5.1b, we show the fluorescence spectra of 25 µM curcumin in different SiNp formulations in aqueous solutions.

a)

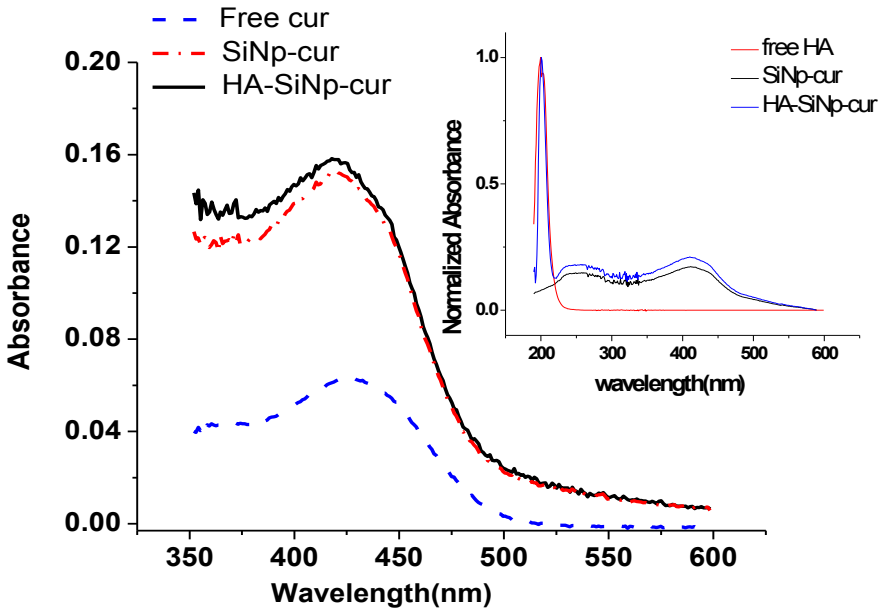

b)

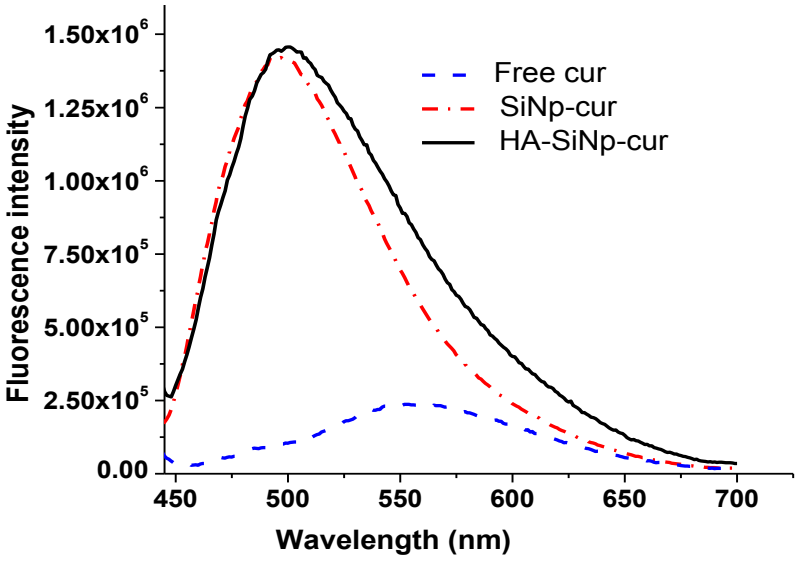

Figure 5.1: Absorption (a) and Fluorescence spectra (b) of free curcumin, SiNp-cur and HA-SiNp-cur in aqueous environment.

The fluorescence spectrum of HA conjugated SiNp-cur was similar to that of HA free SiNp-cur complex. Compared to free curcumin, curcumin fluorescence from HA conjugated and HA free SiNp-cur complex was blue shifted by ~62 and ~58 nm respectively and fluorescence intensity enhanced by a factor of ~6. After conjugation with HA, size of SiNp increased from ~45 nm to ~70 nm. The zeta potential of SiNp-cur complex increased to −33.25 ± 2.5 mV from −26 ± 1.6 mV.

5.3.2. Stability and release of curcumin

To assess the stability, the absorbance of different nanoformulations of curcumin in aqueous media was compared at different time intervals. In Figure 5.2 a, we show change in curcumin peak absorbance at 425 nm with time. While absorbance of free curcumin (dissolved in DMSO) decreased by 90% in water by 4 h, only ~20% change was observed for SiNp-cur. Curcumin absorbance in HA-SiNp-cur formulation did not change with time. This indicated that curcumin was very stable in HA conjugated SiNp formulation.

To understand the mechanism of release of curcumin from HA-SiNp, a known volume of HA conjugated SiNp-cur complex was incubated with and without hyaluronidase enzyme and release of curcumin was compared with curcumin release from SiNp without HA. The cumulative release of curcumin in all the three cases is shown in (Figure 5.2 b). After 4 h, the amount of curcumin released from SiNp-cur was ~35%, ~28% in case of HA-SiNp-cur in presence of enzyme. Curcumin release increased with time from both SiNp-cur and HA-SiNp-cur incubated with hylauronidase and was comparable in both cases. However, curcumin release observed in the same amount of time from HA-SiNp without enzyme was negligible.

a)

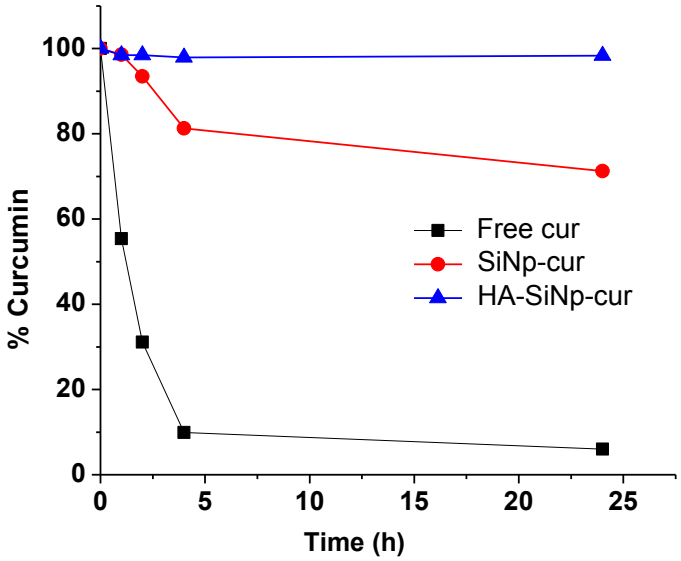

b)

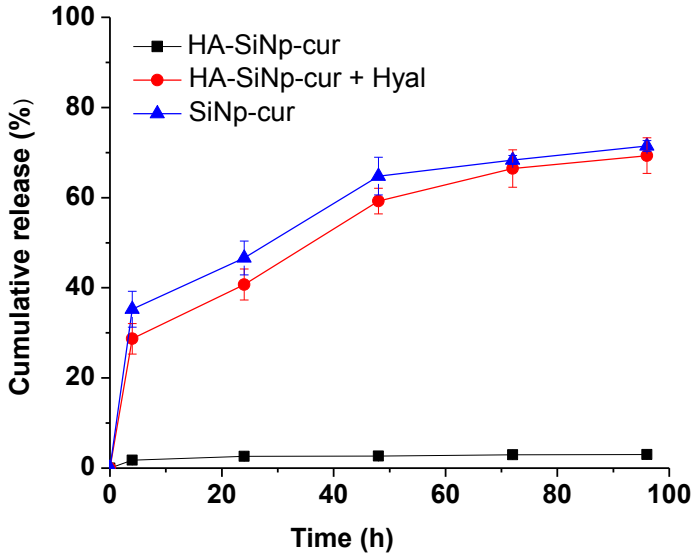

Figure 5.2: Stability of different formulations of curcumin in aqueous environment (a), Time dependent release of curcumin from HA-SiNp in presence and absence of hyaluronidase enzyme (b).

5.3.3. Intracellular localization and uptake of curcumin

Cellular targeting efficacy of HA free and HA conjugated SiNp-cur was studied by visualizing the intrinsic fluorescence of curcumin by fluorescence microscopy. In Figure 5.3 a (first row) we show the fluorescence microscopic and corresponding transmitted light images (second row) of cells incubated with free curcumin, SiNp-cur and HA-SiNp-cur for 4 h. Compared to free curcumin and its SiNp complex, fluorescence of curcumin from cells incubated with HA-SiNp-cur was strongest. While fluorescence of curcumin appeared to be arising from membrane in cells treated with free curcumin, fluorescence of curcumin in HA-SiNp-cur treated cells was observed throughout the cytoplasm. This suggests that HA-SiNp-cur was more easily internalized by the colo-205 cells than HA-free Nps. To confirm the involvement of CD44 receptors in the uptake of HA-SiNp-cur by colo-205 cells, HA-SiNp-cur was co incubated with free HA. While the presence of HA did not alter the fluorescence of curcumin significantly in cells incubated with either free curcumin or SiNp-cur, in cells incubated with HA-SiNp-cur complex a very large decrease in fluorescence was observed due to competitive binding of free HA with receptors (Figure 5.3 a, third row). Differences in uptake of curcumin nanoformulations in cells incubated with free curcumin, SiNp-cur, and HA-SiNp-cur (25 μM, 4 h) was quantified by measuring the intracellular curcumin extracted in methanol (Figure 5.3 b). These results showed that as compared to free curcumin uptake of curcumin in cells incubated with SiNp-cur and HA-SiNp-cur increased by ~2.9 and ~4.5 times respectively.

a)

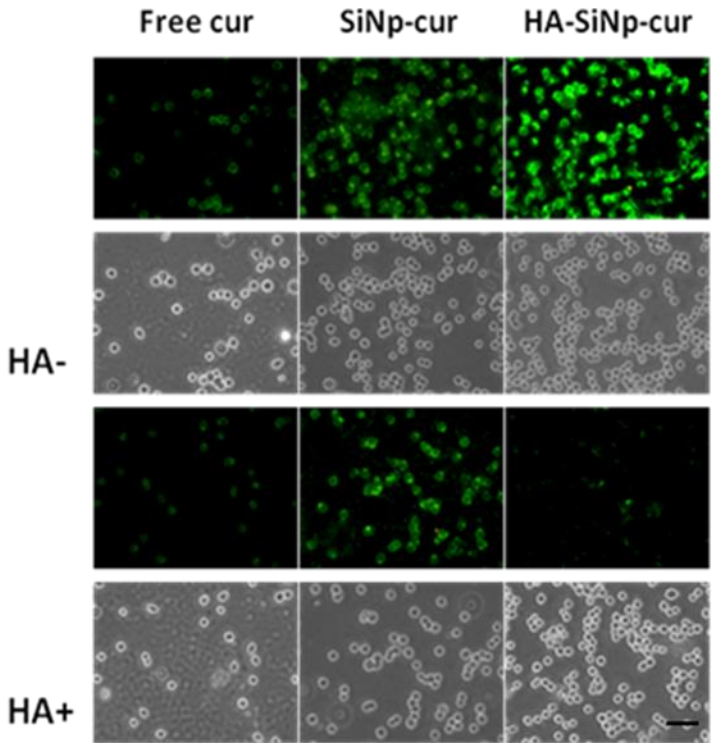

b)

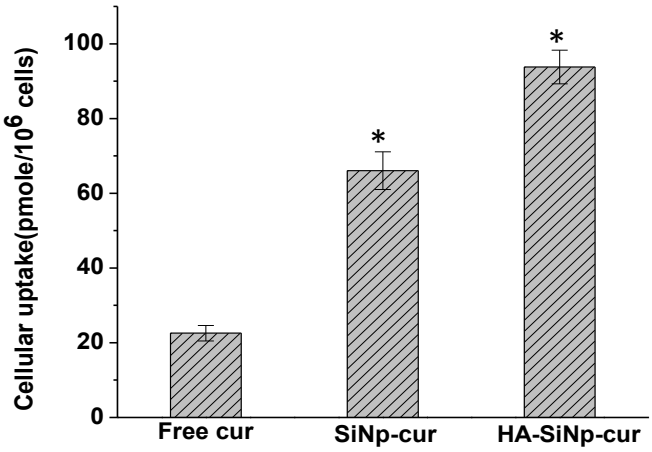

Figure 5.3: Fluorescence and transmitted light microscopic images of cells incubated with free curcumin, SiNp-cur, and HA-SiNp-cur for 4 h in presence and absence of HA (free) (Scale bar: 50 µm) (a). Uptake of curcumin in cells incubated with free curcumin, SiNp-cur, and HA-SiNp-cur for 4 h at 37 ºC (b). *$p<0.05$, with respect to free curcumin**.**

5.3.4. Uptake in tumor spheroids

Figure 5.4 (a & b) show the uptake of curcumin in spheroids incubated with different formulations of curcumin for different durations and the microscopic images of spheroids (intact & dissociated) incubated with different formulations of curcumin for 24 h. It is apparent from the Figure 5.4 (a) that at all the incubation time points the uptake of curcumin from HA-SiNp-cur was higher than free curcumin and its SiNp complex.

a)

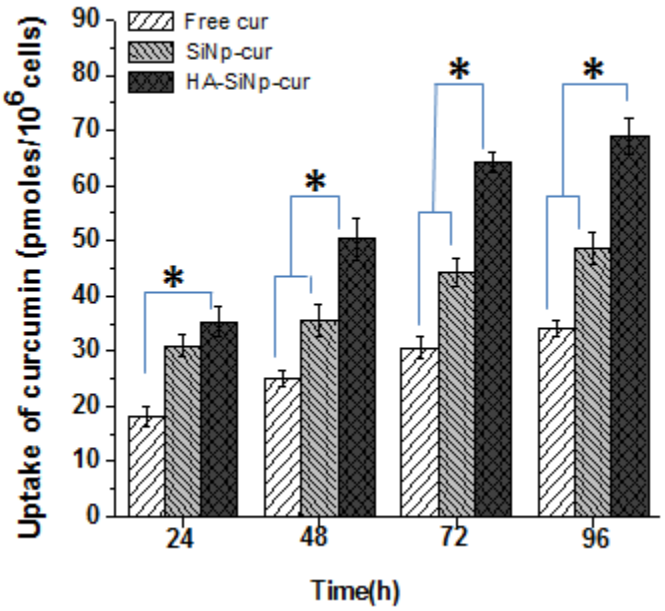

b)

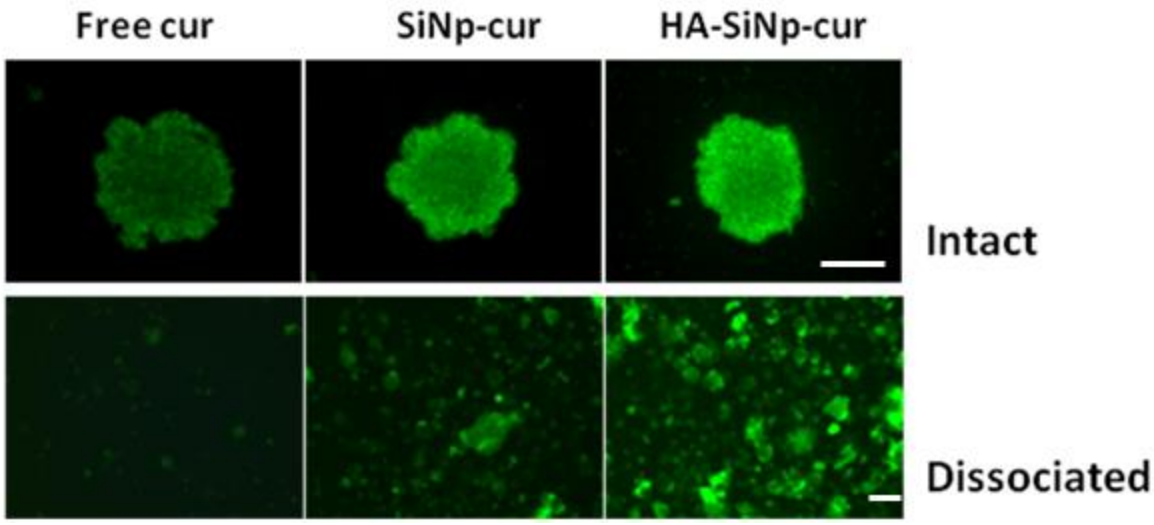

Figure 5.4: Time dependent uptake of curcumin in spheroids incubated with 25 μM of free curcumin, SiNp-cur, and HA-SiNp-cur. *$p<0.05$, with respect to free and SiNp-cur (a). Fluorescence microscopic images of spheroids (intact and dissociated) (b). Spheroids were incubated with free curcumin and HA free and HA conjugated SiNp-cur complex for 24 h before imaging. Concentration of curcumin was 25 μM. Scale bar: (100 μm, upper panel), (50 μm, lower panel)**.**

As compared to free curcumin, uptake of SiNp-cur and HA-SiNp-cur increased ~1.5 and ~2.2 times respectively at 96 h. Correspondingly, the curcumin fluorescence visualized by fluorescence microscopy from intact as well as cells dissociated from spheroids treated with HA-SiNp-cur for 24 h was stronger as compared to HA free SiNp-cur and free curcumin (Figure 5.4 b).

5.3.5. Cytotoxicity of nanoformulated curcumin in monolayer and spheroids

Figure 5.5a shows the time dependent changes in viability of colo-205 cells grown in monolayer incubated with 25 μM curcumin in different formulations. As compared to control (untreated), all the treatments reduced the cell viability. The reduction in viability observed in cells incubated with free curcumin, SiNp-cur and HA-SiNp-cur for 96 h was ~46%, ~67% and ~88% respectively.

Figure 5.5b shows the cytotoxicity of different formulations of curcumin in spheroids. The effect of different formulations of curcumin in spheroids was similar to monolayer. Cytotoxicity induced by all the formulations of curcumin increased with increase in incubation time. Significant differences in cytotoxicity were observed after 48 h treatment. At 96 h, as compared to free curcumin, about ~ 2.0 times enhancement in cell death was observed in HA-conjugated SiNp-cur, whereas in HA free SiNp complex the cell death was about ~1.6 higher than free curcumin.

a)

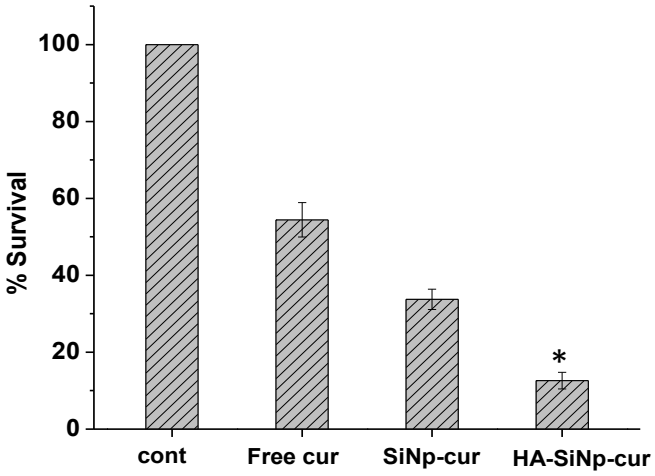

b)

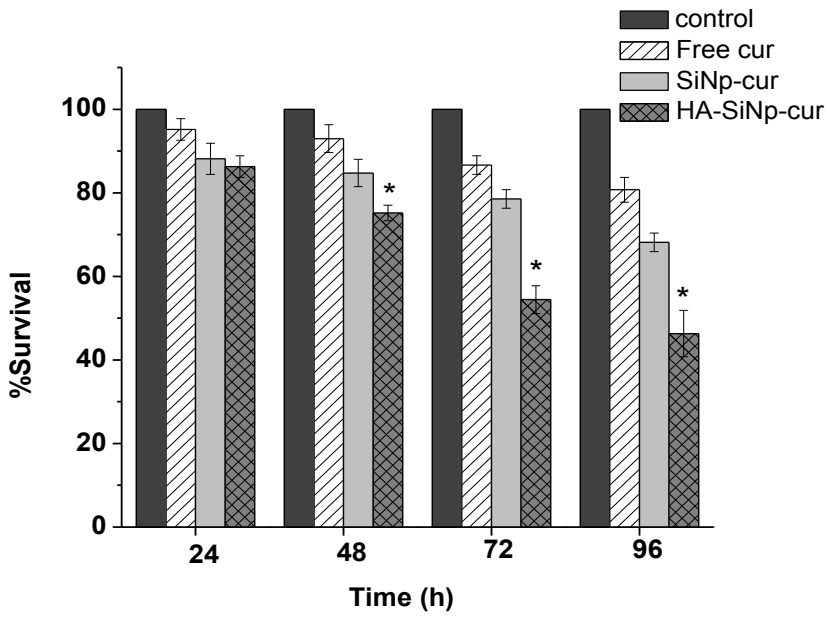

Figure 5.5: Viability of cells incubated with free curcumin, HA free or HA conjugated SiNp-cur complex. Monolayer (a), Multicellular spheroids (b). Cells grown in monolayer were incubated for 96 h; Spheroids were incubated for different durations. MTT assay was done to assess viability of cells. Concentration of curcumin in free and nanoformulation was 25 μM. *$p<0.05$ compared to SiNp-cur treated group.

5.3.6. Post treatment growth of spheroids

To confirm the cytotoxic efficacy of HA conjugated nanoformulated curcumin, post treated spheroids were incubated in fresh culture medium on non adherent surfaces after washing the spheroids and growth was followed for 6 days. Figure 5.6 a shows the growth of spheroids after treating with different formulation of curcumin. The changes in diameter of spheroids with time

are shown in Figure 5.6 b. While the size increased in untreated and spheroids treated with void SiNp with increase in time, ~18%, ~38% and ~57% decrease in diameter was observed in spheroids regrown after treatment with free curcumin, SiNp-cur and HA-conjugated SiNp-curcumin respectively.

a)

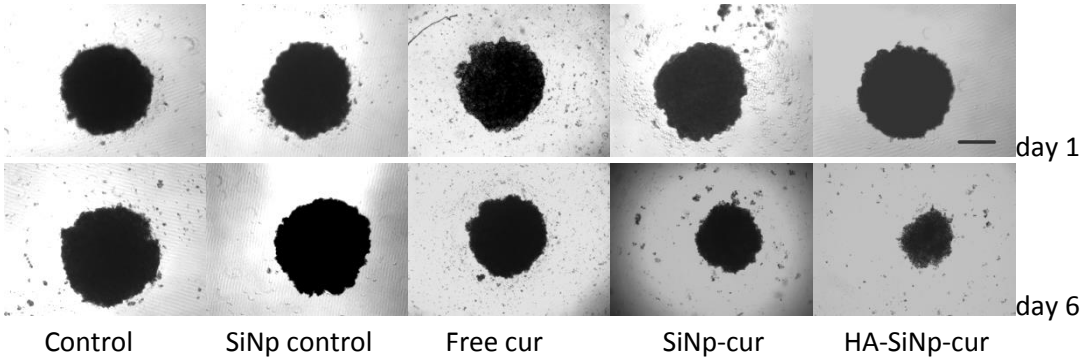

b)

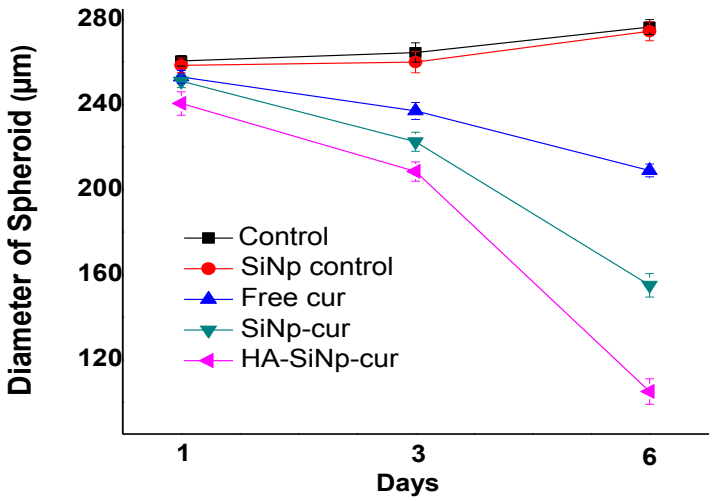

Figure 5.6: Phase-contrast images of spheroids grown for different days after treatment with 25 µM of free curcumin or its different nanoformulations for 24 h, imaged at day 1 (upper panel) and day 6 (lower panel) (a), Scale bar (—100µm). Changes in diameter of spheroids subjected to different treatments (b).

5.3.7. Effect of different formulations of curcumin on invasion of cells

In order to study if CD44 targeted HA-SiNp had any influence on antimetastatic effect of curcumin, invasion of spheroids were assessed by embedding the treated spheroids in collagen matrix and tumor cell invasion was monitored up to 72 h. Figure 5.7 shows the effect of curcumin treatment on invasion of cells from spheroids embedded in collagen matrix. Compared to untreated controls, while cells in spheroids treated with 25 μM of free curcumin, SiNp-cur showed less migration, cells in spheroids treated with HA-SiNp-cur containing similar concentration of curcumin did not migrate even after 72 h of incubation.

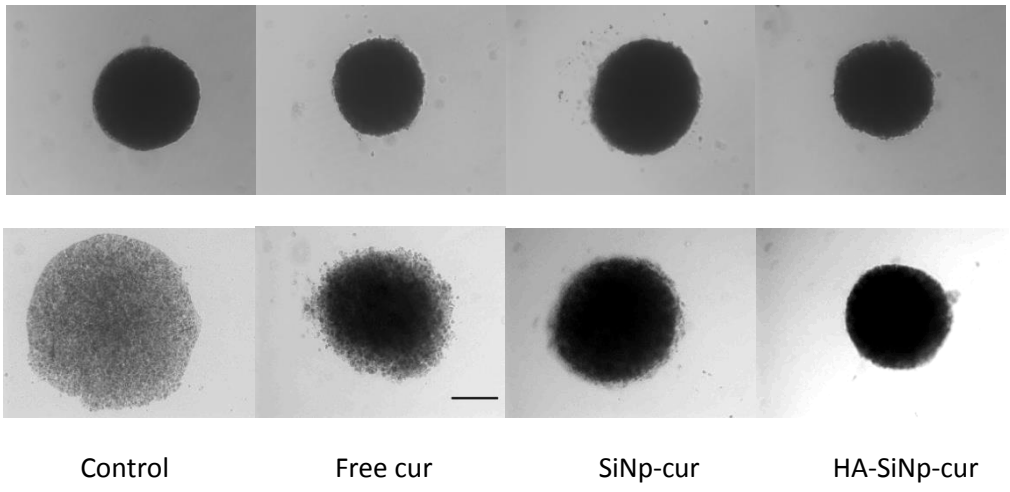

Figure 5.7: Phase-contrast images of spheroids showing effect of curcumin on invasion of cells from spheroids embedded in collagen matrix. Spheroids were treated with 25 μM free curcumin, SiNp-cur and HA-SiNp-cur for 24 h before embedding on collagen matrix. Scale bar (—100μm).

5.4. Discussions

The objective of this study was to investigate the cytotoxic potential of HA conjugated curcumin SiNp complex on CD44 expressing colon cancer cells. As reported in previous studies [244], since SiNps have hydrophobic core and porous matrix, curcumin post loaded in these particles formed stable complexes. This is confirmed from observed blue shift and enhancement in the fluorescence peak intensity of curcumin (Figure 5.1b). The absorption peak of HA observed at 215 nm in the spectrum of HA-SiNp-cur (inset) confirmed that HA is conjugated to SiNp [273]. This led to enhancement in the size (from ~45 nm to ~70 nm) and increase in the negative charge (-33.2 ± 3.0 mV from -26 ± 2.0 mV) as surface amino groups in SiNp were utilized for conjugating with HA and these results are consistent with other reports [274, 275]. The results presented in Figure (5.2 b) show that curcumin loaded in HA free SiNp and HA conjugated SiNp (HA-SiNp-cur) incubated with hyaluronidase enzyme is released from SiNp with time in a biphasic manner, whereas in absence of hyaluronidase curcumin is not released from HA-SiNp-cur. Initial high release of curcumin observed from SiNp without HA coating may be due to escape of curcumin associated on the pore surface. The gradual release of curcumin observed from SiNp is because curcumin is physically entrapped and it may diffuse out from Np slowly through pores which are of the order of nm size [47]. Diffusion of curcumin may occur due to differences in concentration gradients. However, in HA coated SiNp, network of HA is likely to cause hindrance to release. The increase in curcumin release from HA-SiNp in presence of enzyme with time suggests that on degradation of HA, the pores may open up, and the drug is released from pores. This is consistent with the report wherein it has been shown that the release

of chemotherapeutic drug loaded in mesoporous silica Nps gets hindered upon capping with HA [74].

Results presented on fluorescence microscopic study (Figure 5.3 a) and quantitation of curcumin uptake (Figure 5.3 b) shows that uptake is enhanced in cells incubated with curcumin in nanoformulation as compared to free curcumin and the uptake of curcumin from HA-SiNp-cur is the highest. This is due to its enhancement in stability as compared free curcumin. In nanoformulation, curcumin is in the hydrophobic core of SiNp and protected from rapid hydrolysis and degradation in physiological pH (7.4) [244]. Another reason for observed enhanced uptake of nanoformulated curcumin could be due to differences in the mechanism of internalization. While free curcumin internalizes through diffusion, both the nanoformulations are uptaken by cells through endocytosis. Among the two nanoformulations, uptake of HA-SiNp-cur is more because it is internalized through CD44 receptors present in these cells [272]. This is consistent with the fluorescence microscopic study which shows a large decrease in fluorescence of curcumin in cells incubated with HA-SiNp-cur in presence of free HA due to competitive binding with receptors (Figure 5.3 a, third row).

The results presented in Figure 5.4, show that uptake of nanoformulated curcumin is higher compared to free curcumin even in spheroids which have three dimensional structure with extracellular matrix. The variations in the uptake of different formulations of curcumin could have occurred due to cellular variations within the spheroids in addition to mechanism of uptake. It should be noted although free curcumin is smaller in size than nanoformulated curcumin, its uptake is limited in spheroids. This may be due to resistance exhibited by efflux pumps that are expressed generally in cells of hypoxic regions in spheroids [276]. Since both the formulations of SiNp-cur are internalized by endocytosis, this mechanism of internalization can overcome the

drug resistance exhibited by cells in deeper regions. In fact, in previous studies it has been shown that curcumin and DNA methylating agent co delivered in Nps accumulate more in tumor spheroids than free drugs as they are internalized by endocytosis, whereas free drugs are confined to periphery as these are internalized by diffusion [260]. Further, higher uptake of HA conjugated SiNp-cur observed in cells of spheroids may be attributed to transcytosis where HA nanoparticles exocytosed from cells might have been taken up by the neighboring cells within spheroids. These results are consistent with the previous observation wherein it has been shown that HA coating enhances the permeability of doxorubicin containing Nps by internalization through endocytosis and subsequent exocytosis of particles in 3D multilayered cell culture as well as spheroids [277].

Enhanced cell death observed in both monolayer (Figure 5.5 a) and in spheroids (Figure 5.5 b) after treatment with HA-SiNp-cur as compared to HA free SiNp and free curcumin correlated with the higher accumulation of curcumin due to enhanced uptake of HA conjugated Nps and higher stability of curcumin in this formulation. High accumulation of curcumin would lead to increased cell death. These results are consistent with other studies wherein it has been shown that HA-conjugated nanomaterials have good tumor targeting and penetrating ability for drug delivery under *in vivo* and *in vitro* models [278].

A progressive decrease in growth of spheroids observed after treatment with SiNp-cur and HA-conjugated SiNp-curcumin confirms that nanoformulated curcumin has infiltrated the spheroids and inhibition in cell proliferation due to curcumin leaked out from nanoformulation appears to be sustained and irreversible (Figure 5.6). It should also be noted that under intracellular

conditions hyaluronidase enzyme present in the cytoplasm may facilitate the release of curcumin from HA-SiNp-cur which would induce cytotoxic effects in sustained manner.

The results presented in Figure 5.7, show that migration of cells in spheroids treated with HA-SiNp-cur is reduced considerably as compared to free curcumin. These results suggest that anti migratory activity of curcumin is enhanced in HA formulation. It has been shown that hyaluronan oligomers inhibit invasion of malignant cells by interfering with interactions between endogenous hyaluronan and other matrix components that are necessary for the integrity of hydrated matrix [279]. Thus suggest HA oligomer contribute to inhibition of invasiveness of tumor cells.

5.5. Conclusion

In summary, our study has shown that conjugation of SiNp-curcumin complex with oligomers of hyaluronic acid results in enhanced uptake of curcumin possibly through CD44 mediated endocytosis and improvement in cytotoxicity in colon carcinoma cells. HA curcumin complex also showed improved distribution and internalization in spheroids of colon carcinoma as compared to HA free complex presumably due to exocytosis of endocytosed SiNp. These complexes were more potent in inhibiting growth as well as invasion of tumor spheroids compared to HA free complexes.

CHAPTER 6

UPTAKE AND PHOTODYNAMIC ACTION OF PYROPHEOPHORBIDE-a ENTRAPPED IN FOLATE RECEPTOR TARGETED ORGANICALLY MODIFIED SILICA NANOPARTICLES ON BREAST AND ORAL CANCER CELLS

6.1. Introduction

As discussed in Chapter 1, Photodynamic therapy (PDT) is an established treatment modality for many types of cancer [190, 280]. Successful use of PDT depends on preferential localization of the photosensitizer (PS) in the tumor and high yield of ROS produced on photoexcitation of PS which destroy the diseased tissues. Pyropheophorbide-a (PPa) and their derivatives are second generation PSs and are receiving considerable attention in PDT as these compounds are chemically well characterized, absorb light above 650 nm, have good singlet oxygen yield and low skin toxicity [88, 96]. However, the therapeutic effectiveness of PPa in native form is limited due to poor solubility in water which leads to aggregation and inefficient photodynamic activity. Therefore, suitable formulation is necessary for administration and target specific accumulation of PPa for in vivo applications.

As discussed earlier, ORMOSIL (SiNp) are the suitable delivery vehicles for PSs because of their transparency to light over the region of interest for PDT [88], porosity ensures that molecular oxygen and light can reach the entrapped PS and the generated ROS can diffuse out and inactivate cells [88, 96].

In this chapter, results of our investigations on the use of SiNp as a delivery vehicle for PPa have been presented. Both plain SiNp as well as SiNps conjugated with folic acid, a ligand which binds to receptor over expressed in many of the cancer cells were used for the study. Further, since pH strongly influence the outcome of anticancer drugs by affecting their uptake and release of drugs from the nanocarriers [281-283], as well as the expression of many growth factors [284] and receptors in cells [285], the effect of pH on uptake and photodynamic action of two

nanoformulations of PPa were investigated in two cell lines (squamous cell carcinoma Nt-8e) cells, and adenocarcinoma of breast (MCF-7) a cell line which express folic acid receptors [281].

6.2. Experimental methods

6.2.1. Nanoparticle preparation and Characterization

Preparation of PPa encapsulated in plain SiNp (Np-PPa) and conjugation of folic acid with Np-PPa (FR-Np-PPa) and their characterization are described in chapter 2.

6.2.2. Uptake of nanoformulated PPa

The human breast adenocarcinoma (MCF-7) and human squamous cell carcinoma derived from upper aero-digestive tract (Nt-8e) cells have been used in this study. For studying the pH dependent uptake of PPa loaded Nps, Nt-8e ($\sim 0.6\times10^6$) and MCF-7 ($\sim 0.4\times10^6$) cells were grown in 24 well plastic dishes at 37 ºC. After 24 h, the medium was replaced with fresh HEPES buffered growth media of pH 7.4 or pH adjusted to 6.5. After 1 h of incubation in a medium of specific pH, 0.5 µM of PPa in two nanoformulations was added into each well and cells were incubated for different durations. PPa from cells was extracted by using 0.1 M NaOH-2% SDS after washing the unbound PPa and quantitated by fluorescence spectroscopy. Details are described in chapter 2.

6.2.3. Mechanism of uptake

To study the influence of pH on mechanism of internalization, cells were incubated either at 4 ºC where endocytosis is blocked or 37 ºC in the dark for 2 h with culture medium containing two

formulations of Nps (PPa 0.5 µM) of pH 6.5 or 7.4. After incubation, the cells were rinsed three times with sterile acidified PBS, and cells were solubilized and uptake was measured as described in chapter 2.

6.2.4. Fluorescence confocal imaging

Nt-8e and MCF-7 cells were incubated with the two Np formulations containing PPa (0.5 µM) in a medium of pH 6.5 or 7.4 for 2 h at 37 ºC or 4 ºC in the dark. Unbound Np-PPa were removed by washing cells with PBS and fixed using formaldehyde (4%) for 15 min. Cells were imaged using Near field scanning optical microscope in confocal fluorescence mode as described in chapter 2.

6.2.5. Phototoxicity of PPa loaded Nps

Nt-8e and MCF-7 cells grown in a 96-well plate for 24 h were incubated with growth medium of pH adjusted to 6.5 or 7.4. Specified quantities of Nps containing 0.5 µM of PPa was added and incubated for 2 h in the dark. Details of light source and procedure of MTT assay followed is described in chapter 2.

6.2.6. Statistical analysis

All the experiments were repeated at least three times. Data was represented as mean ± SEM of three experiments. A t-test was used to compare the statistical difference among the groups. P value <0.05 was considered as statistically significant.

6.3. Results

6.3.1. Characterization of the plain and FR targeted PPa entrapped Nps

Figure 6.1a & b show the absorption and fluorescence emission spectra of the two formulations of Np-PPa, free PPa in water and DMF. The absorption spectra of free PPa in water showed soret band at 383 nm and Q band was observed at 699 nm. In contrast, the absorption spectrum of Np-PPa exhibited a strong broad band with a peak around 400 nm and four Q bands at wavelengths 506, 542, 613 and 670 nm and was similar to the absorption spectra of PPa in DMF. The absorbance of Q band at 670 nm was predominant. Np-PPa conjugated with folic acid showed similar spectral profile except that longest Q band was blue shifted by ~2 nm. In comparison to free PPa in water, magnitude of absorbance of the nanoformulated PPa was stronger. The conjugation of folic acid to void Np, was ascertained by observation of a peak at ~290 nm (Inset i). The strong extinction noted in the spectra of the two nanoformulations of PPa in the lower wavelength region (280-350 nm) is due to Rayleigh scattering by the particles. The spectra corrected for scattering is also shown in inset (ii). Figure 6.1(b), we show normalized fluorescence spectra of free PPa and PPa encapsulated in Nps suspended in water. On encapsulation, the emission peak of PPa in Np-PPa and its folate conjugate was seem to red shift by about 5 nm. The zeta potential and size of Np-PPa was −24 ± 6.0 mV and ~65 nm respectively. Upon conjugation with folic acid, both zeta potential and size of Np-PPa increased to −45±4.0 mV and ~75 nm respectively. Encapsulation efficiencies of PPa in the two formulations of Np were above 60- 67%.

a)

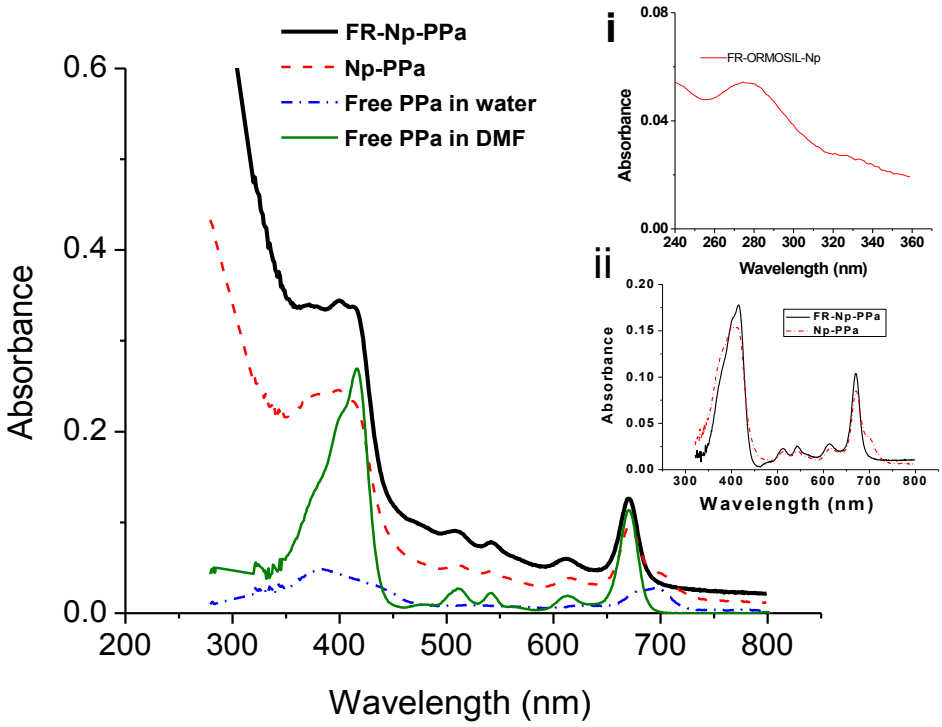

b)

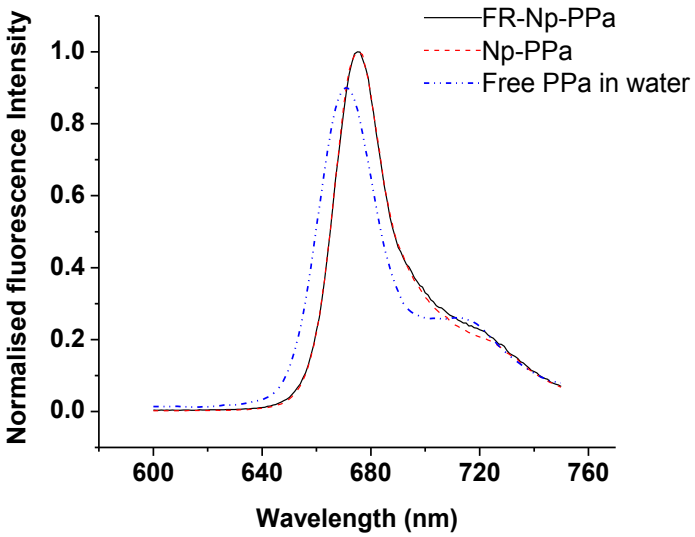

Figure 6.1: The absorption spectra of **a)** FR-Np-PPa, Np-PPa in water; free PPa in water and DMF; Inset (i) shows absorption spectra folic acid conjugated ORMOSIL-Np, inset (ii) shows spectra of FR-Np-PPa, Np-PPa corrected for Rayleigh scattering, Fluorescence spectra of **b)** FR-

Np-PPa, Np-PPa, free PPa in water, all samples were excited at 410 nm. Concentration of PPa in water, DMF and the two formulations ORMOSIL-Np was 2.0 μM.

6.3.2. Effect of pH on intracellular accumulation of nanoformulated PPa

Figure 6.2 shows the fluorescence confocal micrographs of MCF-7 and Nt-8e cells incubated with the two nanoformulation (equivalent to 0.5 μM PPa) in a media of pH 6.5 and 7.4. While the fluorescence of PPa in cells incubated with Np without conjugation (Figure 6.2, right panels) did not show any pH dependent difference, fluorescence of PPa from cells incubated with folate Np conjugate was stronger and cells incubated in a media of pH 6.5 were brighter as compared to 7.4. The fluorescence of PPa was observed mainly from cytoplasm in cells incubated at pH 6.5 as well as pH 7.4.

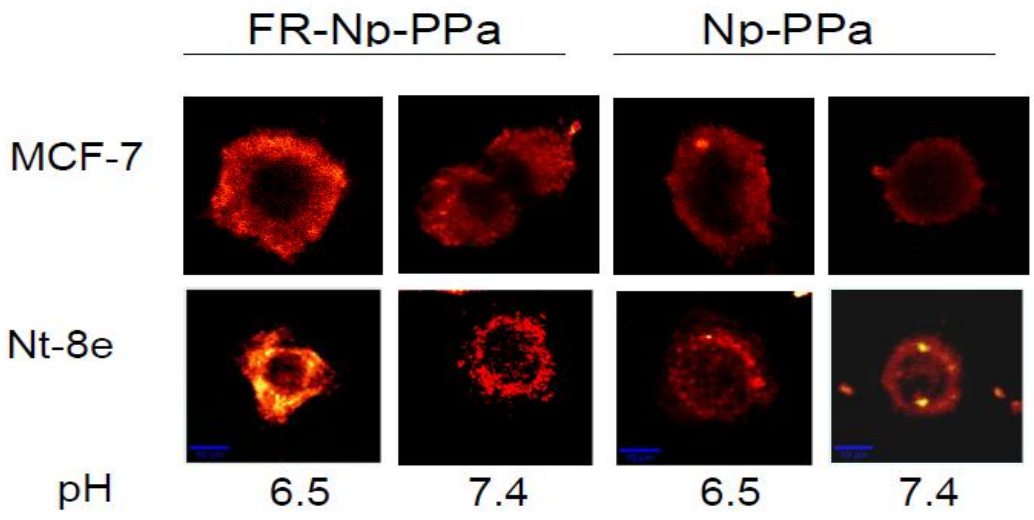

Figure 6.2: Fluorescence confocal micrographs of MCF-7 or Nt-8e cells incubated with FR-Np-PPa and Np-PPa (PPa (0.5 μM) in a medium of pH 6.5 and 7.4 for 2 h in dark.

6.3.3. Effect of pH on uptake

In Figure 6.3 a & b, we show time dependent uptake of PPa by MCF-7 and Nt-8e cells incubated with either Np-PPa or its folate conjugate (PPa 0.5 µM) in a media of pH 6.5 and 7.4. Uptake of PPa via FR-Np-PPa formulation was higher than Np-PPa for all the incubation time points. The folate nanoformulation mediated uptake was more at pH 6.5. Compared to physiological pH, uptake of PPa at pH 6.5 was ~1.4 times higher after 2 and 4 h of incubation in MCF-7 cells and in Nt-8e the increase was ~1.4 and ~1.5 times at similar incubation times. Nevertheless, PPa accumulated via Np-PPa did not show any (significant) pH dependence in both types of cells. Among the two cell lines, the uptake of PPa through both the formulations was higher for MCF-7 cells compared to Nt-8e cells. However, as compared to MCF-7, difference in uptake between the folate receptor targeted and untargeted nanoformulation was larger for Nt-8e cells at all the incubation time points at both the pH.

a)

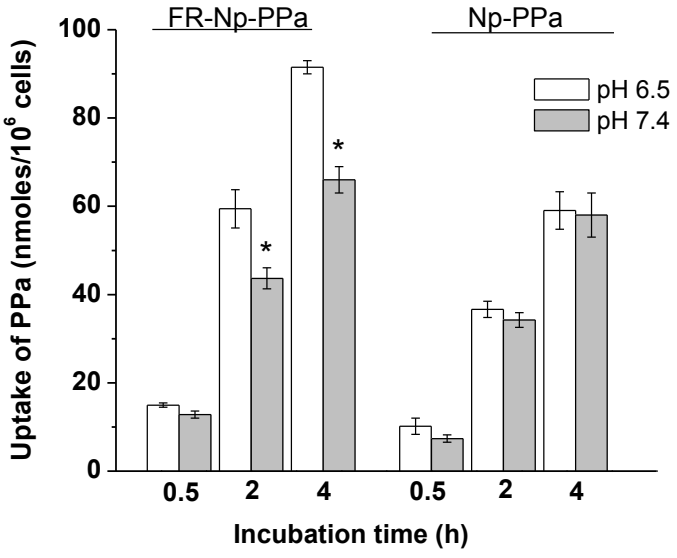

b)

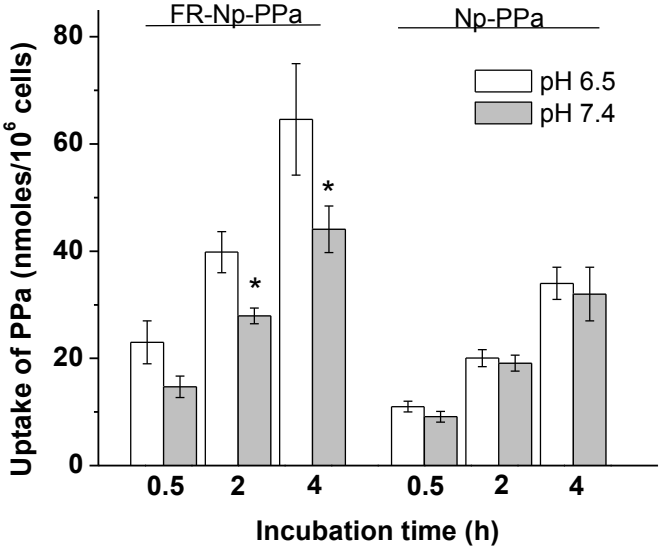

Figure 6.3: Time dependent uptake of FR-Np-PPa and Np-PPa by MCF-7 **a)** and Nt-8e cells **b)** incubated with FR-Np-PPa and Np-PPa (PPa (0.5 μM) in a medium of pH 6.5 and 7.4. Cell bound PPa was quantitated by measuring the fluorescence of PPa extracted with 2% SDS-0.1M NaOH. (*P<0.05 as compared to pH 6.5 group).

6.3.4. Effect of pH on uptake in presence of free folic acid

In order to confirm involvement of folate receptor in pH dependent uptake of FR-Np-PPa, a competitive binding assay was performed. This was done by incubating MCF-7 and Nt-8e cells with 1mM free folic acid (FA) in a medium of pH 6.5 and 7.4 prior to incubating with FR targeted Nps for 4 h. As shown Figure 6.4, uptake of PPa via FR-Np in MCF-7 cells was reduced by ~67 % and ~ 41.6 % when incubated in a medium of pH 6.5 and 7.4 respectively. In Nt-8e

cells, presence of FA reduced the uptake of PPa by ~83.8 % and ~ 71 % at pH 6.5 and 7.4 respectively.

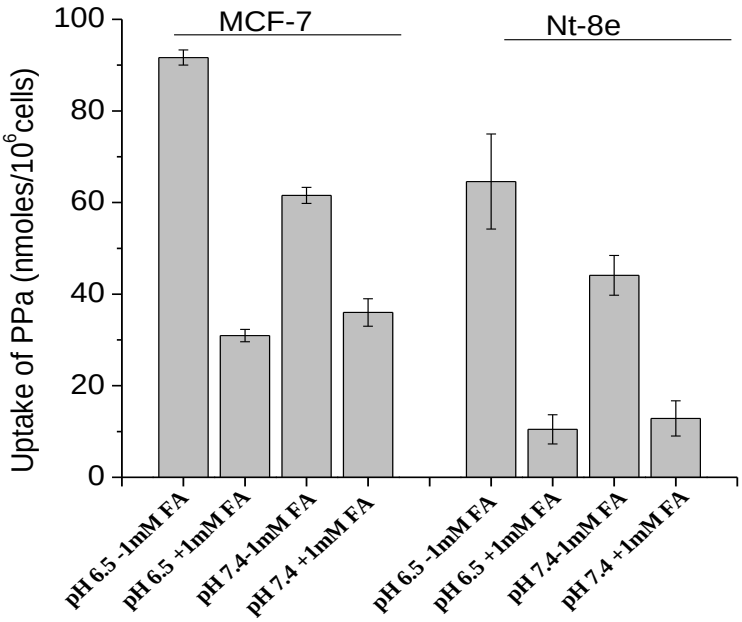

Figure 6.4: Uptake of PPa by MCF-7 and Nt-8e cells incubated with FR-Np-PPa (PPa (0.5 μM) in presence of 1mM free FA in a medium of pH 6.5 and 7.4 for 4 h in dark. Cell bound PPa was quantitated by measuring the fluorescence of PPa extracted with 2% SDS-0.1M NaOH.

6.3.5. Effect of pH on morphology

Figure 6.5 shows the morphology of cells incubated with growth medium of different pH. Whereas MCF-7 cells incubated in a medium of pH 6.5 for 4 h showed distinct change in morphology such as increase in cell size and projections, at physiological pH cells appeared

more spherical (Figure 6.5, left upper panel). Similar observations were noted in Nt-8e cells although the differences were less distinct as compared to MCF-7 cells (Fig 6.5, bottom right panel).

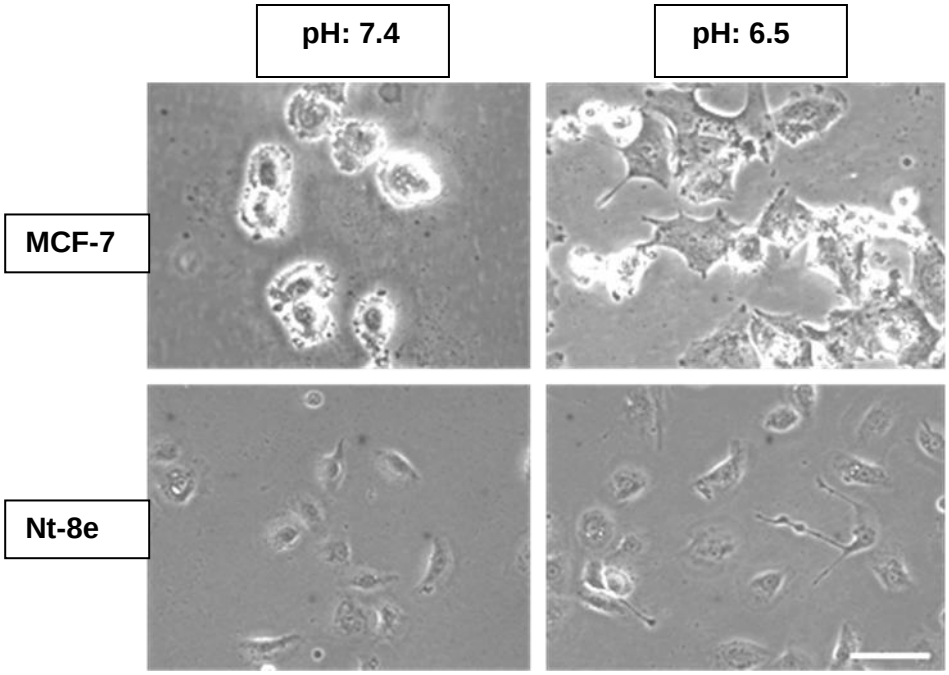

Figure 6.5: Morphology of MCF-7 and NT-8e cells grown for 30 h then incubated in medium of pH 6.5 and 7.4 for 4 h. Scale bar: 50 µm.

6.3.6. Effect of pH on mechanism of uptake

Effect of pH on internalization of two formulations of PPa, by cells is shown in Figure 6.6 a & b. Compared to cells incubated at 37 ^{0}C, uptake of PPa in MCF-7 cells incubated with FR-Np-PPa at 4 ^{0}C was reduced by ~80 % and ~70 % at pH 6.5 and 7.4 respectively. In cells were incubated at 4 ^{0}C with Np-PPa in a medium of pH 6.5 and 7.4, the uptake of PPa reduced by ~73 % and ~ 68 % respectively. Similarly, low temperature dependent inhibition in uptake of PPa from the FR-Np-PPa was observed to be higher (~82 %) at pH 6.5 as compared to physiological pH

(76%) and the pH dependent differences in uptake of Np-PP was reduced in Nt-8e cells (Figure 6.6 b). In (Figure 6.6 c), we show confocal microscopic images of Nt-8e cells incubated at 4 ^{0}C and 37 ^{0}C with the two formulations of Nps. Compared to cells incubated at 37 ^{0}C, fluorescence of PPa from the cytoplasm of cells incubated with targeted and untargeted Np-PPa at 4 ^{0}C was weak. This indicated that some PPa was internalized nonspecifically.

a)

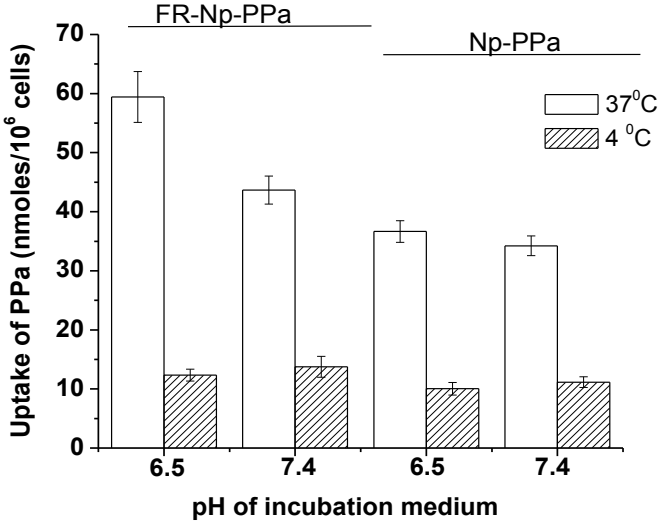

b)

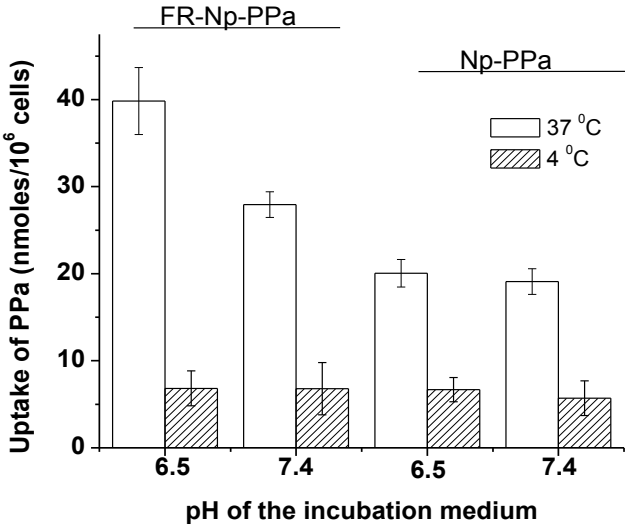

(c)

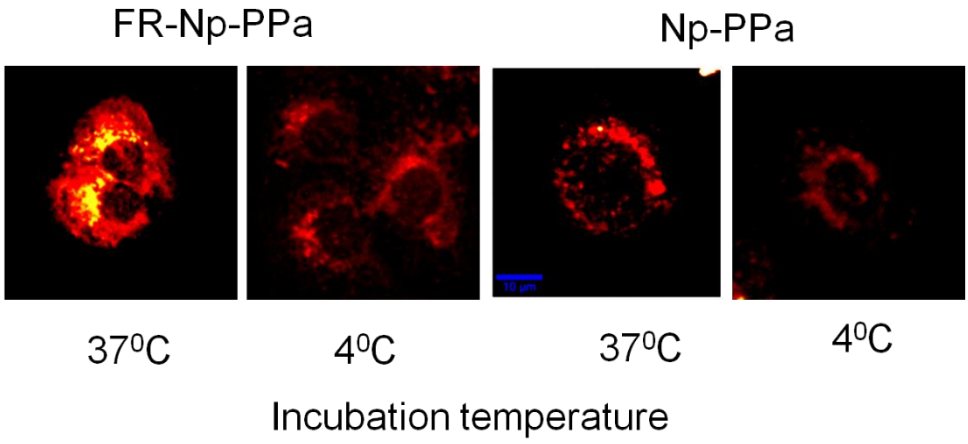

Figure 6.6: Uptake of PPa by MCF-7 **a)** and Nt-8e cells **b)** incubated with FR-Np-PPa or Np-PPa (PPa (0.5μM) in a medium of pH 6.5 and pH 7.4 at 4 ^{0}C, and at 37 ^{0}C for 2 h in dark. Confocal images of Nt-8e cells incubated with Np-PPa or FR-Np-PPa (PPa 0.5 μM) in a medium of pH 6.5 at 4 ^{0}C, and at 37 ^{0}C for 2 h in dark **c)**.

6.3.7. Effect of pH on phototoxicity

The pH dependence on phototoxicity of cells incubated with Np-PPa or its folate conjugates (PPa concentration 0.5 μM) for 2 h in the dark and then exposed to light is shown in Figure 6.7a & b. While no significant dark toxicity of the two formulations was observed in MCF-7 cells at pH 6.5 as well as pH 7.4, a dose dependent loss of survival was observed on exposure to light. The loss of survival was ~77 % and ~67 % in cells incubated with FR-Np-PPa in a medium of pH 6.5 and 7.4 after light exposure (5 J/cm^2). On the other hand, about ~60% loss of survival was observed in cells treated with Np-PPa in a media of pH 6.5 or 7.4 under similar irradiation

conditions. pH dependent phototoxicity was also observed in Nt-8e cells. Compared to MCF-7 cells, phototoxicity was slightly lower in these cells.

a)

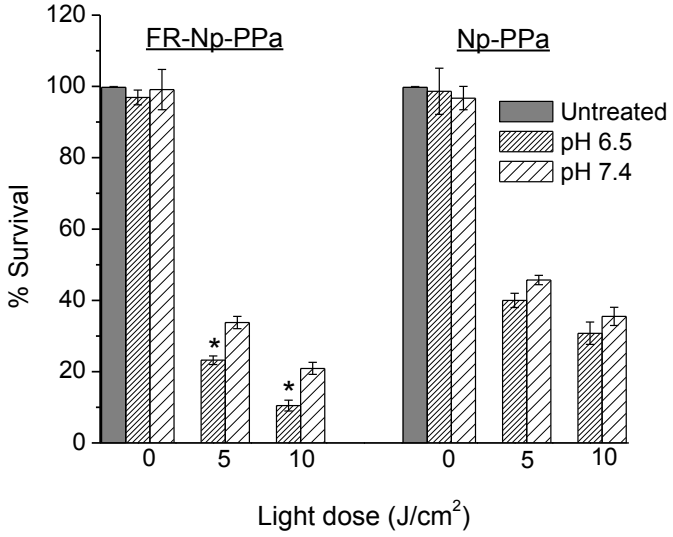

b)

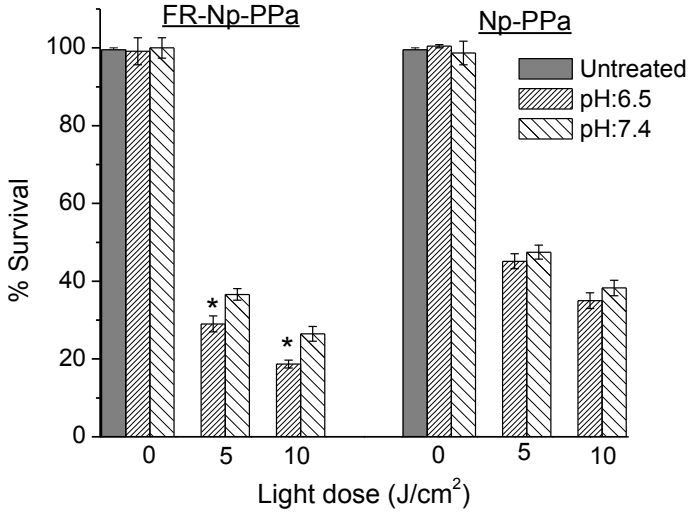

Figure 6.7: Phototoxicity of PPa in MCF-7 **a)**, and Nt-8e **b)** cells incubated in a medium of pH 6.5 and 7.4. Cells were treated with FR-Np-PPa and Np-PPa (PPa (0.5 μM) for 2h in dark prior to irradiation with red light. After 24 h MTT assay was performed. (*P<0.05 as compared to pH 7.4 group).

6.4. Discussions

The objective of the present study was to investigate the use of SiNp for targeted delivery of PPa and study the influence of extracellular pH on uptake and photodynamic efficacy of PPa entrapped in folate targeted and untargeted SiNp. Results presented in Figure 6.1 (a) show that whereas free PPa gets aggregated when suspended in aqueous media as evidenced by blue shifted soret band and a red shifted Q band (699 nm) [190], PPa in nanoformulations (SiNp) is in hydrophobic environment. This is confirmed by observation of strong absorbance of red shifted soret band and blue shifted Q band (670 nm) and red shift (5 nm) in the fluorescence spectra. These spectral features are similar to free PPa in hydrophobic solvents like DMF [286] and the PPa doped SiNps are monodisperse and stable in aqueous solution. The absorption peak of folic acid observed at 290 nm in the spectrum of SiNp confirmed that folic acid is conjugated to Np [287]. This led to enhancement in the size and increase in the negative charge as surface amino groups in SiNp were utilized for conjugating with folic acid. Our results on confocal microscopic study (Figure 6.2) and quantitative PPa fluorescence measurements (Figure 6.3 a & b) suggests that the uptake of folate conjugated nanoformulation of PPa is mediated through folate receptors and dependent on pH. This is evident from the enhanced intracellular fluorescence of PPa and higher accumulation of PPa observed in MCF-7 and Nt-8e cells incubated with folate conjugated nanoformulation as compared to cells incubated with unconjugated nanoformulation. Involvement of folate receptors is further confirmed by reduced uptake of PPa observed in presence of free folic acid which binds to folate receptors competitively (Figure 6.4). One reason for increase in uptake of PPa delivered via folate conjugated Np in Nt-8e and MCF-7 cells incubated under acidic (pH 6.5) condition might be due to increase in the activity and level of

folate receptor expression. Indeed, studies have shown that acidification affects the expressions of many receptor genes as receptors in the cytoplasmic membranes generally have a domain located outside the cells [284]. The activity of these may be more sensitive to external acidosis and have optimum activity at acidic pH compared with the cytosolic proteins which are exposed to alkaline pH (7.4) and many of the growth factors like VEGF, MMP-9 have been shown to get expressed within short durations of exposure to acidic conditions [288, 289]. Indeed, degree of folate expression is reported to have correlation with malignancy of tumors which are likely to have more acidic environment compared to non malignant cells [290]. Changes in morphology such as enhancement in projections and size of MCF-7 and Nt-8e cells incubated in a media of pH 6.5 observed in this study could have also contributed to increase in folate binding sites which in turn could have enhanced the uptake of PPa via folate receptor targeted Np (Figure 6.5). These changes are more evident in MCF-7 cells as compared to Nt-8e which explains the higher accumulation of PPa (both formulation) observed in these cells. However, the large difference in folate receptor dependent uptake observed in Nt-8e compared to MCF-7 cells indicates presence of higher levels of folate receptors. It should be noted that Nt-8e cell line is derived from grade III tumor therefore it is more likely that these cells have high density of folate receptors than MCF-7 cells.

Results presented in Figure 6.4 indicate that difference in uptake of folate conjugated Np could also be due to pH dependent difference in the binding affinity of folate conjugated Np to receptors. Our observation of higher inhibition in uptake of PPa observed at pH 6.5 in presence of free folic acid as compared to physiological pH suggests increased affinity of folic acid to folate receptor at slightly acidic pH (pH 6.5) which may be due to changes in protonation of amino acids residues [291]. It has been reported that binding of folic acid to folate receptors is

pH dependent and have different pH optima in different type of cells. Binding of folic acid to receptors of rat kidney brush border membrane vesicles have pH optimum at 5.6 [292], FR isolated from porcine kidney shows a broad pH optimum ranging from 5.5 to 7.6, whereas pH of 6.5 is optimum for folate receptor mediated influx of antifolate-methotrexate in F2-MTX A a leukemia cell line with a functional defect folate carrier [291]. The higher uptake of PPa by cells could be due to increase in affinity of folate conjugated Np to folate receptors in acidic pH (6.5) and consistent with other reports. Variation in the inhibition of uptake of folate conjugated Np observed in the two cell lines could be due to differences in the density of folate receptors. Our results (Figure 6.4) also show that uptake of FR-Np-PPa in presence of free folic acid (1 mM) is lower (more than two fold in MCF-7 and three fold in Nt-8e cells at pH 6.5) than the uptake of Np-PPa. This implies that nonspecific uptake of folate targeted particles is reduced in both the types of cells. The reduced nonspecific interaction of FR-Np-PPa with cells might be due to their higher negative zeta potential (-45 mV) as compared to non targeted particle (-24 mV). Nps with positive zeta potential are internalized more readily by cells due to their negative surface charge as compared to particles with negative zeta potential and it has been observed that surface charge on cell surface also influences the uptake of Np [293]. Thus it is possible that Zeta potential of particles as well as differences in the cell surface charges between MCF-7 and Nt-8e could have also contributed to reduction in non specific uptake of FR-Np-PPa in our study. Our study on mechanism of internalization suggests that uptake of both the formulation of PPa occurs predominantly through endocytosis (Figure 6.6). Since our results show significant differences inhibition of endocytosis of FR-targeted Np in both the cells at acidic pH (6.5) as compared to physiological pH, it implies pathway of internalization may be different. There have been conflicting reports on FR-mediated pathways of internalizations [294]. Studies have suggested

that FR is organized in the lipid rafts or receptor rich complexes of cholesterol in the membrane [295] and not associated with clathrin-coated pits [296]. Since the internalization of clatharin mediated endocytosis occurs at a slower rate when extracellular pH is low due slower rate of pinching of clatharin-coated vesicles [297], it is possible that FR-Np may be internalized through clatharin independent pathway when extracellular pH is mildly acidic (pH 6.5). Since internalization pathway also depends on surface charge and size of Nps [298], it is possible that untargeted nanoformulation and folate targeted PPa at physiological pH may follow a different pathway. Our study shows that pH dependent uptake of PPa through both the nanoformulations correlates with phototoxic studies. Low pH (acidic pH) induced enhancement in the phototoxicity of PPa taken up through folate targeted Np observed in our study (Figure 6.7) is attributed to an increase in PPa uptake. Although both the nanoformulations induce high phototoxicity in MCF-7 cells, when drug uptake is compared with cell killing Nt-8e appears to be more photosensitive compared to MCF-7 cells. The observed differences in pH dependent phototoxicity of the two nanoformulations may also be due to a difference in the uptake pathways as well as their localization in different subcellular organelles. It is reported that drugs internalized through the clathrin-mediated pathway may be localized initially in the early endosomes then in late endosomes and subsequently transferred to lysosomes [299]. On the other hand, drug Np entered through caveolae mediated pathway may get localized in the Golgi complex via early endosomes and caveosomes. Depending upon the pathway the relative distribution of targeted and nontargeted Np-PPa in the sensitive sites may vary and contribute to differences in the phototoxicity of the two nanoformulation observed between the MCF-7 and Nt-8e cells.

6.5. Conclusion

In summary, pH dependent uptake and phototoxicity of FR targeted Np doped with PPa is significantly different as compared to untargeted Np-PPa in MCF-7 and Nt-8e cells. While the uptake and phototoxicity of untargeted Np-PPa is independent of pH of the incubation media for both the cell lines, uptake and phototoxicity of FR targeted Np-PPa increases with decrease in pH from 7.4 to 6.5. These results suggests that efficacy of FR-targeted nanoformulated PPa is higher under acidic pH have implications in photodynamic therapy of cancer.

CHAPTER 7

BIODISTRIBUTION AND CLEARANCE STUDIES OF PYROPHEOPHORBIDE–a ENTRAPPED IN FOLATE RECEPTOR TARGETED ORGANICALLY MODIFIED SILICA NANOPARTICLES IN TUMOR BEARING MICE

7.1. Introduction

For successful use of Np based drug delivery system for cancer therapy, it is required that drug delivered through Nps should be high at the tumor site, it should have a fast clearance from the normal organs, stable retention of the drug in Nps while in circulation [78]. Another important criterion of Np based drug delivery is its biosafety or biocompatibility under *in vivo* conditions. It is therefore essential that efficacy of any new drug Np complexes have to be evaluated under *in vivo* conditions [300].

Although several studies have demonstrated the use of ORMOSIL (SiNp) for imaging and delivery of photosensitizer (PS) for photodynamic therapeutic application under *in vitro* conditions [87, 88], there are a few reports on *in vivo* distribution of drug encapsulated SiNp in tumor models. In one of the studies, Kumar et al [107] have studied the biodistribution and toxicity of near infra-red fluorophore/ radioactive iodine conjugated SiNp of size 20-25 nm in nude mice by optical fluorescence imaging, as well by measuring the radioactivity from harvested organs and showed these particles were not toxic under *in vivo* conditions. However, biodistribution and clearance and toxicity of SiNp under *in vivo* conditions may vary depending upon size, surface charge and targeting moiety [301]. This is because under *in vivo*, environmental conditions are extremely complicated and the interactions of the nanostructures with biological components, such as proteins and cells, could lead to unique biodistribution, clearance, immune response, and metabolism [301].

In the previous chapter, we have presented results of our study on evaluation of uptake and photodynamic efficacies of folic acid conjugated (FR-Np-PPa) and plain SiNp encapsulating PPa (Np-PPa) on folate receptor expressing cells. Results showed that under *in vitro* conditions the

uptake and photodynamic efficacies of FR-Np-PPa is higher for breast carcinoma and oral cancer cells than folic acid free Np-PPa. Also our study showed that uptake of FR targeted SiNp is pH dependent [274]. It is, however necessary to understand the tumor uptake efficacies of targeted and untargeted Np-PPa under *in vivo* conditions for evaluating their clinical potential. In this chapter, we present results of study on biodistribution of free PPa, Np-PPa and FR-Np–PPa in mice bearing mammary tumors. Possible toxicity induced by these SiNp on different organs has been evaluated.

7.2. Experimental methods

Preparation and characterization of plain Np-PPa, FR-Np-PPa, used in this study, procedures used for maintainace of C127I (a cell line used for induction of tumor), tumor induction in mice, method used for studying biodistribution and tumor uptake of nanoformulated PPa, histology, biochemical assays (lipid peroxidation and GSH estimation) carried out in tissue homogenates for evaluating the toxicities of Nps have been described in detail in chapter 2.

Size and zeta potential of plain Np-PPa are ~65 nm, −24 ± 6.0 mV, FR-Np-PPa is ~75 nm, −45 ± 4.0 mV.

In this study, tumors in mice were developed by injecting subcutaneously mouse mammary tumor cells (C127I). For biodistribution studies, mice were injected intraperitoneally with different formulations of PPa containing 5.0 μM of PPa and concentration of SiNp used was 3 mg / kg body weight of mice.

7.2.1. Statistical Analysis

Mice were divided in three groups for studying biodistribution and clearance studies of free PPa and nanoformulated PPa (Np-PPa and FR-Np-PPa). Organs resected from the same mice were

used for histology and biochemical (LPO and GSH) measurements. Data presented on tumor uptake and biodistribution of PPa are mean ± standard error of mean of two or three animals. Student's t-test was applied for evaluating the significance and P value <0.05 was considered as statistically significant.

7.3. Results

7.3.1. Uptake of Np-PPa and FR-Np-PPa by C127I cells

Figure 7.1 shows the fluorescence microscopic images of C127I cells incubated with either Np-PPa or FR-Np-PPa (PPa, 0.5 μM) in presence and absence of free folic acid (0.5 mM). As seen in the figure, fluorescence of PPa in cells incubated with FR-Np-PPa is bright as compared to Np-PPa. While in cells incubated with FR-Np-PPa in presence of free folic acid, fluorescence of PPa is reduced considerably, in Np-PPa treated cells the change in fluorescence of PPa is not very obvious. These results suggest involvement of folate receptors in uptake of FR-Np-PPa by C127I cells.

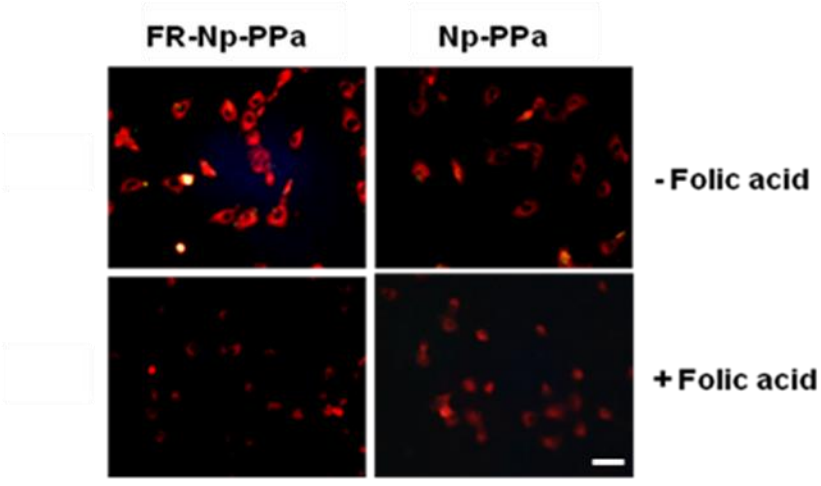

Figure 7.1: Fluorescence microscopic image of C127I cells. Cells were incubated with folic acid (0.5 mM) for 2 h followed by incubation with FR-Np-PPa or Np-PPa for 2 h in dark. (Scale bar: 50 μm).

7.3.2. Uptake of different formulations of PPa by tumor

Figure 7.2 shows the accumulation of PPa in tumor bearing mice injected with different formulations of PPa. As seen in the figure, at 4 h, PPa accumulation in the tumor of the animals injected with free PPa is ~30 nmoles/gm of tissue at 24 h, PPa concentration is enhanced by ~4 fold and at around 120 h PPa concentration is negligible in the tumor. In animals injected with Np-PPa, the concentration of PPa at 4 h and 24 h was ~2 and ~ 1.4 times higher respectively than in animals injected with free PPa. Compared to Np-PPa, accumulation of PPa in tumor of animals injected with FR-Np-PPa, was ~ 1.4 and ~1.5 times higher at 4 and 24 h respectively. Even after 120 h, concentration of PPa retained in the tumor injected with FR-Np-PPa was higher as compared to Np-PPa and free PPa. This indicated that FR-Np-PPa is targeted to tumors.

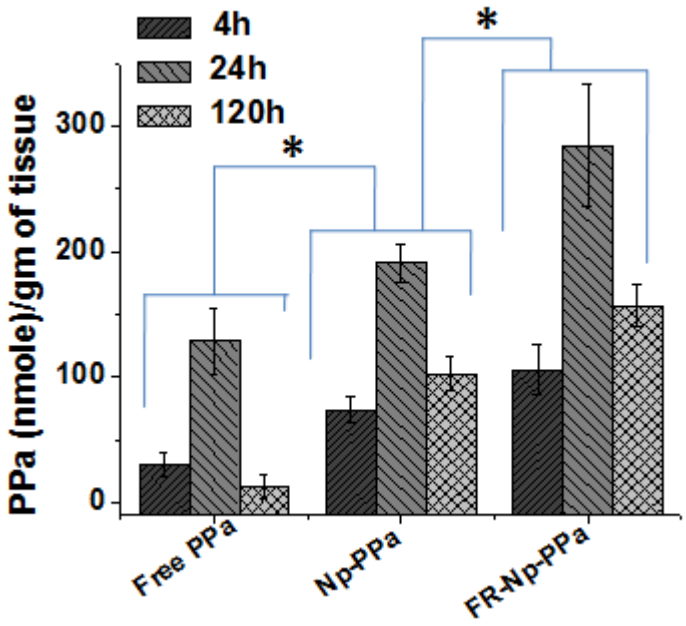

Figure 7.2: Accumulation of PPa in tumor of the mice injected with free PPa, Np-PPa and FR-Np-PPa after 4, 24 and 120 h. PPa concentration is 5.0 µM. (*P<0.05, statistical significance).

7.3.3. Biodistribution of different formulations of PPa

The biodistribution of PPa entrapped in folate receptor targeted Np and untargeted Np was studied by quantitating the PPa extracted from different organs at 4, 24, 72 and 120 h post injection. This was compared with PPa extracted from mice injected with free PPa at similar time points (Figure 7.3 a, b & c).

a)

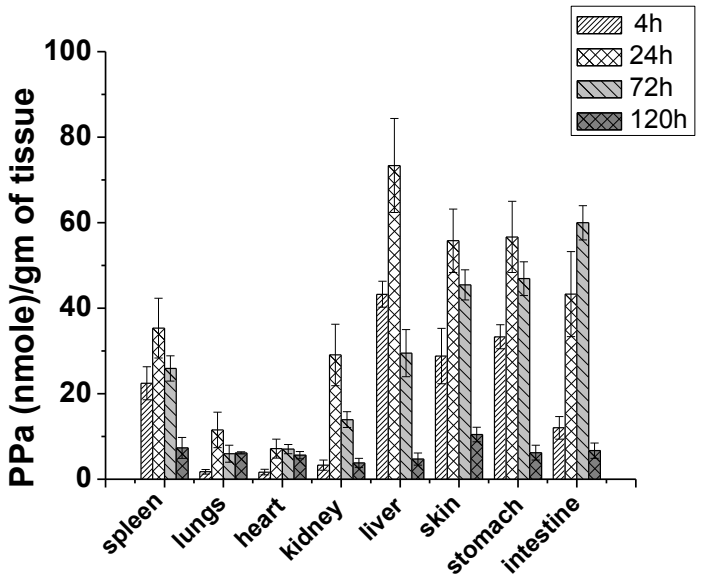

b)

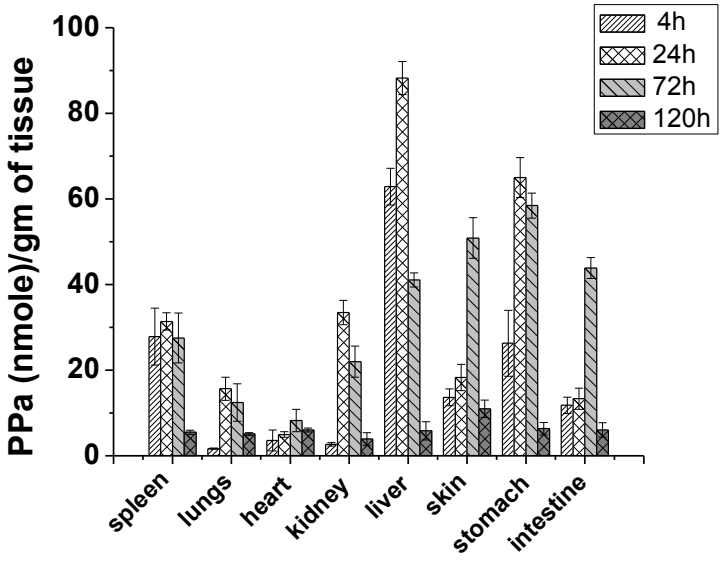

c)

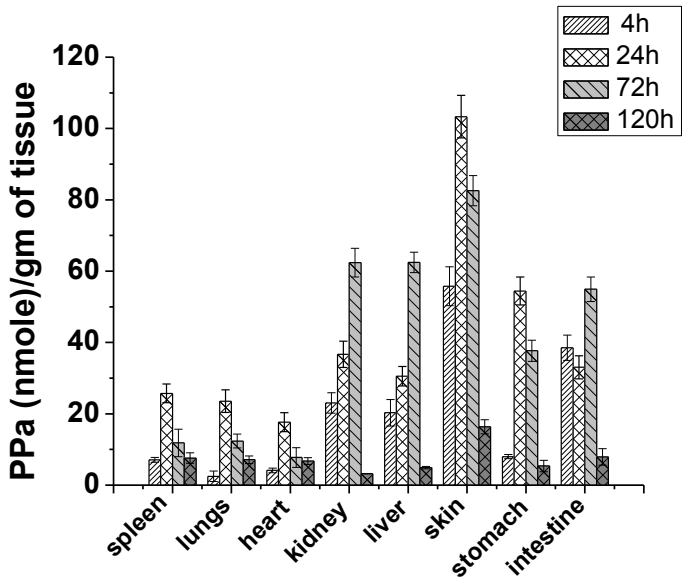

Figure 7.3: Quantitation of PPa accumulated in various organs of mice injected with (a) Np-PPa (b) FR-Np-PPa (c) free PPa at 4, 24, 72 and 120 h.

As shown in the figure 7.3a, at 4 h after injection of Np–PPa, the accumulation of PPa was observed to be highest in liver which was followed by stomach, spleen, skin and intestine. The accumulation of PPa was negligible in kidney, lung and heart at this time point. At 24 h, the concentration of PPa increased in liver, spleen, skin, stomach, intestine and kidney. However, overall concentration PPa in kidney was lower than liver, stomach, intestine and skin. With further increase in time the PPa accumulation increased in intestine but in all other organs decreased and at 120 h the concentration was negligible in all the organs.

After 4 h of injection of FR-Np-PPa , PPa accumulation in the liver was maximum (Figure 7.3b). This was followed by stomach, spleen, skin and intestine. At 24 h the accumulation of PPa

increased in liver, stomach and kidney. At this time point PPa accumulation in skin was much lower than in mice injected with Np-PPa, and did not change significantly in spleen, skin, intestine and heart. At 72 h PPa accumulation increased in skin and intestine, whereas in liver and kidney it decreased. After 5 days, PPa concentration was negligible in all the organs. In contrast, when free PPa was injected maximum accumulation of PPa was observed in skin as compared to all other organs at 4 h (Figure 7.3c). Concentration of PPa in kidney and intestine was high compared to lungs and heart. At 24 h, PPa accumulation increased in all organs and skin showed the highest accumulation. PPa concentration in skin, stomach and spleen decreased slightly at 72 h, whereas in kidney, liver and intestine it increased. With further increase in time the PPa decreased to negligible amount in all the organs.

7.3.4. Plain and folic acid conjugated SiNp induced oxidative stress

Since nanoformulated PPa is retained for longer durations in liver, possible oxidative stress induced by the two nanoformulations on liver was assessed. Figure 7.4, shows the levels of lipid peroxidation (LPO) and glutathione (GSH) in liver tissue homogenates after 72 h of administrating free and the two nanoformulations of PPa. As seen in figure the LPO and GSH levels in liver tissues of mice injected with Np and FR-Np (drug free) were comparable to that of control animals. This indicated that SiNp at the concentration (3 mg/kg) used did not induce any oxidative stress.

a)

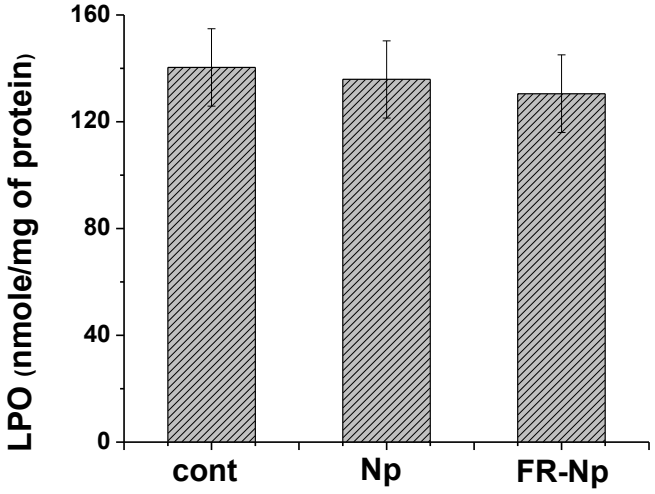

b)

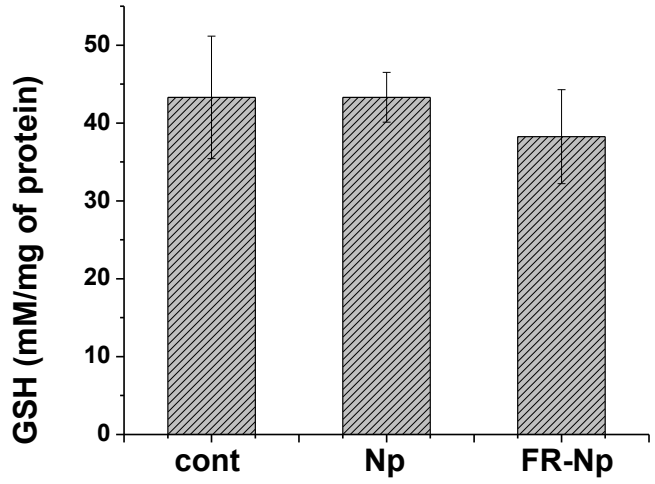

Figure 7.4: Oxidative stress induced by plain and FR conjugated Np in liver tissue (a) Lipid peroxidation (LPO) (b) GSH. Liver tissues were excised from animals after 72 h of injection with Np and FR-Np. Concentration of Np injected was 3 mg/kg.

7.3.5. Histological evaluation

Possible toxicity induced by plain and FR-Np on organs involved in excretion was evaluated through histology. Figure 7.5 shows the histological sections of the liver and kidney of mice after 72 h of injection with the plain Np and FR-Np and untreated control.

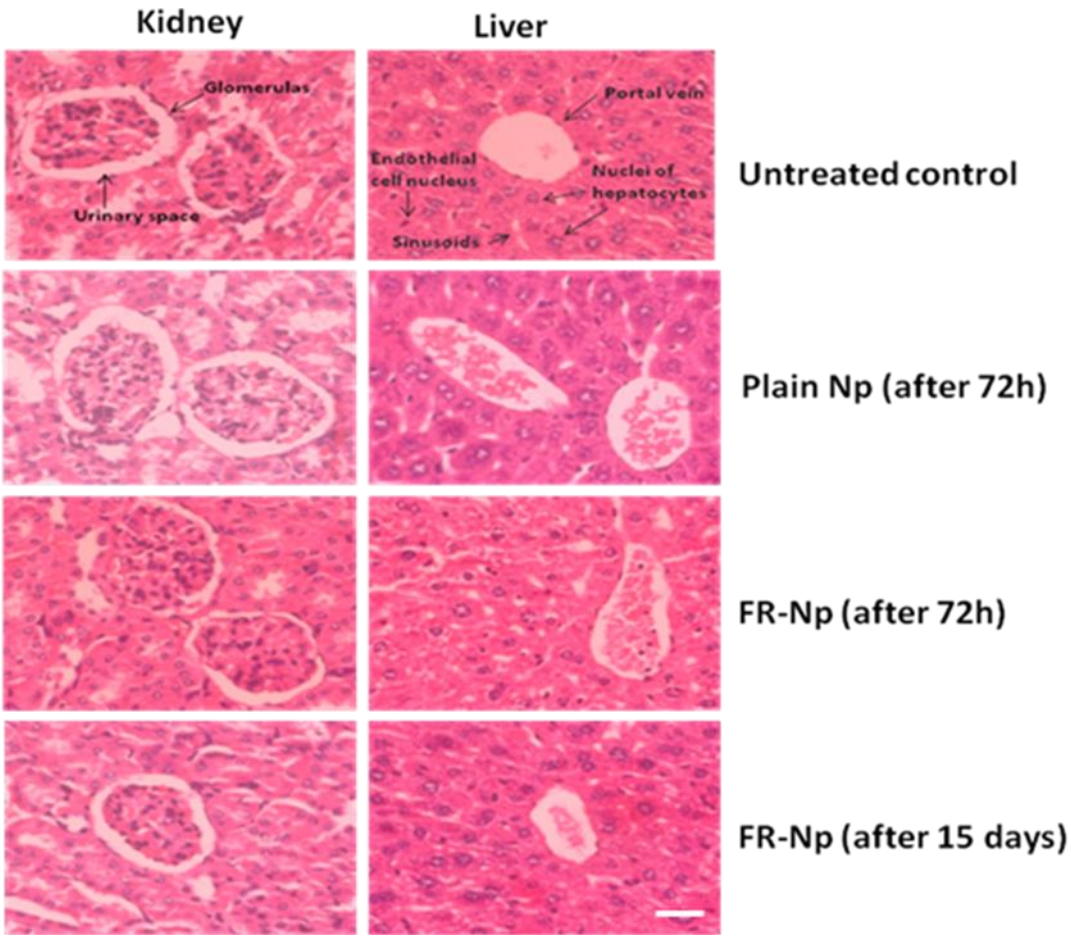

Figure 7.5: Representative histological images of liver and kidney of mice injected with Nps or FR-Np. Liver, and kidney samples were excised after 72 and 360 h after intaperitonial administration of different Nps, fixed and processed for histology. The hematoxylin and eosin stained tissue sections were observed under a microscope at 40×. Concentration of Np injected was 3 mg/kg. Scale bar (— 100 µm).

As seen in figure, no apparent tissue damages were observed in the mice injected with the FR-Np or void Np, when compared with histology of organs of control mice. Histology of liver and kidney were normal even after 15 days of administrating void FR-Np. This indicated that SiNp did not cause any long term toxicity at the concentration used.

7.4. Discussion

The main objective of this study was to evaluate the tumor uptake efficacy and biodistribution of plain and folic acid conjugated SiNp encapsulating PPa under *in vivo* condition and also evaluate their possible toxicities in organs of excretion. As discussed in the previous chapter, the conjugation of Np with folic acid facilitates binding to folate receptors which is over expressed in many types of tumors and relatively absent in most normal tissues [294].

The results presented in Figure 7.2 show that tumor accumulation of PPa delivered using Np is higher than free PPa at all the post injection time points studied. These results indicate that Np-PPa formulation has better tumor localizing property than free PPa which is due to the EPR effect [302]. The concentration of PPa in tumors of mice injected with Np-PPa formulations was relatively higher. This further confirmed that nanoformulated drug is retained better than free PPa. Among the two formulations, accumulation of folic acid receptor targeted Np-PPa was higher (~ 1.5 times) at 24 h and retained for longer period (120 h) than folic acid free Np. This is due to more efficient cellular uptake of Np-PPa which may be due to presence of folate receptors in C127I mammary tumor. These results are in agreement with our *in vitro* studies which shows reduced uptake of FR-Np-PPa in presence of free folic acid (Figure 7.1) due to competitive

binding. These results indicate that cellular uptake of folic acid conjugated Np accumulated at the tumor sites due to EPR is enhanced due to presence of high affinity sites on cells [294, 303].

Results presented in Figure 7.3 (a, b & c) show that biodistribution of Np-PPa and FR-Np-PPa is quite different compared to free PPa. Compared to free PPa, high accumulation of Np-PPa and FR-Np-PPa observed in liver, spleen and stomach initially (4 h) indicates that intraperitonially injected Nps gets absorbed in blood rapidly through peritoneum. It may be possible that nanoformulated PPa may penetrate into stomach and liver directly from peritoneal cavity [304].

Enhanced uptake of the nanoformulated PPa observed in the liver, spleen at 4 h post injection compared to free PPa is attributed due to capture of these particles by the macrophages residing in these organs. Large molecules or particles (>10 nm) and highly charged surfaces are recognized by the RES and are quickly removed from the circulation [300, 305, 306]. Since size of Np-PPa and FR-Np-PPa are of ~65 nm and ~75 nm respectively and both these particles are negatively charged (-25 & -45 mV) and also these particles are not pegylated they are more likely to be recognized and captured by RES in liver and spleen [274].

Pharmacokinetics study shows for mice injected with FR-Np-PPa, uptake of PPa in liver peaks at 24 h and slowly decrease with time (`~120 h), whereas accumulation of PPa in stomach and intestine is more at later time (72 h). This indicates that excretion pathway is mainly by hepatobiliary pathway. Compared to Np-PPa, PPa accumulation in liver of animals injected with FR-Np-PPa is high. One reason for this could be because macrophages have folate receptors therefore the uptake of FR-Np-PPa may be better than Np-PPa in liver [307].

Uptake of PPa observed in the kidney, is not due to excretion of FR-Np-PPa or Np-PPa as the size of these particles are too large (~65 nm, ~75 nm) for glomerular filtration in kidney [300, 305]. The observed accumulation of PPa in kidney at 24 h may be due to excretion of PPa leaked

out from the Nps or degradation Np-PPa in liver and spleen RES system. Interestingly, PPa accumulation in skin also increased after 24 h in Np-PPa injected mice which is also likely to be due to leakage of PPa or degradation of SiNp. In case of FR-Np-PPa injected mice, PPa accumulation in skin was more at later time points (72 h). This indicates that SiNp may get degraded slowly. Rate of leakage may vary in FR conjugated and FR free SiNp. Indeed, previous studies have also reported leakage of PS entrapped in SiNp [107]. However it should be noted that concentration of PPa in skin is much lower than the mice injected with free PPa.

In contrast to nanoformulated PPa, free PPa accumulates less in liver, spleen initially (4 h) which may be because of its small size and being hydrophobic it is less likely to be taken up by RES [308]. Concentration of PPa in liver, stomach, intestine as well as in kidney increases at later time points (72 h) in mice injected with free PPa indicating that both renal and hepatobiliary pathway of excretion may be involved. Since free PPa molecules are small (less than 6 nm) compared to Nps and they can easily go through the renal filtration [300]. Increase in concentration of free PPa in skin with time (upto 72 h) indicates that skin has higher affinity binding sites.

Our results on analysis of LPO and GSH (Figure 7.4) content in liver tissue of the mice injected with the either plain Np or FR-Np indicate that SiNp do not induce any oxidative stress. This is supported by observation of lack of any apparent tissue/cellular damages in the kidney and liver of these mice (Figure 7.5) even after 15 days after administration of Np. These results were consistent with other studies carried out using mesoporous SiNp [309]. In contrast to these studies, it has been reported that colloidal SiO_2 Np induces extensive liver injury due to longer retention of SiO_2 Np in the RES [310-312]. The negligible toxicity observed in mesoporous

SiNp could be due to efficient degradation in liver because of porous nature of SiNps as compared to SiO_2 Np [313].

7.5. Conclusion

In summary, our study show that PPa accumulation in tumor is higher in mice injected with FR-Np-PPa, Np-PPa than the animals injected with free PPa. Biodistribution and clearance studies showed nanoformulated PPa was excreted mainly by hepatobiliary pathway. The results of toxicity showed that these nanoparticles do not induce any oxidative stress in liver. No morphological changes are observed in kidney even after 15 days of administrating Nps. This indicated that SiNp did not cause any long term toxicity and could be an efficient drug delivery system.

CHAPTER 8

SUMMARY AND FUTURE PROSPECTIVES

The main objective of the work reported in this thesis was to investigate the use of SiNp for improvement of bioavailability and therapeutic efficacy of hydrophobic drugs which are of interest to cancer treatment. Towards this objective, efficacy of SiNp for delivery of hydrophobic drugs curcumin, a natural herbal agent and pyropheophorbide-a (PPa), which is a potential PS for PDT of cancer was investigated.

Results of our investigation on uptake of curcumin delivered using SiNp (cur-SiNp) in human oral cancer cells showed that curcumin uptake is more as compared to free curcumin. Increase in uptake was attributed to lower degradation of curcumin incorporated in SiNp. Studies on cytotoxicity showed that cur-SiNp induces enhanced cell killing and inhibition in the activity of NF-kB and its regulated proteins involved in invasion (MMP-9), angiogenesis (VEGF) and inflammation (TNF-α) in dark as well as on exposure to light. This study was extended to multicellular spheroids of human oral cancer cells (Nt-8e) cells which have three dimensional organization, extracellular matrix, complex biochemical and biomechanical environments as in tumors under *in vivo* conditions. Results showed that uptake and phototoxicity of nanoformulated curcumin was higher than free curcumin in spheroids. This resulted in larger inhibition in growth and migration of cells and enhanced reactive oxygen species generation as compared to spheroids treated with free curcumin under similar conditions. Phototoxicity of cur-SiNp decreased in presence of GSH, a ROS scavenger confirming the involvement of ROS in phototoxicity. These results suggest that nanoformulation of curcumin is also able to penetrate in three dimensional tumor models.

To improve targeting efficacy, SiNp-cur was conjugated with Hyaluronic acid (HA-SiNp-cur), which has a strong affinity for CD44 receptor that are over expressed in cancer cells. Results of

our investigations on uptake and cytotoxic efficacy of HA-SiNp-cur on human colon carcinoma (colo-205 cells) showed that uptake of curcumin delivered through HA-SiNp-cur was significantly higher in monolayer and spheroid cultures as compared to free curcumin and HA free SiNp-cur. The uptake of HA-SiNp-cur was found to be receptor mediated. Cytotoxicity, cell death, inhibition in growth and migration of cells was higher in spheroids treated with HA-SiNp-cur complex as compared to HA free SiNp complex and free curcumin. Studies also showed that release of curcumin from HA-SiNp-cur involves enzyme.

Results of study carried out on uptake and photodynamic action of plain Np-PPa as well as folic acid conjugated SiNp entrapping PPa (FR-Np-PPa) in two cell lines (squamous cell carcinoma (Nt-8e) cells, and adenocarcinoma of breast (MCF-7) showed that the uptake of untargeted Np-PPa is independent of pH of the incubation media for both the cell lines, for FR-Np-PPa, uptake of PPa increased with decrease in pH from 7.4 to 6.5. These results suggested that acidic pH influence the binding of FR-Np to cells. Similarly, for FR targeted Np-PPa phototoxicity was pH dependent and showed higher phototoxicity at pH 6.5, whereas phototoxicity of plain Np-PPa was independent of pH of the incubation media for both the cell lines. These results suggests that photodynamic efficacy of FR-targeted nanoformulated PPa is higher under acidic pH.

Results on biodistribution of free PPa, Np-PPa and its folic acid conjugate (FR-Np-PPa) and possible toxicity of these formulations studied in mice bearing mammary tumors showed that tumor uptake of FR-Np-PPa, was higher than in Np-PPa and free PPa. Clearance study showed nanoformulated PPa was excreted mainly by hepatobiliary pathway. The SiNp did not induce any significant change in oxidative stress markers and morphological changes in liver and kidney. This indicated that SiNp did not cause any long term toxicity.

In conclusion, results presented in different cancer cells and spheroids show SiNp is a promising delivery vehicle for curcumin and pyropheophorbide-a. It is therefore worthwhile to explore the photodynamic efficacies of these nanoformulations in *in vivo* tumor models for evaluating their clinical potential.

REFERENCES

[1] Siegel R, Ward E, Brawley O, Jemal A. Cancer statistics, 2011: the impact of eliminating socioeconomic and racial disparities on premature cancer deaths. CA Cancer J Clin. 2011; 61: 212-36.

[2] Treasure J. Herbal medicine and cancer: an introductory overview. Semin Oncol Nurs. 2005; 21: 177–83.

[3] Ahmad A, Sakr WA, Rahman KM. Novel targets for detection of cancer and their modulation by chemopreventive natural compounds. Front Biosci (Elite Ed). 2012; 4: 410–25.

[4] Triesscheijn M, Baas P, Schellens JH, Stewart FA. Photodynamic therapy in oncology. Oncologist 2006; 11: 1034–44.

[5] Oleinick NL, Morris RL, Belichenko I. The role of apoptosis in response to photodynamic therapy: what, where, why, and how. Photochem. Photobiol. Sci. 2001; 1: 1–21.

[6] Dougherty TJ, Gomer CJ, Henderson BW, Jori G, Kessel D, Korbelik M, Moan J, Peng Q. Photodynamic therapy. J. Natl. Cancer Inst. 1998; 90: 889–905.

[7] Williams HD, Trevaskis NL, Charman SA, Shanker RM, Charman WN, Pouton CW. Strategies to address low drug solubility in discovery and development. Pharmacol. Rev. 2013; 65: 315–499.

[8] Hobbs SK, Monsky WL, Yuan F, Roberts WG, Griffith L, Torchilin VP. Regulation of transport pathways in tumor vessels: role of tumor type and microenvironment. Proc. Natl. Acad. Sci. U. S. A. 1998; 95: 4607–12.

[9] Prabhakar U, Maeda H, Jain RK, Sevick-Muraca EM, Zamboni W, Farokhzad OC. Challenges and key considerations of the enhanced permeability and retention effect for nanomedicine drug delivery in oncology. Cancer Res. 2013; 73: 2412–17.

[10] Jain RK, Stylianopoulos T. Delivering nanomedicine to solid tumors. Nat. Rev. Clin. Oncol. 2010; 7: 653–64.

[11] Provenzano PP, Cuevas C, Chang AE, Goel VK, Von Hoff DD, Hingorani SR. Enzymatic targeting of the stroma ablates physical barriers to treatment of pancreatic ductal adenocarcinoma. Cancer Cell 2012; 21: 418–29.

[12] Bareford LM, Swaan PW. Endocytic mechanisms for targeted drug delivery. Adv. Drug Deliv. Rev. 2007; 59: 748–58.

[13] Bhattacharyya S, Bhattacharya R, Curley S, McNiven MA, Mukherjee P. Nanoconjugation modulates the trafficking and mechanism of antibody induced receptor endocytosis. Proc. Natl. Acad. Sci. U. S. A. 2010; 107: 14541–46.

[14] Jhaveri A, Deshpande P, Torchilin V. Stimuli-sensitive nanopreparations for combination cancer therapy. J. Control. Release 2014; 190: 352-70.

[15] Obata Y, Tajima S, Takeoka S. Evaluation of pH-responsive liposomes containing amino acid-based zwitter ionic lipids for improving intracellular drug delivery in vitro and in vivo. J. Control. Release 2010; 142: 267–76.

[16] Du JZ, Du XJ, Mao CQ, Wang J. Tailor-made dual pH-sensitive polymer doxorubicin nanoparticles for efficient anticancer drug delivery. J. Am. Chem. Soc. 2011; 133: 17560–563.

[17] Hu CMJ, Zhang L. Therapeutic nanoparticles to combat cancer drug resistance. Curr. Drug Metab. 2009; 10: 836–41.

[18] Allen TM. Liposomes:Opportunities as drug delivery systems. Drugs 1997; 54: 8-14.

[19] Torchillin VP. Recent advances with Liposomes as Pharmaceutical carriers, Nature drug discovery. 2005; 4: 145-60.

[20] Arshady R. Preparation of biodegradable microspheres and microcapsules: 2. Polyactides and related polyesters. J Control Release 1991; 17: 1–21.

[21] Goyal P, Goyal K, Vijaya Kumar SG. Liposomal drug delivery systems clinical applications. Acta Pharmaceut 2005; 55: 1–25.

[22] Wicki A, Witzigmannb D, Balasubramanian V, Huwyler J. Nanomedicine in cancer therapy: Challenges, opportunities, and clinical applications Journal of Controlled Release 2015; 200: 138–57.

[23] Rangaramanujam MK, Omathanu PP, Sujatha K. Biomedical applications of nanotechnology: dendrimers and hyperbranched polymers for drug delivery. In: V Labhasetwar V and Leslie-Pelecky DL (eds) Biomedical applications of nanotechnology. NJ: John Wiley & Sons, 2007, pp. 107–129.

[24] Gabizon A, Papahadjopoulos D. Liposome formulations with prolonged circulation time in blood and enhanced uptake by tumors. P Natl Acad Sci USA 1988; 85: 6949–53.

[25] Barani H and Montazer M. A review on applications of liposomes in textile processing. J Liposome Res 2008; 18: 249–62.

[26] Müller RH, Mäder K, Gohla S. Solid lipid nanoparticles (SLN) for controlled drug delivery – a review of the state of the art. Eur. J. Pharm. Biopharm. 2000; 50: 161–77.

[27] Bae Y, Kataoka K. Intelligent polymeric micelles from functional poly (ethylene glycol) poly (amino acid) block copolymers. Adv. Drug Deliv. Rev. 2009; 61: 768–84.

[28] Torchilin VP. Structure and design of polymeric surfactant based drug delivery systems. J. Control. Release 2001; 73: 137–72.

[29] Lin W, He Y, Zhang J, Wang L, Wang Z, Ji F, Chen S. Highly hemocompatible zwitterionic micelles stabilized by reversible cross-linkage for anti-cancer drug delivery. Colloids Surf. B: Biointerfaces 2014; 115: 384–90.

[30] Kumari A, Yadav SK, Yadav SC. Biodegradable polymeric nanoparticles based drug delivery systems. Int. J. Pharm. 2010; 75: 1–18.

[31] Nobs L, Buchegger F, Gurny R, Allémann E. Poly(lactic acid) nanoparticles labeled with biologically active Neutravidin TM for active targeting. Eur. J.Pharm. Biopharm. 2004; 58: 483–90.

[32] Ikezoe T, Yang Y, Bandobashi K, Saito T, Takemoto S, Machida H, Togitani K, Koeffler HP, Taguchi H. Oridonin, a diterpenoid purified from Rabdosiarubescens, inhibits the proliferation of cells from lymphoid malignancies in association with blockade of the NF-κB signal pathways. Mol. Cancer Ther. 2005; 4: 578–86.

[33] Xing J, Zhang D, Tan T. Studies on the oridonin loaded poly (D,L-lactic acid) nanoparticles in vitro and in vivo. Int. J. Biol. Macromol. 2007; 40: 153–58.

[34] Prabu P, Chaudhari AA, Dharmaraj N, Khil MS, Park SY, Kim HY. Preparation, characterization, in-vitro drug release and cellular uptake of poly (caprolactone) grafted dextran copolymeric nanoparticles loaded with anticancer drug. J. Biomed. Mater. Res. A 2009; 90: 1128–36.

[35] Sharma RI, Pereira M, Schwarzbauer JE, Moghe PV. Albumin-derived nanocarriers: substrates for enhanced cell adhesive ligand display and cell motility, Biomaterials 2006; 27: 3589–98.

[36] Elsadek B, Kratz F. Impact of albumin on drug delivery new applications on the horizon. J. Control. Release 2012; 157: 4–28.

[37] Kratz F. Albumin as a drug carrier: design of prodrugs, drug conjugates and nanoparticles, J. Control. Release 2008; 132: 171–83.

[38] Dreis S, Rothweiler F, Michaelis M, Cinatl J, Kreuter J, Langer K. Preparation, characterization and maintenance of drug efficacy of doxorubicin loaded human serum albumin (HSA) nanoparticles. Int. J. Pharm. 2007; 341: 207–14.

[39] Matthews OA, Shipway AN, Stoddart JF. Dendrimers branching out from curiosities into new technologies. Prog Polym Sci 1998; 23: 1–56.

[40] Soliman GM, Sharma A, Maysinger D. Dendrimers and miktoarm polymers based multivalent nanocarriers for efficient and targeted drug delivery. Chem Commun 2011; 47: 9572–87.

[41] Majoros IJ, Williams CR, Becker A. Methotrexate delivery via folate targeted dendrimer based nanotherapeutic platform. Wiley Interdiscip Rev Nanomed Nanobiotechnol 2009; 1: 502–10.

[42] McNerny DQ, Leroueil PR, Baker JR. Understanding specific and nonspecific toxicities: a requirement for the development of dendrimer-based pharmaceuticals. Wiley Interdiscip Rev Nanomed Nanobiotechnol 2010; 2: 249–59.

[43] Lubbe AS, Bergemann C, Brock J. Physiological aspects in magnetic drug-targeting. J Magn Mater 1999; 194: 149–55.

[44] Liu YJ, Zhang B, Yan B. Enabling anticancer therapeutics by nanoparticle carriers: the delivery of paclitaxel. Int J Mol Sci 2011; 12: 4395–13.

[45] Wu X, Wu M, Zhao JX. Recent development of silica nanoparticles as delivery vectors for cancer imaging and therapy. Nanomedicine: Nanotech. Biol. and Medicine 2014; 10: 297–312.

[46] Rosenholm JM, Sahlgren C, Linden M. Multifunctional mesoporous silica nanoparticles for combined therapeutic, diagnostic and targeted action in cancer treatment. Curr Drug Targets 2011; 12: 1166-86.

[47] Kwon S, Singh RK, Perez RA, Abou Neel EA, Kim HW, Chrzanowski W. Silica-based mesoporous nanoparticles for controlled drug delivery. J Tissue Eng. 2013; doi: 10.1177/2041731413503357.

[48] Bradbury MS, Phillips E, Montero PH, Cheal SM, Stambuk H, Durack JC, Sofocleous CT, Meester RJ, Wiesner U, Patel S. Clinically-translated silica nanoparticles as dual-modality cancer-targeted probes for image-guided surgery and interventions. Integr. Biol 2013; 5: 74—86.

[49] Slowing II, Vivero-Escoto JL, Wu CW, Lin VS. Mesoporous silica nanoparticles as controlled release drug delivery and gene transfection carriers. Adv. Drug Deliv. Rev 2008; 60: 1278—88.

[50] Bae SW, Tan W, Hong JI. Fluorescent dye-doped silica nanoparticles: new tools for bioapplications. Chem Commun 2012; 48: 2270-82.

[51] Li Z, Barnes JC, Bosoy A, Stoddart JF, Zink JI. Mesoporous silica nanoparticles in biomedical applications. Chem Soc Rev 2012; 41: 2590-605.

[52] Rosenholm JM, Sahlgren C, Lindén M. Towards multifunctional, targeted drug delivery systems using mesoporous silica nanoparticles opportunities & challenges. Nanoscale 2010; 2: 1870-83.

[53] Rao KS, El-Hami K, Kodaki T, Matsushige K, Makino K. A novel method for synthesis of silica nanoparticles, J. Colloid and Interface Sci. 2005; 289: 125-31.

[54] Scherer G W, Brinker C J. Sol-Gel Science, Academic Press, New York (1990). Adv Drug Deliv Rev 2008; 60: 1278-88.

[55] Piao Y, Burns A, Kim J, Wiesner U Hyeon T. Designed Fabrication of Silica Based Nanostructured Particle Systems for Nanomedicine Applications. Adv. Funct. Mater. 2008; 18: 3745–58.

[56] Brevet D, Gary-Bobo M, Raehm L, Richeter S, Hocine O, Amro K, Loock B, Couleaud P, Frochot C, Morere A, Maillard P, Garcia M, Durand J O. Mannose-targeted mesoporous silica nanoparticles for photodynamic therapy. Chem. Commun. 2009; 12: 1475–77.

[57] Cheng SH, Lee CH, Yang CS, Tseng FG, Mou CY, Lo LW. Mesoporous silica nanoparticles functionalized with an oxygen-sensing probe for cell photodynamic therapy: potential cancer theranostics. J. Mater. Chem. 2009; 19: 1252–57.

[58] Tu BHL, Lin YS, Hung Y, Lo LW, Chen YF, Mou CY. In vitro studies of functionalized mesoporous silica nanoparticles for photodynamic therapy. Adv. Mater. 2009; 21: 172–77.

[59] Kim S, Ohulchanskyy TY, Pudavar HE, Pandey RK, Prasad PN. Organically modified silica nanoparticles co-encapsulating photosensitizing drug and aggregation-enhanced two-photon absorbing fluorescent dye aggregates for two-photon photodynamic therapy. J. Am. Chem. Soc., 2007; 129: 2669–75.

[60] Coll C, Bernardos A, Martínez-Máñez R, Sancenón F. Gated silica mesoporous supports for controlled release and signaling applications. Acc Chem Res. 2013; 46: 339-49.

[61] Lai CY, Trewyn BG, Jeftinija DM, Jeftinija K, Xu S, Jeftinija S, et al. A mesoporous silica nanosphere based carrier system with chemically removable CdS nanoparticle caps for stimuli responsive controlled release of neurotransmitters and drug molecules. J Am Chem Soc 2003; 125: 4451-59.

[62] Singh N, Karambelkar A, Gu L, Lin K, Miller JS, Chen CS, et al. Bioresponsive mesoporous silica nanoparticles for triggered drug release. J Am Chem Soc 2011; 133: 19582-85.

[63] Chen C, Geng J, Pu F, Yang X, Ren J, Qu X. Polyvalent nucleic acid/mesoporous silica nanoparticle conjugates: dual stimuli-responsive vehicles for intracellular drug delivery. Angew Chem Int Ed 2011; 50: 882-86.

[64] Meng H, Xue M, Xia T, Zhao Y-L, Tamanoi F, Stoddart JF, et al. Autonomous in vitro anticancer drug release from mesoporous silica nanoparticles by pH-sensitive nanovalves. J Am ChemSoc 2010; 132: 12690-97.

[65] Saito G, Swanson JA, Lee KD. Drug delivery strategy utilizing conjugation via reversible disulfide linkages: role and site of cellular reducing activities. Adv Drug Deliv Rev 2003; 55: 199-215.

[66] Wang Y, Zhao Q, Han N, Bai L, Li J, Liu J, Che E, Hu L, Zhang Q, Jiang T, Wang S. Mesoporous silica nanoparticles in drug delivery and biomedical applications. Nanomedicine. 2015; 11: 313-27.

[67] Gan Q, Dai D, Yuan Y, Qian J, Sha S, Shi J, Liu C. Effect of size on the cellular endocytosis and controlled release of mesoporous silica nanoparticles for intracellular delivery. Biomed Microdevices. 2012; 14: 259-70.

[68] Slowing II, Trewyn BG, Giri S, Lin VSY. Mesoporous Silica Nanoparticles for Drug Delivery and Biosensing Applications. Adv. Funct. Mater. 2007; 17: 1225–36.

[69] Jambhrunkar S, Qu Z, Popat A, Yang J, Noonan O, Acauan L, Ahmad Nor Y, Yu C, Karmakar S. Effect of surface functionality of silica nanoparticles on cellular uptake and cytotoxicity. Mol Pharm. 2014; 11: 3642-55.

[70] Ekkapongpisit M, Giovia A, Follo C, Caputo G, Isidoro C. Biocompatibility, endocytosis, and intracellular trafficking of mesoporous silica and polystyrene nanoparticles in ovarian cancer cells: effects of size and surface charge groups. Int J Nanomedicine. 2012; 7: 4147-58.

[71] Huang DM, Hung Y, Ko BS, Hsu SC, Chen WH, Chien CL, Tsai CP, Kuo CT, Kang JC, Yang CS, Mou CY, Chen YC. Highly efficient cellular labeling of mesoporous nanoparticles in human mesenchymal stem cells: implication for stem cell tracking. FASEB J. 2005; 19: 2014-16.

[72] Yu M, Jambhrunkar S, Thorn P, Chen J, Gu W, Yu C. Hyaluronic acid modified mesoporous silica nanoparticles for targeted drug delivery to CD44-overexpressing cancer cells. Nanoscale. 2013; 5: 178-83.

[73] Ma X, Qu Q, Zhao Y. Targeted delivery of 5-aminolevulinic Acid by multifunctional hollow mesoporous silica nanoparticles for photodynamic skin cancer therapy. ACS Appl Mater Interfaces. 2015; 7: 10671-76.

[74] Chen Z, Li Z, Lin Y, Yin M, Ren J, Qu X. Bioresponsive hyaluronic acid-capped mesoporous silica nanoparticles for targeted drug delivery. Chemistry 2013; 19: 1778-83.

[75] Gary-Bobo M, Hocine O, Brevet D, Maynadier M, Raehm L, Richeter S, Charasson V, Loock B, Morère A, Maillard P, Garcia M, Durand JO. Cancer therapy improvement with mesoporous silica nanoparticles combining targeting, drug delivery and PDT. Int J Pharm. 2012; 423: 509-15.

[76] Ma'mani L, Nikzad S, Kheiri-Manjili H, Al-Musawi S, Saeedi M, Askarlou S, Foroumadi A, Shafiee A. Curcumin-loaded guanidine functionalized PEGylated I3ad mesoporous silica nanoparticles KIT-6: practical strategy for the breast cancer therapy. Eur J Med Chem. 2014; 83: 646-54.

[77] Lu J, Liong M, Zink JI, Tamanoi F. Mesoporous silica nanoparticles as a delivery system for hydrophobic anticancer drugs. Small 2007; 3: 1341-46.

[78] Lu J, Liong M, Li Z, Zink JI, Tamanoi F. Biocompatibility, biodistribution, and drug delivery efficiency of mesoporous silica nanoparticles for cancer therapy in animals. Small 2010; 6: 1794-805.

[79] He X, Hai L, Su J, Wang K, Wu X. One-pot synthesis of sustained released doxorubicin silica nanoparticles for aptamer targeted delivery to tumor cells. Nanoscale 2011; 3: 2936-42.

[80] Qian J, Gharibi A, He S. Colloidal mesoporous silica nanoparticles with protoporphyrin IX encapsulated for photodynamic therapy. J Biomed Opt. 2009; 14: 014012.

[81] Yang Y, Song W, Wang A, Zhu P, Fei J, Li J. Lipid coated mesoporous silica nanoparticles as photosensitive drug carriers. Phys Chem Chem Phys. 2010; 12: 4418-22.

[82] Zhu J, Wang H, Liao L, Zhao L, Zhou L, Yu M, Wang Y, Liu B, Yu C. Small mesoporous silica nanoparticles as carriers for enhanced photodynamic therapy. Chem Asian J. 2011; 6: 2332-38.

[83] Teng IT, Chang YJ, Wang LS, Lu HY, Wu LC, Yang CM, Chiu CC, Yang CH, Hsu SL, Ho JA. Phospholipid functionalized mesoporous silica nanocarriers for selective photodynamic therapy of cancer. Biomaterials. 2013; 34: 7462-70.

[84] Tu J, Wang T, Shi W, Wu G, Tian X, Wang Y, Ge D, Ren L. Multifunctional ZnPc loaded mesoporous silica nanoparticles for enhancement of photodynamic therapy efficacy by endolysosomal escape. Biomaterials. 2012; 33: 7903-14.

[85] Chen C, Zhou L, Geng J, Ren J, Qu X. Photosensitizer incorporated quadruplex DNA gated nanovechicles for light triggered, targeted dual drug delivery to cancer cells. Small. 2013; 9: 2793-800.

[86] Idris NM, Gnanasammandhan MK, Zhang J, Ho PC, Mahendran R, Zhang Y. *In vivo* photodynamic therapy using up conversion nanoparticles as remote controlled nanotransducers. Nat Med. 2012; 18: 1580-85.

[87] Ohulchanskyy TY, Roy I, Goswami LN, Chen Y, Bergey EJ, Pandey RK, Oseroff AR, Prasad PN. Organically modified silica nanoparticles with covalently incorporated photosensitizer for photodynamic therapy of cancer. Nano Lett. 2007; 7: 2835-42.

[88] Roy I, Ohulchansky T, Pudavar HE, Bergey EJ, Morgan J, Oseroff AR, Dougherty TJ, Prasad PN. Ceramic-based nanoparticles entrapping water insoluble photosensitizing anticancer

drugs: a novel drug-carrier system for photodynamic therapy (PDT). J Am Chem Soc 2003; 125: 7860–65.

[89] Das S, Jain TK, Maitra AN. Inorganic-organic hybrid nanoparticles from n-octyl triethoxy silane. J. Colloid Interface Sci. 2002; 252: 82–88.

[90] Jain TK, Roy I, De TK, Maitra AN. Nanometer silica particle encapsulating active compound: a novel ceramic drug carrier. J. Am. Chem. Soc. 1998; 120: 11092–95.

[91] Zhao B, Yin JJ, Bilski PJ, Chignell CF, Roberts JE, He YY. Enhanced photodynamic efficacy towards melanoma cells by encapsulation of Pc4 in silica nanoparticles. Toxicol Appl Pharmacol. 2009; 241: 163-72.

[92] Compagnin C, Baù L, Mognato M, Celotti L, Miotto G, Arduini M, Moret F, Fede C, Selvestrel F, Rio Echevarria IM, Mancin F, Reddi E. The cellular uptake of meta-tetra(hydroxyphenyl) chlorin entrapped in organically modified silica nanoparticles is mediated by serum proteins. Nanotechnology 2009; 20: 345101.

[93] Kim S, Ohulchanskyy TY, Bharali D, Chen Y, Pandey RK, Prasad PN. Organically Modified Silica Nanoparticles with Intraparticle Heavy Atom Effect on the Encapsulated Photosensitizer for Enhanced Efficacy of Photodynamic Therapy. J Phys Chem C Nanomater Interfaces. 2009; 113: 12641–44.

[94] Uppal A, Jain B, Gupta PK, Das K. Photodynamic action of Rose Bengal silica nanoparticle complex on breast and oral cancer cell lines. Photochem Photobiol. 2011; 87: 1146-51.

[95] Qian J, Li X, Wei M, Gao X, Xu Z, He S. Bio-molecule-conjugated fluorescent organically modified silica nanoparticles as optical probes for cancer cell imaging. Opt Express. 2008; 16: 19568-78.

[96] Qian J, Wang D, Cai F, Zhan Q, Wang Y, He S. Photosensitizer encapsulated organically modified silica nanoparticles for direct two-photon photodynamic therapy and in vivo functional imaging. Biomaterials 2012; 33: 4851-60.

[97] Yong KT, Roy I, Swihart MT, Prasad PN. Multifunctional nanoparticles as biocompatible targeted probes for human cancer diagnosis and therapy. J Mater Chem 2009; 19: 4655–72.

[98] Tang L, Cheng J. Nonporous Silica Nanoparticles for Nanomedicine Application. Nano Today 2013; 8: 290-312.

[99] Roy I, Ohulchanskyy TY, Bharali DJ, Pudavar HE, Mistretta RA, Kaur N, Prasad PN. Optical tracking of organically modified silica nanoparticles as DNA carriers: a nonviral, nanomedicine approach for gene delivery. Proc Natl Acad Sci U S A 2005; 102: 279-84.

[100] Bharali DJ, Klejbor I, Stachowiak EK, Dutta P, Roy I, Kaur N, Bergey EJ, Prasad PN, Stachowiak MK. Organically modified silica nanoparticles: a nonviral vector for in vivo gene delivery and expression in the brain. Proc Natl Acad Sci U S A 2005; 102: 11539-44.

[101] Klejbor I, Stachowiak EK, Bharali DJ, Roy I, Spodnik I, Morys J, Bergey EJ, Prasad PN, Stachowiak MK. ORMOSIL nanoparticles as a non viral gene delivery vector for modeling polyglutamine induced brain pathology. J. Neurosci Methods 2007; 165: 230-43.

[102] Yang X, Liu J, He H, Zhou L, Gong C, Wang X, Yang L, Yuan J, Huang H, He L, Zhang B, Zhuang Z. SiO2 nanoparticles induce cytotoxicity and protein expression alteration in HaCaT cells. Part Fibre Toxicol. 2010; 7: 1.

[103] Panas A, Marquardt C, Nalcaci O, Bockhorn H, Baumann W, Paur HR, Mülhopt S, Diabaté S, Weiss C. Screening of different metal oxide nanoparticles reveals selective toxicity and inflammatory potential of silica nanoparticles in lung epithelial cells and macrophages. Nanotoxicology 2013; 7: 259-73.

[104] Moret F, Selvestrel F, Lubian E, Mognato M, Celotti L, Mancin F, Reddi E. PEGylation of ORMOSIL nanoparticles differently modulates the in vitro toxicity toward human lung cells. Arch Toxicol. 2015; 89: 607-20.

[105] Huang X, Teng X, Chen D, Tang F, He J. The effect of the shape of mesoporous silica nanoparticles on cellular uptake and cell function. Biomaterials 2010; 31: 438-48.

[106] Kasper J, Hermanns MI, Bantz C, Koshkina O, Lang T, Maskos M, Pohl C, Unger RE, Kirkpatrick CJ. Interactions of silica nanoparticles with lung epithelial cells and the association to flotillins. Arch Toxicol. 2013; 87: 1053-65.

[107] Kumar R, Roy I, Ohulchanskky TY, Vathy LA, Bergey EJ, Sajjad M, Prasad PN. In vivo biodistribution and clearance studies using multimodal organically modified silica nanoparticles. ACS Nano. 2010; 4: 699-708.

[108] Barandeh F, Nguyen PL, Kumar R, Iacobucci GJ, Kuznicki ML, Kosterman A, Bergey EJ, Prasad PN, Gunawardena S. Organically modified silica nanoparticles are biocompatible and can be targeted to neurons in vivo. PLoS One 2012; 7: e29424.

[109] Goel A, Kunnumakkara AB, Aggarwal BB. Curcumin as "Curcumin": from kitchen to clinic. Biochem Pharmacol 2008; 75: 787–809.

[110] Prasad S, Gupta SC, Tyagi AK, Aggarwal BB. Curcumin, a component of golden spice: from bedside to bench and back. Biotechnol Adv. 2014; 32: 1053-64.

[111] Grynkiewicz G, Ślifirski P. Curcumin and curcuminoids in quest for medicinal status. Acta Biochim Pol. 2012; 59: 201-12.

[112] Priyadarsini KI. J. Photophysics, photochemistry and photobiology of curcumin: Studies from organic solutions, bio-mimetics and living cells. Photochem. Photobiol. C Photochem. Rev. 2009, 10, 81–95.

[113] Aggarwal BB, Sung B. Pharmacological basis for the role of curcumin in chronic diseases: an age-old spice with modern targets. Trends Pharmacol. Sci. 2009; 30: 85–94.

[114] Aggarwal BB, Harikumar KB. Potential therapeutic effects of curcumin, the anti-inflammatory agent, against neurodegenerative, cardiovascular, pulmonary, metabolic, autoimmune and neoplastic diseases. Int J Biochem Cell Biol. 2009; 41: 40-59.

[115] Satoskar RR, Shah SJ, Shenoy SG. Evaluation of anti-inflammatory property of curcumin (diferuloyl methane) in patients with postoperative inflammation. Int. J. Clin. Pharmacol. Ther Toxicol. 1986; 24: 651–54.

[116] Akbik D, Ghadiri M, Chrzanowski W, Rohanizadeh R. Curcumin as a wound healing agent. Life Sci. 2014; 116: 1-7.

[117] Moghadamtousi SZ, Kadir HA, Hassandarvish P, Tajik H, Abubakar S, Zandi K. A review on antibacterial, antiviral, and antifungal activity of curcumin. Biomed Res Int. 2014; doi: 10.1155/2014/186864.

[118] Nayak AP, Tiyaboonchai W, Patankar S, Madhusudhan B, Souto EB. Curcuminoids-loaded lipid nanoparticles: novel approach towards malaria treatment. Colloids Surf B Biointerfaces 2010; 81: 263-73.

[119] Ravindran J, Prasad S, Aggarwal BB. Curcumin and cancer cells: how many ways can curry kill tumor cells selectively? AAPS J. 2009; 11: 495-510.

[120] Anand P, Sundaram C, Jhurani S, Kunnumakkara AB, Aggarwal BB. Curcumin and cancer: an "old-age" disease with an "age-old" solution. Cancer Lett. 2008 18; 267: 133-64.

[121] Sinha D, Biswas J, Sung B, Aggarwal BB, Bishayee A. Chemopreventive and chemotherapeutic potential of curcumin in breast cancer. Curr Drug Targets. 2012; 13: 1799-819.

[122] Kunnumakkara AB, Diagaradjane P, Guha S, Deorukhkar A, Shentu S, Aggarwal BB, Krishnan S. Curcumin sensitizes human colorectal cancer xenografts in nude mice to gamma-radiation by targeting nuclear factor-kappa B-regulated gene products. Clin Cancer Res. 2008; 14: 2128-36.

[123] Bernd A. Visible light and/or UVA offer a strong amplification of the anti-tumor effect of curcumin. Phytochem Rev. 2014; 13: 183-89.

[124] Mukhopadhyay A, Banerjee S, Stafford LJ, Xia C, Liu M, Aggarwal BB. Curcumin-induced suppression of cell proliferation correlates with down-regulation of cyclin D1 expression and CDK4-mediated retinoblastoma protein phosphorylation. Oncogene 2002; 21: 8852-61.

[125] Duvoix A, Blasius R, Delhalle S, Schnekenburger M, Morceau F, Henry E. Chemopreventive and therapeutic effects of curcumin. Cancer Lett 2005; 223: 181-90.

[126] Bar-Sela G, Epelbaum R, Schaffer M. Curcumin as an anti-cancer agent: review of the gap between basic and clinical applications. Curr Med Chem 2010; 17: 190-7.

[127] Maheshwari RK, Singh AK, Gaddipati J, Srimal RC. Multiple biological activities of curcumin: a short review. Life Sci 2006; 78: 2081-87.

[128] Shishodia S, Chaturvedi MM. Role of curcumin in cancer therapy. Curr Prob Cancer 2007; 31: 243-305.

[129] Hatcher H, Planalp R, Cho J, Torti FM, Torti SV. Curcumin: from ancient medicine to current clinical trials. Cell Mol Life Sci. 2008; 65: 1631–52.

[130] Brondino N, Re S, Boldrini A, Cuccomarino A, Lanati N, Barale F, Politi P. Curcumin as a therapeutic agent in dementia: a mini systematic review of human studies. Scientific World Journal. 2014; 2014: 174282.

[131] Anand P, Kunnumakkara AB, Newman RA, Aggarwal BB. Bioavailability of curcumin: problems and promises. Mol Pharm. 2007; 4: 807–18.

[132] Kurien BT, Singh A, Matsumoto H, Scofield RH. Improving the solubility and pharmacological efficacy of curcumin by heat treatment. Assay Drug Dev Techn 2007; 5: 567-76.

[133] Tønnesen HH, Másson M, Loftsson T. Studies of curcumin and curcuminoids. XXVII. Cyclodextrin complexation: solubility, chemical and photochemical stability. Int J Pharm 2002; 244: 127-35.

[134] Wang YJ, Pan MH, Cheng AL, Lin LI, Ho YS, Hsieh CY. Stability of curcumin in buffer solutions and characterization of its degradation products. J Pharm Biomed Anal. 1997; 15: 1867-76.

[135] Yang KY, Lin LC, Tseng TY, Wang SC, Tsai TH. Oral bioavailability of curcumin in rat and the herbal analysis from Curcuma longa by LC-MS/MS. J Chromatogr B Analyt Technol Biomed Life Sci. 2007; 853: 183-89.

[136] Shoba G, Joy D, Joseph T, Majeed M, Rajendran R, Srinivas PS. Influence of piperine on the pharmacokinetics of curcumin in animals and human volunteers. Planta Med. 1998; 64: 353-56.

[137] Wahlstromand B, Blennow G. “A study on the fate of curcumin in the rat,”. Acta Pharmacologica et Toxicologica 1978; 43: 86–92.

[138] Vareed SK, Kakarala M, Ruffin MT. Pharmacokinetics of curcumin conjugate metabolites in healthy human subjects. Cancer Epidemiol Biomarkers Prev. 2008; 17: 1411–17.

[139] Sharma RA, Euden SA, Platton SL. Phase I clinical trial of oral curcumin: biomarkers of systemic activity and compliance. Clin Cancer Res. 2004; 10: 6847–54.

[140] Singh DV, Godbole MM, Misra K. A plausible explanation for enhanced bioavailability of P-gp substrates in presence of piperine: simulation for next generation of P-gp inhibitors. J Mol Model. 2013; 19: 227-38.

[141] Parvathy K, Negi P, Srinivas P. Curcumin amino acid conjugates: synthesis, antioxidant and antimutagenic attributes. Food Chem 2010; 120: 523-30.

[142] Manju S, Sreenivasan K. Conjugation of curcumin on to hyaluronic acid enhances its aqueous solubility and stability. J Colloid Interface Sci 2011; 359: 318-25.

[143] Tang H, Murphy CJ, Zhang B, Shen Y, Sui M, Van Kirk EA. Amphiphilic curcumin conjugate-forming nanoparticles as anticancer prodrug and drug carriers: in vitro and in vivo effects. Nanomedicine 2010; 5: 855-65.

[144] Yallapu MM, Jaggi M, Chauhan SC. beta-Cyclodextrin-curcumin self assembly enhances curcumin delivery in prostate cancer cells. Colloids Surf B Biointerfaces. 2010; 79: 113–25.

[145] Duan J, Zhang Y, Han S, et al. Synthesis and in vitro/in vivo anticancer evaluation of curcumin loaded chitosan /poly(butyl cyanoacrylate) nanoparticles. Int J Pharm. 2010; 400: 21120.

[146] Rejinold NS, Sreerekha PR, Chennazhi KP, Nair SV, Jayakumar R. Biocompatible, biodegradable and thermo-sensitive chitosan-g-poly (N-isopropylacrylamide) nanocarrier for curcumin drug delivery. Int J Biolog Macromol. 2011; 49: 161–72.

[147] Babaei E, Sadeghizadeh M, Hassan ZM, Feizi MA, Najafi F, Hashemi SM. Dendrosomal curcumin significantly suppresses cancer cell proliferation in vitro and in vivo. Int Immuno pharmacol. 2012; 12: 226–34.

[148] Nair KL, Thulasidasan AK, Deepa G, Anto RJ, Kumar GS. Purely aqueous PLGA nanoparticulate formulations of curcumin exhibit enhanced anticancer activity with dependence on the combination of the carrier. Int J Pharm. 2012; 425: 44–52.

[149] Anand P, Nair HB, Sung B. Design of curcumin-loaded PLGA nanoparticles formulation with enhanced cellular uptake, and increased bioactivity in vitro and superior bioavailability invivo. Biochem Pharmacol. 2010; 79: 330–38.

[150] Bisht S, Mizuma M, Feldmann G. Systemic administration of polymeric nanoparticle encapsulated curcumin (NanoCurc) blocks tumor growth and metastases in preclinical models of pancreatic cancer. Mol Cancer Ther. 2010; 9: 2255–64.

[151] Sahu A, Bora U, Kasoju N, Goswami P. Synthesis of novel biodegradable and self assembling methoxy poly(ethylene glycol)- palmitate nanocarrier for curcumin delivery to cancer cells. Acta Biomater. 2008; 4: 1752–61.

[152] Zhang L, Zhu W, Yang C. A novel folate-modified self-microemulsifying drug delivery system of curcumin for colon targeting. Int J Nanomedicine. 2012; 7: 151–62.

[153] Saengkrit N, Saesoo S, Srinuanchai W, Phunpee S, Ruktanonchai UR. Influence of curcumin-loaded cationic liposome on anticancer activity for cervical cancer therapy. Colloids and Surfaces B: Biointerfaces 2014; 114: 349-56.

[154] Manju S, Sreenivasan K. Gold nanoparticles generated and stabilized by water soluble curcumin–polymer conjugate: Blood compatibility evaluation and targeted drug delivery onto cancer cells. Journal of Colloid and Interface Science 2012; 368: 144-51.

[155] Ranjan AP, Mukerjee A, Helson L, Vishwanatha JK. Scale up, optimization and stability analysis of Curcumin C3 complex-loaded nanoparticles for cancer therapy. J. Nanobiotechnology. 2012; 10: 38.

[156] Khalil NM, Nascimento TC, Casa DM, Dalmolin LF, Mattos AC, Hoss I, Romano MA, Mainardes RM. Pharmacokinetics of curcumin-loaded PLGA and PLGA-PEG blend nanoparticles after oral administration in rats. Colloids Surf. B: Biointerfaces. 2013; 101: 353-60.

[157] Tsai YM, Chang-Liao WL, Chien CF, Lin LC, Tsai TH. Effects of polymer molecular weight on relative oral bioavailability of curcumin. Int. J. Nanomedicine. 2012; 7: 2957–66.

[158] Shaikh J, Ankola DD, Beniwal V, Singh D, Kumar MN. Nanoparticle encapsulation improves oral bioavailability of curcumin by at least 9-fold when compared to curcumin administered with piperine as absorption enhancer. Eur. J. Pharm. Sci. 2009; 37: 223–30.

[159] Wang W, Zhu R, Xie Q, Li A, Xiao Y, Li K, Liu H, Cui D, Chen Y, Wang S. Enhanced bioavailability and efficiency of curcumin for the treatment of asthma by its formulation in solid lipid nanoparticles. Int. J. Nanomedicine. 2012; 7: 3667–77.

[160] Li C, Zhang Y, Su T, Feng L, Long Y, Chen Z. Silica-coated flexible liposomes as a nanohybrid delivery system for enhanced oral bioavailability of curcumin. Int. J. Nanomedicine. 2012; 7: 5995–6002.

[161] Pawar YB, Purohit H, Valicherla GR, Munjal B, Lale SV, Patel SB, Bansal AK. Novel lipid based oral formulation of curcumin: development and optimization by design of experiments approach. Int. J. Pharm. 2012; 436: 617–23.

[162] Yu H, Huang Q. Improving the oral bioavailability of curcumin using novel organogel-based nanoemulsions. J. Agric. Food. Chem. 2012; 60: 5373–79.

[163] Mohanty C, Sahoo SK. The *in vitro* stability and *in vitro* pharmacokinetics of curcumin prepared as an aqueous nanoparticulate formulation. Biomaterials. 2010; 31: 6597–611.

[164] Feng R, Song Z, Zhai G. Preparation and *in vivo* pharmacokinetics of curcumin-loaded PCL-PEG-PCL triblock copolymeric nanoparticles. Int. J. Nanomedicine. 2012; 7 :4089–98.

[165] Onoue S, Takahashi H, Kawabata Y, Seto Y, Hatanaka J, Timmermann B, Yamada S. Formulation design and photochemical studies on nanocrystal solid dispersion of curcumin with improved oral bioavailability. J. Pharm. Sci. 2010; 99: 1871–81.

[166] Gao Y, Li Z, Sun M, Li H, Guo C, Cui J, Li A, Cao F, Xi Y, Lou H, Zhai G. Preparation, characterization, pharmacokinetics, and tissue distribution of curcumin nanosuspension with TPGS as stabilizer. Drug. Dev. Ind. Pharm. 2010; 36: 1225–34.

[167] Dujic J, Kippenberger S, Hoffmann S, Ramirez-Bosca A, Miquel J, Diaz-Alperi J, Bereiter-Hahn J, Kaufmann R, Bernd A. Low concentrations of curcumin induce growth arrest

and apoptosis in skin keratinocytes only in combination with UVA or visible light. J Invest Dermatol. 2007; 127: 1992–2000.

[168] Ye Y, Li Y, Fang F. Upconversion nanoparticles conjugated with curcumin as a photosensitizer to inhibit methicillin-resistant Staphylococcus aureus in lung under near infrared light. Int J Nanomedicine 2014; 9: 5157-65.

[169] Chignell CF, Bilski P, Reszka KJ, Motten AN, Sik RH, Dhal TA. Spectral and photochemical properties of curcumin. Photochem. Photobiol. 1994; 59: 295–302.

[170] Gorman AA, Hamblett I, Srinivasan VS, Wood PD. Curcumin-derived transients: a pulsed laser and pulse radiolysis study. Photochem. Photobiol. 1994; 59: 389–98.

[171] Dahl TA, Bilski P, Reszka KJ, Chignell CF. Photocytotoxicity of curcumin. Photochem Photobiol. 1994; 59: 290–94.

[172] Dahl TA, McGowan WM, Shand MA, Srinivasan VS. Photokilling of bacteria by the natural dye curcumin. Arch Microbiol. 1989; 151: 183–85.

[173] Koon HK, Leung AWN, Yue KKM, Mak NK. Photodynamic effect of curcumin on NPC/CNE2 cells. J. Environ. Pathol. Toxicol. Oncol. 2006; 25: 205-15.

[174] Dujic J, Kippenberger S, Ramirez-Bosca A, Diaz-Alperi J, Bereiter-Hahn J, Kaufmann R, Bernd A, Hofmann M. Curcumin in combination with visible light inhibits tumor growth in a xenograft tumor model. Int J Cancer 2009; 124: 1422–28.

[175] Bruzell EM, Morisbak E, Tonnesen HH. Studies on curcumin and curcuminoids. XXIX. Photoinduced cytotoxicity of curcumin in selected aqueous preparations. Photochem. Photobiol. Sci. 2005; 4: 523–30.

[176] Dolmans DE, Fukimura D, Jain RK. Photodynamic therapy for cancer. Nat Rev Cancer, 2003; 3: 380-87.

[177] Dougherty TJ, Gomer CJ, Henederson BW, Jori G, Kessel D, Korbelik M, Moan J, Peng Q. Photodynamic Therapy. J Natl Cancer Inst. 1998; 90: 889-905.

[178] Dougherty T. Photochemistry in the treatment of cancer. Adv.Photochem. 1992; 17: 275–312.

[179] Foote CS. Definition of Type I and Type II photosensitized oxidation. Photochem. Photobiol. 1991; 54: 659.

[180] Nyman ES, Hynninen PH. Research advances in the use of tetrapyrrolic photosensitizers for photodynamic therapy. J. Photochem. and Photobio. B: Biology 2004; 73: 1–28.

[181] Jori G. Far-red absorbing photosensitizers: their use in the photodynamic therapy of tumours, J. Photochem. Photobiol. A 1992; 62: 371–78.

[182] Usuda J, Kato H, Okunaka T, Furukawa K, Tsutsi H, Yamada K, Suga Y, Honda H, Nagatsuka Y, Ohira T, Tsuboi M, Hirano T. Photodynamic therapy (PDT) for lung cancers. J. Thorac. Oncol. 2006; 1: 489–93.

[183] Bonnett R. Photosensitizers of the porphyrin and phthalocyanine series for photodynamic therapy. Chem. Soc. Rev. 1995; 24: 19-33.

[184] Ormond AB, Freeman HS. Dye Sensitizers for Photodynamic Therapy. Materials 2013; 6: 817-40.

[185] Spikes JD, Bommer JC. Chlorophylls and related pigments as photosensitizers in biology and medicine. H. Scheer (Ed.), Chlorophylls, CRC Press, Boca Raton, FL 1991; 1181–1204.

[186] Egorov SY, Krasnovsky AA. Laser-induced luminescence of singlet molecular oxygen. Generation by drugs and pigments of biological importance. Proc. SPIE – Int. Soc. Opt. Eng. 1990; 1403: 611–21.

[187] Sengee GI, Badraa N. Shim YK. Synthesis and Biological Evaluation of New Imidazolium and Piperazinium Salts of Pyropheophorbide-a for Photodynamic Cancer Therapy. Int J Mol Sci. 2008; 9: 1407–15.

[188] Al-Omari S, Ali A. Photodynamic activity of pyropheophorbide methyl ester and pyropheophorbide a in dimethylformamide solution. Gen. Physiol. Biophys. 2009; 28: 70–77

[189] Pandey RK, Sumlin AB, Constantine S, Aoudia M, Smith WR, Dougherty TJ. Alkyl ether analogs of chlorophyll-a derivatives: Part 1. Synthesis, photophysical properties and photodynamic efficacy. Photochem. Photobiol. 1996; 64: 194–204.

[190] Stamati I, Kuimova MK, Lion M, Yahioglu G, Phillips D, Deonarain MP. Novel photosensitisers derived from pyropheophorbide-a: uptake by cells and photodynamic efficiency in vitro. Photochem Photobiol Sci. 2010; 9: 1033-41.

[191] Savellano MD, Pogue BW, Hoopes PJ, Vitetta ES, Paulsen KD. Multiepitope HER2 targeting enhances photoimmunotherapy of HER2-overexpressing cancer cells with pyropheophorbide-aimmunoconjugates. Cancer Res. 2005; 65: 6371-79.

[192] Kuimova MK, Bhatti M, Deonarain M, Yahioglu G, Levitt JA, Stamati I, Suhling K, Phillips D. Fluorescence characterisation of multiply-loaded anti-HER2 single chain Fv-photosensitizer conjugates suitable for photodynamic therapy. Photochem Photobiol Sci. 2007; 6: 933-39.

[193] Bhatti M, Yahioglu G, Milgrom LR, Garcia-Maya M, Chester KA, Deonarain MP. Targeted photodynamic therapy with multiply loaded recombinant antibody fragments. Int J Cancer 2008; 122: 1155-63.

[194] Liu T, Wu LY, Choi JK, Berkman CE. In vitro targeted photodynamic therapy with a pyropheophorbide--a conjugated inhibitor of prostate-specific membrane antigen. Prostate. 2009; 69: 585-94.

[195] Liu T, Wu LY, Choi JK, Berkman CE. Targeted photodynamic therapy for prostate cancer: inducing apoptosis via activation of the caspase-8/-3 cascade pathway. Int J Oncol. 2010; 36: 777-84.

[196] Fernandez Gacio A, Fernandez-Marcos C, Swamy N, Dunn D, Ray R. Photodynamic cell kill analysis of breast tumor cells with a tamoxifen-pyropheophorbide conjugate. J Cell Biochem. 2006; 99: 665-70.

[197] Sadler S, Persons KS, Jones GB, Ray R. Internalization of a C17α-alkynylestradiol-porphyrin conjugate into estrogen receptor positive MCF-7 breast cancer cells. Bioorg Med Chem Lett 2011; 21: 4638-41.

[198] Stefflova K, Li H, Chen J, Zheng G. Peptide-based pharmacomodulation of a cancer targeted optical imaging and photodynamic therapy agent. Bioconjug Chem. 2007; 18: 379-88.

[199] Cinteza LO, Ohulchanskyy TY, Sahoo Y, Bergey EJ, Pandey RK, Prasad PN. Diacyllipid micelle-based nanocarrier for magnetically guided delivery of drugs in photodynamic therapy. Mol Pharm. 2006; 3: 415-23.

[200] Guelluy PH, Fontaine-Aupart MP, Grammenos A, Lécart S, Piette J, Hoebeke M. Optimizing photodynamic therapy by liposomal formulation of the photosensitizer pyropheophorbide-a methyl ester: in vitro and ex vivo comparative biophysical investigations in a colon carcinoma cell line. Photochem Photobiol Sci. 2010; 9: 1252-60.

[201] Wang S, Fan W, Kim G, Hah HJ, Lee YE, Kopelman R, Ethirajan M, Gupta A, Goswami LN, Pera P, Morgan J, Pandey RK. Novel methods to incorporate photosensitizers into nanocarriers for cancer treatment by photodynamic therapy. Lasers Surg Med. 2011; 43: 686-95.

[202] Zhou A, Wei Y, Wu B, Chen Q, Xing D. Pyropheophorbide A and c(RGDyK) comodified chitosan-wrapped upconversion nanoparticle for targeted near-infrared photodynamic therapy. Mol Pharm. 2012; 9: 1580-9.

[203] Stile RA, Barber TA, Castner DG, Healy KE. Sequential robust design methodology and X ray photoelectron spectroscopy to analyze the grafting of hyaluronic acid to glass substrates. J Biomed Mater Res 2002; 61: 391-8.

[204] Oueslati N, Leblanc P, Harscoat-Schiavo C, Rondags E, Meunier S, Kapel R, Marc I. CTAB turbidimetric method for assaying hyaluronic acid in complex environments and under cross-linked form. Carbohydr. Polym 2014; 112: 102–8.

[205] Mulherkar R, Goud AP, Wagle AS. Establishment of ahuman squamous cell carcinoma cell line of the upper aerodigestive tract. Cancer Letters 1997; 118: 115—21.

[206] Zölzer F, Hillebrandt S, Streffer C. Radiation induced G1-block and p53 status in six human cell lines. Radiother Oncol 1995; 37: 20–28.

[207] Sharma M, Verma Y, Rao KD, Nair R, Gupta PK. Imaging growth dynamics of tumor spheroids using optical coherence tomography. Biotechnol Lett 2007; 2: 273-78.

[208] Kunwar A, Barik A, Mishra B, Rathinasamy K, Pandey R, Priyadarsini KI. Quantitative cellular uptake, localization and cytotoxicity of curcumin in normal and tumor cells. Biochim Biophys Acta 2008; 1780: 673–79.

[209] García-Díaz M, Nonell S, Villanueva A. Do folate receptor targeted liposomal photosensitizers enhance photodynamic therapy selectivity, Biochimica Biophysica Acta 2011;1808:1063- 71.

[210] Mosmann T. Rapid colorimetric assay for cellular growth and survival: application to proliferation and cytotoxicity assays. Journal of Immunological Methods 1983; 65:55- 63.

[211] Xu WH, Han M, Dong Q, Fu ZX, Diao YY, Liu H, Xu J, Jiang HL, Zhang SZ, Zheng S, Gao JQ, Wei QC. Doxorubicin-mediated radiosensitivity in multicellular spheroids from a lung cancer cell line is enhanced by composite micelle encapsulation. Int J Nanomedicine 2012; 7: 2661-71.

[212] Mohanty C, Sahoo SK. The in vitro stability and in vivo pharmacokinetics of curcumin prepared as an aqueous nanoparticulate formulation. Biomaterials 2010; 31:6597–611.

[213] Placer ZA, Cushman LL, Johnson BC. Estimation of product of lipid peroxidation (malonyldialdehyde) in biochemical systems. Anal. Biochem 1966; 16: 359–64.

[214] Akerboom TP, Sies H. Assay of glutathione, glutathione disulfide, and glutathione mixed disulfides in biological samples. Methods Enzymol. 1981; 77: 373-82.

[215] Joe B, Vijaykumar M, Lokesh BR. Biological properties of curcumin-cellular and molecular mechanisms of action. Crit Rev Food Sci Nutr 2004; 44: 97–111.

[216] Xu YX, Pindolia KR, Janakiraman N, Noth CJ, Chapman RA, Gautam SC. Curcumin a compound with anti-inflammatory and anti-oxidant properties, down regulates chemokine expression in bone marrow stromal cell. Exp Hematol 1997; 25: 413–22.

[217] Ribeiro AP, Pavarina AC, Dovigo LN, Brunetti IL, Bagnato VS. Phototoxic effect of curcumin on methicillin-resistant Staphylococcus aureus and L929 fibroblasts. Lasers Med Sci 2013; 28: 391–98.

[218] Kunwar A, Barik A, Pandey R, Priyadarsini KI. Transport of liposomal and albumin loaded curcumin to living cells; an absorption and fluorescence spectroscopic study. Biochim Biophys Acta 2006; 1760: 1513–20.

[219] Bisht S, Feldmann G, Soni S, Ravi R, Karikar C, Maitra. Polymeric nanoparticle-encapsulated curcumin ("nanocurcumin"): a novel strategy for human cancer therapy. J Nanobiotechnol 2007; 5:3.

[220] Sou K, Inenaga S, Takeoka S, Tsuchida E. Loading of curcumin into macrophages using lipid-based nanoparticles. Int J Pharm 2008; 352: 287–93.

[221] Damoiseau X, Schuitmaker HJ, Lagerberg JW, Hoebeke M. Increase of the photosensitizing efficiency of the Bacteriochlorin a by liposome-incorporation. J Photochem Photobiol B 2001; 60: 50–60.

[222] Qian J, Li X, Wei M, Gao X, Xu Z. Bio-molecule conjugated fluorescent organically modified silica nanoparticles as optical probes for cancer cell imaging. Opt Express 2008; 16: 19568–578.

[223] Lin CL, Lin JK. Curcumin: a potential cancer chemopreventive agent through suppressing NF-κB signaling. J Cancer Mol 2008; 4: 11–16.

[224] Besic Gyenge E, Darphin X,Wirth A, Pieles U,Walt H, Bredell M, Maake C. Uptake and fate of surface modified silica nanoparticles in head and neck squamous cell carcinoma. J Nanobiotechnology 2011; 9: 32.

[225] Chaudhary LR, Hruska KA. Inhibition of cell survival signal protein kinase B/Akt by curcumin in human prostate cancer cells. J Cell Biochem 2003; 89: 1–5.

[226] Squires MS, Hudson EA, Howells L, Sale S, Houghton CE, Jones JL, Fox LH, Dickens M, Prigent SA, Manson MM. Relevance of mitogen activated protein kinase (MAPK) and phosphotidylinositol-3-kinase/protein kinase B (PI3K/PKB) pathways to induction of apoptosis by curcumin in breast cells. Biochem Pharmacol 2003; 65: 361–76.

[227] Korutla L, Kumar R. Inhibitory effect of curcumin on epidermal growth factor receptor kinase activity in A431 cells. Biochim Biophys Acta 1994; 1224: 597–600.

[228] Das KC, Das CK. Curcumin (diferuloylmethane), a singlet oxygen $^{1}O_2$ quencher. Biochem Biophys Res Commun 2002; 295: 62–66.

[229] Began G, Sudharshan E, Udaya Sankar K, Appu Rao AG. Interaction of curcumin with phosphatidylcholine: a spectrofluorimetric study. J Agric Food Chem 1999; 47:4992–97.

[230] Aggarwal S, Takada Y, Singh S, Myers JN, Aggarwal BB. Inhibition of growth and survival of human head and neck squamous cell carcinoma cells by curcumin via modulation of nuclear factor-κB signaling. Int J Cancer 2004; 111:679–92.

[231] Kunnumakkara AB, Anand P, Aggarwal BB. Curcumin inhibits proliferation, invasion, angiogenesis and metastasis of different cancers through interaction with multiple cell signaling proteins. Cancer Lett 2008; 269: 199–225.

[232] Philip M, Rowley DA, Schreiber H. Inflammation as a tumor promoter in cancer induction. Semin Cancer Biol 2004; 14: 433–39.

[233] Sanna V, Pala N, Sechi M. Targeted therapy using nanotechnology: focus on cancer. Int J Nanomedicine 2014; 9: 467-83.

[234] Guo S, Huang L. Nanoparticles containing insoluble drug for cancer therapy. Biotechnol Adv. 2014; 32: 778-88.

[235] Minchinton AI, Tannock IF. Drug Penetration in Solid Tumors. Nature Rev Cancer 2006; 6: 583–92.

[236] Cabral H, Matsumoto Y, Mizuno K, Chen Q, Murakami M, Kimura M, Terada Y, Kano MR, Miyazono K, Uesaka M, Nishiyama N, Kataoka K. Accumulation of sub-100 nm polymeric micelles in poorly permeable tumours depends on size. Nature Nanotech. 2011; 6: 815–23.

[237] Chauhan VP, Stylianopoulos T, Boucher Y, Jain RK. Delivery of molecular and nanoscale medicine to tumors: transport barriers and strategies. Annu Rev Chem Biomol Eng. 2011; 2: 281–98.

[238] Chithrani BD, Chan WC. Elucidating the mechanism of cellular uptake and removal of protein-coated gold nanoparticles of different sizes and shapes. Nano Lett. 2007; 7: 1542–50.

[239] Chithrani BD, Ghazani AA, Chan WC. Determining the size and shape dependence of gold nanoparticle uptake into mammalian cells. Nano Lett. 2006; 6: 662–68.

[240] Jiang W, Kim BY, Rutka JT, Chan WC. Nanoparticle-mediated cellular response is size-dependent. Nature Nanotech. 2008; 3: 145-50.

[241] Lu F, Wu SH, Hung Y, Mou CY. Size effect on cell uptake in well suspended, uniform mesoporous silica nanoparticles. Small 2009; 5: 1408–13.

[242] Hirschhaeuser F, Menne H, Dittfeld C, West J, Mueller-Klieser W, Kunz-Schughart LA. Multicellular tumor spheroids: an underestimated tool is catching up again. J of Biotech. 2010; 148: 3–15.

[243] Mehta G, Hsiao A Y, Ingram M, Luker G D, Takayama S. Opportunities and challenges for use of tumor spheroids as models to test drug delivery and efficacy. J of Controlled Rel. 2012; 164: 192–204.

[244] Singh SP, Sharma M, Gupta PK. Enhancement of phototoxicity of curcumin in human oral cancer cells using silica nanoparticles as delivery vehicle. Lasers Med Sci. 2014; 29: 645-52.

[245] Valko M, Rhodes CJ, Moncol J, Izakovic M, Mazur M. Free radicals, metals and antioxidants in oxidative stress-induced cancer. Chemi. Biololo. Interactions 2006; 160: 1-40.

[246] Perotti C, Casas A, Del C, Batlle AM. Scavengers protection of cells against ALA-based photodynamic therapy-induced damage. Lasers Med Sci. 2002; 17: 222-29.

[247] Timmins GS, Davies MJ. An EPR spin trapping study of albumin protein radicals formed by the photodynamic action of haematoporphyrin. J Photochem Photobiol B. 1993; 21: 167-73.

[248] Huang K, Ma H, Liu J, Huo S, Kumar A, Wei T, Zhang X, Jin S, Gan Y, Wang PC, He S, Zhang X, Liang XJ. Size-dependent localization and penetration of ultrasmall gold nanoparticles in cancer cells, multicellular spheroids, and tumors in vivo. ACS Nano 2012; 6: 4483-93.

[249] Jin S, Ma X, Ma H, Zheng K, Liu J, Hou S, Meng J, Wang PC, Wu X, Liang XJ. Surface chemistry-mediated penetration and gold nanorod thermotherapy in multicellular tumor spheroids. Nanoscale 2013; 5: 143-6.

[250] Davies CD, Berk DA, Pluen A, Jain RK. Comparison of IgG diffusion and extracellular matrix composition in rhabdomyosarcomas grown in mice versus in vitro as spheroids reveals the role of host stromal cells. British J Cancer 2002; 86: 1639–44.

[251] Ramanujan S, Pluen A, McKee TD, Brown EB, Boucher Y, Jain RK. Diffusion and convection in collagen gels: Implications for transport in the tumor interstitium. Biophys J. 2002; 83: 1650–60.

[252] Kim B, Han G, Toley BJ, Kim CK, Rotello VM, Forbes NS. Tuning payload delivery in tumour cylindroids using gold nanoparticles. Nature Nanotech 2010; 5: 465-72.

[253] Dubessy C, Merlin JM, Marchal C, Guillemin F. Spheroids in radiobiology and photodynamic therapy. Crit Rev Oncol Hematol. 2000; 36: 179-92.

[254] Olive PL, Durand RE. Drug and radiation resistance in spheroids: cell contact and kinetics. Cancer Metastasis Rev 1994; 13: 121-38.

[255] West CM. Size-dependent resistance of human tumour spheroids to photodynamic treatment. British J Cancer 1989; 59: 510-14.

[256] Chaudhary LR, Hruska KA. Inhibition of cell survival signal protein kinase B/Akt by curcumin in human prostate cancer cells. J Cellular Biochem 2003; 89: 1–5.

[257] Madsen SJ, Sun CH, Tromberg BJ, Cristini V, De Magalhães N, Hirschberg H. Multicell tumor spheroids in photodynamic therapy. Lasers Surg Med. 2006; 38: 555-64.

[258] Weston MA, Patterson MS. Validation and Application of a Model of Oxygen Consumption and Diffusion During Photodynamic Therapy In Vitro. Photochem Photobiol. 2014; 90: 1359-67.

[259] Nichols MG, Foster TH. Oxygen diffusion and reaction kinetics in the photodynamic therapy of multicell tumour spheroids. Phys Med Biol. 1994; 39: 2161-81.

[260] Dilnawaz F, Sahoo SK. Enhanced accumulation of curcumin and temozolomide loaded magnetic nanoparticles executes profound cytotoxic effect in glioblastoma spheroid model. Eur J Pharm Biopharm. 2013; 85: 452-62.

[261] Etminan N, Peters C, Ficnar J, Anlasik S, Bünemann E, Slotty PJ, Hänggi D, Steiger HJ, Sorg RV, Stummer W. Modulation of migratory activity and invasiveness of human glioma spheroids following 5-aminolevulinic acid-based photodynamic treatment. Laboratory investigation. J Neurosurg. 2011; 11: 281-8.

[262] Wang A Z, Langer R, Farokhzad O C. Nanoparticle delivery of cancer drugs. Annu. Rev. Med 2012; 63: 185–98.

[263] Wang Y, Wei X, Zhang C, Zhang F, Liang W. Nanoparticle delivery strategies to target doxorubicin to tumor cells and reduce side effects. Ther Deliv 2010; 2: 273-87.

[264] Aslan B, Ozpolat B, Sood AK, Lopez-Berestein G. Nanotechnology in cancer therapy. J Drug Target 2013; 10: 904-13.

[265] Lammers T, Kiessling F, Hennink WE, Storm G. Drug targeting to tumors: principles, pitfalls and (pre) clinical progress. J Control Release 2012; 161: 175-87.

[266] Toole BP. Hyaluronan-CD44 Interactions in Cancer: Paradoxes and Possibilities. Clin Cancer Res 2009; 15: 7462-68.

[267] Karbownik MS, Nowak JZ. Hyaluronan: towards novel anti-cancer therapeutics. Pharmacol Rep 2013; 65: 1056-74.

[268] Cui X, Xu H, Zhou S, Zhao T, Liu A, Guo X, Tang W, Wang F. Evaluation of angiogenic activities of hyaluronan oligosaccharides of defined minimum size. Life Sci 2009; 85: 573–77.

[269] Jin P, Kang Z, Zhang N, Du G, Chen J. High-yield novel leech hyaluronidase to expedite the preparation of specific hyaluronan oligomers. Sci. Rep 2014; 4: 1–8.

[270] Toole BP, Ghatak S, Misra S. Hyaluronan oligosaccharides as a potential anticancer therapeutic. Curr. Pharm. Biotechnol 2008; 9: 249–52.

[271] Toole BP, Slomiany MG. Hyaluronan, CD44 and Emmprin: partners in cancer cell chemoresistance. Drug Resist. Updat 2008; 11: 110–21.

[272] Li YF, Xiao B, Tu SF, Wang YY, Zhang XL. Cultivation and identification of colon cancer stem cell-derived spheres from the Colo205 cell line. Braz. J. Med. Biol. Res 2012; 45: 197–204.

[273] Alkrad JA, Mrestani Y, Stroehl D, Wartewig S, Neubert R. Characterization of enzymatically digested hyaluronic acid using NMR, Raman, IR, and UV-Vis spectroscopies. J. Pharm. Biomed.Anal 2003; 31: 545–50.

[274] Singh SP, Sharma M, Patel H, Gupta PK. Extra cellular pH influences uptake and photodynamic action of pyropheophorbide-a entrapped in folate receptor targeted organically modified silica nanoparticle. Photodiagnosis Photodyn. Ther 2014; 11: 156–64.

[275] Chen Z, Chen J, Wu L, Li W, Chen J, Cheng H, Pan J, Cai B. Hyaluronic acid-coated bovine serum albumin nanoparticles loaded with brucine as selective nanovectors for intra-articular injection. Int. J. Nanomed 2013; 9: 3843–53.

[276] Wartenberg M, Fery C, Diedershagen H, Ritgen J, Hescheler J, Saurer H. Development of an intrinsic P-glycoprotein-mediated doxorubicin resistance in quiescent cell layers of large, multicellular prostate tumor spheroids. Int.J. Cancer 1998; 75: 855–63.

[277] El-Dakdouki MH, Puré E, Huang X. Development of drug loaded nanoparticles for tumor targeting. Part 2: Enhancement of tumor penetration through receptor mediated transcytosis in 3D tumor models. Nanoscale 2013; 5: 3904–11.

[278] Lee H, Lee K, Kim IK, Park TG. Synthesis, characterization, and in vivo diagnostic applications of hyaluronic acid immobilized gold nanoprobes. Biomaterials 2008; 29: 4709–18.

[279] Ward JA, Huang L, Guo H, Ghatak S, Toole BP. Perturbation of hyaluronan interactions inhibits malignant properties of glioma cells. Am. J. Pathol 2003; 162: 1403–09.

[280] Bhatti M, Yahioglu G, Milgrom LR, Garcia-Maya M, Chester KA, Deonarain MP. Targeted photodynamic therapy with multiply-loaded recombinant antibody fragments. International Journal of Cancer 2008; 122:1155-63.

[281] Lee ES, Na K, Bae YH. Polymeric micelle for tumor pH and folate-mediated targeting. J Control Release 2003; 91: 103–113.

[282] Kim D, Gao ZG, Lee ES, Bae YH. In vivo evaluation of doxorubicin-loaded polymeric micelles targeting folate receptors and early endosomal pH in drug-resistant ovarian cancer. Mol Pharm. 2009; 6: 1353-62.

[283] Lee ES, Gao Z, Bae YH. Recent progress in tumor pH targeting nanotechnology. J Control Release 2008; 132: 164-70.

[284] Fukamachi T, Ikeda S, Wang X, Saito H, Tagawa M, Kobayashi H. Gene Expressions for Signal Transduction under Acidic Conditions. Genes 2013; 4: 65-85.

[285] Olszewski-Hamilton U, Hamilton G. Dependence of Relative Expression of NTR1 and EGFR on Cell Density and Extracellular pH in Human Pancreatic Cancer Cell Lines. Cancers 2011; 3: 182-197.

[286] Al-Omari S, Ali A. Photodynamic activity of pyropheophorbide methyl ester and pyropheophorbide-a in dimethylformamide solution. Gen Physiol Biophys 2009; 28:70—7.

[287] Zhao D, Zhao X, Zu Y, Li J, Zhang Y, Jiang R, Zhang Z. Preparation, characterization, and in vitro targeted delivery of folate-decorated paclitaxel-loaded bovine serum albumin nanoparticles. Int J Nanomedicine 2010; 5:669-77.

[288] Xu L, Fukumura D, Jain RK. Acidic extracellular pH induces vascular endothelial growth factor (VEGF) in human glioblastoma cells via ERK1/2 MAPK signaling pathway: Mechanism of low pH-induced VEGF. J Biolog Chemist 2002; 277:11368-74.

[289] Kato Y, Lambert CA, Colige AC, Mineur P, Noël A, Frankenne F, Foidart JM, Baba M, Hata R, Miyazaki K. Acidic extracellular pH induces matrix metalloproteinase-9 expression in mouse metastatic melanoma cells through the phospholipase D-mitogen activated protein kinase signalling. J Biolog Chemist 2005; 280: 10938-44.

[290] Toffoli G, Cernigoi C, Russo A, Gallo A, Bagnoli M, Boiocchi M. Overexpression of folate binding protein in ovarian cancers. Int J Cancer 1997; 74:193-8.

[291] Sierra EE, Brigle KE, Spinella MJ, Goldman ID. pH dependence of methotrexate transport by the reduced folate carrier and the folate receptor in L1210 leukemia cells. Further evidence for a third route mediated at low pH. Biochem Pharmacol 1997; 53:223-31.

[292] Bhandari SD, Joshi SK, McMartin KE. Folate binding and transport by rat kidney brush border membrane vesicles. Biochim Biophy Acta 1988 ; 937:211-8.

[293] Zhang Y, Yang M, Park JH, Singelyn J, Ma H, Sailor MJ, Ruoslahti E, Ozkan M, Ozkan C. A surface-charge study on cellular-uptake behavior of F3-peptide-conjugated iron oxide nanoparticles. Small 2009; 17:1990-96.

[294] Lu Y, Low PS. Folate-mediated delivery of macromolecular anticancer therapeutic agents. Adv Drug Deliv Rev 2002; 54:675-93.

[295] Varma R, Mayor S. GPI-anchored proteins are organized in submicron domains at the cell surface. Nature 1998; 394:798-801.

[296] Rothberg KG, Ying YS, Kolhouse JF, Kamen BA, Anderson RG. The glycophospholipid-linked folate receptor internalizes folate without entering the clathrin coated pit endocytic pathway. J Cell Biology 1990; 110: 637-49.

[297] Cosson P, de Curtis I, Pouysségur J, Griffiths G, Davoust J. Low cytoplasmic pH inhibits endocytosis and transport from the trans-Golgi network to the cell surface. J Cell Biology 1989; 108: 377-87.

[298] Chung TH, Wu SH, Yao M, Lu CW, Lin YS, Hung Y, Mou CY, Chen YC, Huang DM. The effect of surface charge on the uptake and biological function of mesoporous silica nanoparticles in 3T3-L1 cells and human mesenchymal stem cells. Biomaterials 2007; 28:2959-66.

[299] Singh J, Michel D, Chitanda JM, Verrall RE, Badea I. Evaluation of cellular uptake and intracellular trafficking as determining factors of gene expression for amino acid substituted Gemini surfactant-based DNA nanoparticles. J Nanobiotechnology 2012; 10:7.

[300] Longmire M, Choyke PL, Kobayashi H. Clearance properties of nano-sized particles and molecules as imaging agents: considerations and caveats. Nanomedicine 2008; 3: 703-17.

[301] Fischer HC, Chan WC. Nanotoxicity: the growing need for in vivo study. Curr Opin Biotechnol 2007; 18: 565-71.

[302] Fang J, Nakamura H, Maeda H. The EPR effect: Unique features of tumor blood vessels for drug delivery, factors involved, and limitations and augmentation of the effect. Adv Drug Delivery Rev. 2011; 63: 136-51.

[303] Lu J, Li Z, Zink JI, Tamanoi F. In vivo tumor suppression efficacy of mesoporous silica nanoparticles-based drug-delivery system: enhanced efficacy by folate modification. Nanomedicine. 2012; 8: 212-20.

[304] Harivardhan RL, Sharma RK, Chuttani K, Mishra AK, Murthy RS. Influence of administration route on tumor uptake and biodistribution of etoposide loaded solid lipid nanoparticles in Dalton's lymphoma tumor bearing mice. J Control Release. 2005; 105: 185-98.

[305] Kobayashi H, Watanabe R, Choyk PL. Larger molecules or particles are readily recognized by the RES. Molecules or particles with highly charged surfaces are also recognized by the RES and are quickly removed from the circulation. Theranostics 2014; 4: 81-89.

[306] Li SD, Huang L. Pharmacokinetics and biodistributation of nanoparticles. Mol.Pharm. 2008; 5: 496-504.

[307] Turk MJ, Waters DJ, Low PS. Folate-conjugated liposomes preferentially target macrophages associated with ovarian carcinoma. Cancer Lett. 2004; 213: 165-72.

[308] Ernsting MJ, Murakami M, Roy A, Li SD. Factors Controlling the Pharmacokinetics, Biodistribution and Intratumoral Penetration of Nanoparticles. J Control Release. 2013; 172: 782–94.

[309] Park JH, Gu L, von M, G, Ruoslahti E, Bhatia SN, Sailor MJ. Biodegradable luminescent porous silicon nanoparticles for in vivo applications. Nat. Mater. 2009; 8: 331–36.

[310] Xie G, Sun J, Zhong G, Shi L, Zhang D. Biodistribution and toxicity of intravenously administered silica nanoparticles in mice. Arch. Toxicol. 2010; 84: 183–90.

[311] Nishimori H, Kondoh M, Isoda K, Tsunoda S, Tsutsumi Y, Yagi K. Silica nanoparticles as hepatotoxicants. Eur. J. Pharm. Biopharm. 2009; 72: 496–501.

[312] Nishimori H, Kondoh M, Isoda K, Tsunoda S, Tsutsumi Y, Yagi K. Histological analysis of 70-nm silica particles-induced chronic toxicity in mice. Eur. J. Pharm. Biopharm. 2009; 72: 626–29.

[313] Ivanov S, Zhuravsky S, Yukina G, Tomson V, Korolev D, Galagudza M. In Vivo Toxicity of Intravenously Administered Silica and Silicon Nanoparticles. Materials 2012; 5: 1873-89.